



**SYNTHESIS AND CHARACTERIZATION OF  
LONG-CHAINED PORPHYRIN DERIVATIVES AND  
THEIR COBALT COMPLEXES**

**BY**

**MR. WOOTHIPHAN JANTAYOT**

**A THESIS SUBMITTED IN PARTIAL FULFILLMENT OF  
THE REQUIREMENTS FOR THE DEGREE OF  
MASTER OF SCIENCE IN CHEMISTRY  
FACULTY OF SCIENCE AND TECHNOLOGY  
THAMMASAT UNIVERSITY  
ACADEMIC YEAR 2014  
COPYRIGHT OF THAMMASAT UNIVERSITY**

**SYNTHESIS AND CHARACTERIZATION OF  
LONG-CHAINED PORPHYRIN DERIVATIVES AND  
THEIR COBALT COMPLEXES**

**BY**

**MR. WOOTHIPHAN JANTAYOT**

**A THESIS SUBMITTED IN PARTIAL FULFILLMENT OF  
THE REQUIREMENTS FOR THE DEGREE OF  
MASTER OF SCIENCE IN CHEMISTRY  
FACULTY OF SCIENCE AND TECHNOLOGY  
THAMMASAT UNIVERSITY  
ACADEMIC YEAR 2014  
COPYRIGHT OF THAMMASAT UNIVERSITY**



THAMMASAT UNIVERSITY  
FACULTY OF SCIENCE AND TECHNOLOGY

THESIS

BY

MR. WOOTHIPHAN JANTAYOT

ENTITLED

SYNTHESIS AND CHARACTERIZATION OF LONG-CHAINED PORPHYRIN  
DERIVATIVES AND THEIR COBALT COMPLEXES

was approved as partial fulfillment of the requirements for  
the degree of master of science in chemistry  
on July, 2015

Chairman



(Assistant Professor Kittipong Chainok, Ph.D.)

Member and Advisor



(Assistant Professor Supakorn Boonyuen, Ph.D.)

Member and Co-advisor



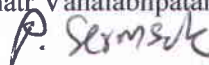
(Nanthawat Wannarit, Ph.D.)

Member



(Parichatr Vanalabhpattana, Ph.D.)

Dean



(Associate Professor Pakorn Sermsuk)

Thesis Title	SYNTHESIS AND CHARACTERIZATION OF LONG-CHAINED PORPHYRIN DERIVATIVES AND THEIR COBALT COMPLEXES
Author	Mr. Wootthiphan Jantayot
Degree	Master Degree
Major Field/Faculty/University	Chemistry Science and Technology Thammasat University
Thesis Advisor	Assistant Professor Supakorn Boonyuen, Ph.D.
Thesis Co-Advisor	Nanthawat Wannarit, Ph.D.
Academic Years	2014

## ABSTRACT

Porphyrins and metalloporphyrins are heterocyclic macrocycle compounds with biochemically importance in nature. Porphyrins applications include molecular electronic devices due to their rich electronic properties. A series of long-chained porphyrin have received much attention. All the porphyrins and complexes have been synthesized and investigated by nuclear magnetic resonance ( $^1\text{H}$  and  $^{13}\text{C}$ -NMR) spectroscopy, mass spectrometry (MS), infrared spectroscopy (IR), elemental analysis (CHN), X-ray diffraction analysis (XRD), thermal gravimetric analysis (TGA), UV-Vis spectroscopy and fluorescence spectroscopy.

This present work focuses on the synthesis and property study of porphyrin with long chain alkane and their cobalt(II) complexes. The porphyrin and their derivatives were synthesized by Adler-Longo method using aldehyde and pyrrole. The long chain aldehydes were synthesized by refluxing 4-hydroxybenzaldehyde with alkyl bromide and  $\text{K}_2\text{CO}_3$  in DMF. Various substituents on *para*-position of phenyl ring in porphyrin are tetrakis(4-methoxyphenyl)porphyrin (TOMPP), tetrakis(4-butyloxyphenyl) porphyrin (TOBPP), tetrakis(4-octyloxyphenyl) porphyrin (TOOPP), tetrakis(4-decyloxyphenyl) porphyrin (TODPP) and tetrakis(4-hydroxyphenyl) porphyrin (THPP). Furthermore, reaction between cobalt acetate

and the described porphyrins were performed the results providing Co-TOMPP, Co-TOBPP, Co-TOOPP and Co-TODPP by refluxing long-chained porphyrins and cobalt acetate in DMF.

**Keywords:** Long-chained porphyrin, Cobalt(II) porphyrins, Spectroscopy



*“Hark, ô Goddess! You do see clearly the results of actions, don’t you? All the others have drowned in the ocean; we alone, are still swimming and have seen you hovering near us. As for us, we are going to endeavour further to the utmost of our ability; we are going to strive like a man should to reach the shores of the ocean.”*

His Majesty King Bhumibol Adulyadej

The Story of Mahajanaka

## ACKNOWLEDGEMENTS

First and foremost, I would like to express my appreciation to my supervisor, Asst. Prof. Dr. Supakorn Boonyuen for his continued support, guidance and encouragement during the course of my research and in the preparation of this thesis. For their generous assistance in this research, I would like to thank Asst. Prof. Dr. Kittipong Chainok, Dr. Nanthawat Wannarit and Dr. Parichatr Vanalabhpatana and the technical staff at Thammasat and Chulalongkorn Universities. My thanks also to Central Scientific Instrument Center (CSIC), Faculty of Science and Technology, Thammasat University, for performing mass and UV studied.

My sincere appreciation to all the member of lab C404, during the past few years, who have entertained me inside and outside of working hours: Jantima Sukjan and all project students. I would be thankful to my parents and my friends for supporting and encouragement. I couldn't have done it without all of you, thank you. Finally, the authors acknowledge the Department of Chemistry, Faculty of science and Technology, Thammasat University.

Wootthiphan Jantayot

## TABLE OF CONTENTS

	Page
ABSTRACT	(1)
ACKNOWLEDGEMENTS	(4)
LIST OF TABLES	(8)
LIST OF FIGURES	(9)
LIST OF ABBREVIATIONS	(12)
CHAPTER 1 INTRODUCTION	1
1.1 Overview of porphyrins and metalloporphyrin	1
1.2 Natural Porphyrins	3
1.2.1 Heme	4
1.2.2 Chlorophyll	5
1.2.3 Vitamin B12	5
1.2.4 Coenzyme F430	6
1.3 The Synthetic porphyrins	6
1.3.1 Synthesis of porphyrins by Rothmund Method	6
1.3.2 Synthesis of porphyrins by Adler-Longo Method	7
1.3.3 Synthesis of porphyrins by Lindsey Method	8
1.3.4 Synthesis of porphyrins by MacDonald [2+2] Condensation	8
1.3.5 Synthesis of porphyrins by MacDonald [3+1] Condensation	9
1.4 Application of porphyrins and metalloporphyrins	9
1.5 Research objectives	10
1.6 Scope and limitations of study	10
1.7 Expected results	11



CHAPTER 2 LITERATURE REVIEW	12
2.1 Synthesis of meso-substituted porphyrins and metal complexes	12
2.2 Synthesis of porphyrins long chain and metal complexes	14
2.3 Characterization of porphyrins long chain and metal complexes	23
2.4 Applications of porphyrins long chain and metal complexes	25
CHAPTER 3 RESEARCH METHODOLOGY	28
3.1 Materials	28
3.1.1 Reagents	28
3.1.2 Apparatus	29
3.1.2.1 NMR spectroscopy	29
3.1.2.2 FT-IR spectroscopy	29
3.1.2.3 Mass spectrometry	29
3.1.2.4 The elemental analysis	30
3.1.2.5 Absorption and fluorescence emission spectroscopy	30
3.1.2.6 Thermal analysis	30
3.1.2.7 Crystallography	30
3.2 Methods	31
3.2.1 Synthesis of aldehydes	31
3.2.2 Synthesis of porphyrin and its derivatives	32
3.2.3 Synthesis of metalloporphyrins	35
CHAPTER 4 RESULTS AND DISCUSSION	37
4.1 Aldehydes synthesis and characterization	37
4.1.1 Mass spectrometry	38
4.1.2 NMR spectroscopy	39
4.1.3 Infrared spectra	43
4.2 Porphyrins and cobalt(II)porphyrins synthesis and characterization	45
4.2.1 Elemental analysis	50

4.2.2 Mass spectrometry	50
4.2.3 NMR spectroscopy	52
4.2.4 Infrared spectroscopy	56
4.2.5 UV-Vis spectroscopy	59
4.2.6 Fluorescence spectroscopy	62
4.2.7 Thermal gravimetric analysis (TGA)	64
4.2.8 X-ray crystal structure of tetrakis(4-butyloxyphenyl)porphyrin	67
CHAPTER 5 CONCLUSIONS AND RECOMMENDATIONS	73
REFERENCES	76
APPENDICES	
APPENDIX A (Mass spectra)	83
APPENDIX B (NMR spectra)	87
APPENDIX C (Infrared spectra)	93
APPENDIX D (UV-Vis spectra)	97
APPENDIX E (Fluorescence spectra)	104
APPENDIX F (Thermogravimetric analysis (TGA) curves)	106
BIOGRAPHY	109

**LIST OF TABLES**

Tables	Page
1 Structures of the <i>meso</i> -alkoxyphenylporphyrins	15
2 The structures of the porphyrins	16
3 Characteristic data for aldehydes <b>1-3</b>	37
4 <sup>1</sup> H and <sup>13</sup> C NMR spectroscopic data for aldehydes <b>1-3</b>	42
5 The IR data of aldehydes <b>1-3</b>	44
6 Characteristic data for porphyrins and cobalt(II) porphyrins	49
7 <sup>1</sup> H-NMR and <sup>13</sup> C-NMR spectroscopic data for free base porphyrins and cobalt porphyrins	53
8 The IR data of free base porphyrins and cobalt(II) porphyrins	58
9 The absorption data of porphyrins and cobalt complexes	61
10 The absorption-emission wavelength and the estimated energy gap of free base porphyrins in dichloromethane	63
11 Temperatures of decomposition of free base porphyrins and cobalt(II) porphyrins	65
12 Crystal data and structure refinement for TOBPP <b>5</b>	69
13 Selected geometric parameters (Å, °) of TOBPP <b>5</b>	70
14 Selected intra/intermolecular interactions in TOBPP <b>5</b> (Å, °)	70

## LIST OF FIGURES

Figures	Page
1 Structure of porphyrin and the IUPAC numbering system	1
2 Delocalised 18 $\pi$ -electron conjugation pathways of the porphyrin ring system	2
3 Types of porphyrins: (a) <i>meso</i> -substituted porphyrin and (b) $\beta$ -substituted porphyrin	2
4 (a) Formation of metalloporphyrin (b) $\sigma$ - and $\pi$ -bond in metalloporphyrin	3
5 Structure of (a) heme, (b) chlorophyll, (c) vitamin B12 and (d) coenzyme F430	4
6 Synthesis of TPP using Rothmund conditions	7
7 Synthesis of TPP using Adler-Longo conditions	7
8 Synthesis of TPP using Lindsey conditions	8
9 Synthesis of TPP using MacDonald [2+2] condensation	8
10 Synthesis of TPP using MacDonald [3+1] condensation	9
11 Synthesis of tetrakis ( <i>p</i> -nitrophenyl)porphyrin <b>1a</b>	12
12 Synthesis of Schiff-base phenylporphyrins <b>2a</b> and their zinc (II) complexes <b>3a</b>	13
13 Synthesis of tetrakis(2-hydroxy-5-nitrophenyl)porphyrin <b>4a</b>	13
14 Synthesis of <i>meso</i> -aryl-substituted porphyrins <b>9-12a</b>	14
15 The structures of the porphyrin <b>13a</b> and silver complex <b>14a</b>	17
16 The structures of the porphyrin <b>15-18a</b> and Zn(II) complex <b>16-18b</b>	18
17 Synthesis of tetrakis-[4-(hexadecyloxy)phenyl]porphyrin <b>19a</b> and Cu(II) complex <b>20a</b>	18
18 Synthesis of porphyrin <b>21-23a</b> and Zn(II) complexes <b>24-26a</b>	19
19 The structure of porphyrins, Ni(II) and Cu(II) complexes	20
20 Synthesis of porphyrins marker	21
21 The structure of palladium porphyrin <b>34a</b>	22
22 The structure of porphyrins and metalloporphyrins <b>35-37a</b>	23
23 UV-Vis absorption spectrum of porphyrin long chain	24
24 Fluorescence spectra of porphyrin long chain	24
25 The structure of <i>meso</i> -tetrakis[4-(pentyloxy)phenyl]porphyrin <b>39a</b>	25

26	Synthesis of the coupling product from palladium catalyst	26
27	Structure of 5,10,15,20-tetrakis-{4-[2-(3-pentadecyl) phenoxy]-ethoxy} phenylporphyrin <b>40a</b>	27
28	Synthesis of alkyloxybenzaldehydes	31
29	Synthesis of porphyrin and their derivatives	32
30	Synthesis of cobalt(II) porphyrins	35
31	Synthesis of Butyloxybenzaldehyde <b>1</b>	37
32	The structure of various alkyloxybenzaldehyde <b>1-3</b>	38
33	Mass spectrum of butyloxybenzaldehyde <b>1</b>	39
34	The <sup>1</sup> H-NMR spectrum of butyloxybenzaldehyde <b>1</b> in CDCl <sub>3</sub>	40
35	The <sup>13</sup> C-NMR spectrum of butyloxybenzaldehyde <b>1</b> in CDCl <sub>3</sub>	41
36	The IR spectrum of butyloxybenzaldehyde <b>1</b> in NaCl	44
37a	The structure of TOMPP <b>4</b> and TOBPP <b>5</b>	45
37b	The structure of TOOPP <b>6</b> , TOOPP <b>7</b> and THPP <b>8</b>	46
38	The structure of Co-TOBPP <b>9</b> , Co-TOBPP <b>10</b> , Co-TOOPP <b>11</b> and Co-TODPP <b>12</b>	47
39	Synthesis of tetra-methoxyphenyl porphyrin (TOMPP <b>4</b> )	48
40	Synthesis of cobalt(II)-methoxyphenyl porphyrin (Co-TOMPP <b>9</b> )	48
41	The mass spectrum of TOBPP <b>5</b>	50
42	The mass spectrum of Co-TOBPP <b>10</b>	51
43	The <sup>1</sup> H-NMR spectrum of TOBPP <b>5</b> in CDCl <sub>3</sub>	52
44	The <sup>13</sup> C-NMR spectrum of TOBPP <b>5</b> in CDCl <sub>3</sub>	55
45	The IR spectra of TOBPP <b>5</b> and Co-TOBPP <b>10</b> in KBr	56
46	UV-Vis absorption spectrum of free base porphyrin (TOBPP <b>5</b> ) in CH <sub>2</sub> Cl <sub>2</sub>	59
47	UV-Vis absorption spectra of all cobalt(II) complexes in CH <sub>2</sub> Cl <sub>2</sub>	60
48	The emission spectra of free base ligands in dichloromethane	62
49	Excitation spectrum and emission spectrum of TOBPP <b>5</b> in CH <sub>2</sub> Cl <sub>2</sub>	63
50	Thermogravimetric analysis (TGA) curves of TOBPP <b>5</b> and Co-TOBPP <b>10</b>	64
51	Correlation between decomposition temperatures with number of carbon in alkyl chain porphyrins	66
52	The molecular structure of TOBPP <b>5</b> , showing 50 % probability displacement ellipsoids and labelling atoms of the asymmetric unit	68

- 53 View of CH $\cdots\pi$  interactions in crystallographic *bc* plane, forming the 2D network of TOBPP **5** 71
- 54 The packing view of the porphyrin (TOBPP **5**) in crystallographic *ac* plane, showing very weak  $\pi\cdots\pi$  interactions between TOBPP molecules. All H atoms and alkyl chains group have been omitted for clarity. 72



## LIST OF ABBREVIATIONS

Symbols/Abbreviations	Terms
1a	Tetrakis(4-nitrophenyl)porphyrin
2a	<i>meso</i> -Tetra(schiff-base phenyl)porphyrins
3a	Zinc(II)(schiff-base phenyl)porphyrins
4a	Tetrakis(2-hydroxy-5-nitrophenyl)porphyrin
5a	4-Tetradecyloxybenzaldehyde
6a	4-Tetradecanoyloxybenzaldehyde
7a	<i>meso</i> -Tetradecyloxyphenyl dipyrromethane
8a	<i>meso</i> -Tetradecanoyloxyphenyl dipyrromethane
9a	5,10,15,20-Tetra(4-tetradecyloxyphenyl)porphyrin
10a	5,10,15,20-Tetra(4-tetradecanoyloxyphenyl)porphyrin
11a	5,15-Bis(4-tetradecyloxyphenyl)-10,20-diphenylporphyrin
12a	5,15-Bis(4-tetradecyloxyphenyl)-10,20-diphenylporphyrin
13a	<i>meso</i> -Tetrakis[4-(pentyloxy)phenyl]porphyrin
14a	<i>meso</i> -Tetrakis[4-(heptyloxy)phenyl]porphyrin
15a	Tetrakis(4-hydroxylphenyl)porphyrin
16a	Tetraheptanolyoxyphenylporphyrin
17a	Tetranonanolyoxyphenylporphyrin
18a	Tetraundecanolyoxyphenylporphyrin
16b	Zinc-heptanolyoxyphenylporphyrin
17b	Zinc-nonanolyoxyphenylporphyrin
18b	Zinc-undecanolyoxyphenylporphyrin
19a	Tetrakis-[4-(hexadecyloxy)phenyl]porphyrin
20a	Copper(II)[4-(hexadecyloxy)phenyl]porphyrin
21a	5,10-bis(4-pyridyl)-15,20-bis(4-octadecyloxyphenyl) porphyrin
22a	5,10-bis(4-pyridyl)-15,20-bis(4-hexyloxyphenyl)porphyrin
23a	5,10-bis(4-pyridyl)-15,20-bis(4-methoxyphenyl)porphyrin

- 24a Zinc-5,10-bis(4-pyridyl)-15,20-bis(4-octadecyloxyphenyl) porphyrin
- 25a Zinc-5,10-bis(4-pyridyl)-15,20-bis(4-hexyloxyphenyl) porphyrin
- 26a Zinc-5,10-bis(4-pyridyl)-15,20-bis(4-methoxyphenyl) porphyrin
- 27a Nickel-2-formyl-5,10,15,20-tetra(4-decyloxyphenyl) porphyrin-fullerene
- 28a Copper-2-formyl-5,10,15,20-tetra(4-decyloxyphenyl) porphyrin-fullerene
- 29a Nickel-2-formyl-5,10,15,20-tetra(4-tetradecyloxyphenyl) porphyrin-fullerene
- 30a Copper-2-formyl-5,10,15,20-tetra(4-tetradecyloxyphenyl) porphyrin-fullerene
- 31a *meso*-Tetrakis(pentafluorophenyl)porphyrin
- 32a *meso*-Tetrakis(2,3,5,6-tetrafluoro-4-(hexadecyloxy)phenyl)porphyrin
- 33a *meso*-Tetrakis(2,3,5,6-tetrafluoro-4-(ethoxy)phenyl) porphyrin
- 34a Palladium porphyrin
- 35a Tetrakis-*p*-octyl-4-phenylporphyrin
- 36a Oxonaphthoporphyrin
- 37a Copper-oxonaphthoporphyrin
- 38a Nickel-oxonaphthoporphyrin
- 39a *meso*-Tetrakis[4-(pentyloxy)phenyl]porphyrin
- 40a 5,10,15,20-Tetrakis-{4-[2-(3-pentadecyl)phenoxy]-ethoxy}phenylporphyrin



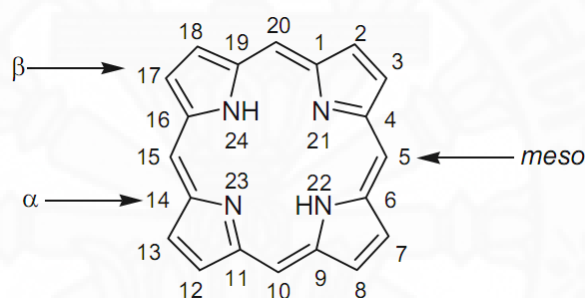
$^1\text{H-NMR}$	Proton Nuclear Magnetic Resonance Spectroscopy
$^{13}\text{C-NMR}$	Carbon Nuclear Magnetic Resonance Spectroscopy
Å	Length
$\delta$	Chemical shift
$J$	Coupling constant
°	Angle
calcd	Calculated
Co-TOBPP	Cobalt-butyloxyphenylporphyrin
Co-TODPP	Cobalt-decyloxyphenylporphyrin
Co-TOMPP	Cobalt-methoxyphenylporphyrin
Co-TOOPP	Cobalt-octyloxyphenylporphyrin
ESI-MS	Electrospray Ionization Mass Spectrometry
IR	Infrared
K	Kelvin
TGA	Thermogravimetric Analysis
TOBPP	Tetrakis(4-butyloxyphenyl)porphyrin
THPP	Tetrakis(4-hydroxyphenyl)porphyrin
TODPP	Tetrakis(4-decyloxyphenyl)porphyrin
TOMPP	Tetrakis(4-methoxyphenyl)porphyrin
TOOPP	Tetrakis(4-octyloxyphenyl)porphyrin
UV-Vis	Ultraviolet-Visible

## CHAPTER 1

### INTRODUCTION

#### 1.1 Overview of porphyrins and metalloporphyrin

The word porphyrin stems from the ancient Greek word *porphura*, which was used to describe the color purple. The basic structure of the porphyrin macrocycles consists of four pyrrole rings (a five-membered ring containing a nitrogen atom) joined by four methylene bridges (=CH-). Fig. 1 shows the basic porphyrin, also referred to porphine, together with the IUPAC numbering of the ring system [1].



$\alpha$ -positions (1, 4, 6, 9, 11, 14, 16, 19)

$\beta$ -positions (2, 3, 7, 8, 12, 13, 17, 18)

*meso*-positions (5, 10, 15, 20)

**Fig. 1** Structure of porphyrin and the IUPAC numbering system [1]

Porphyrins are planar and have an extended  $\pi$ -system, in which only 18  $\pi$ -electron aromatic system out of 22  $\pi$ -electrons contribute to the delocalized (conjugation pathway) which follows Huckel's  $[4n + 2]$  rule for aromaticity shown in Fig. 2 [2]. Due to their delocalized system, the highest occupied molecular orbital (HOMO)-lowest unoccupied molecular orbital (LUMO) gap shrinks and light absorption is seen in the visible region, which explains their intense colors.

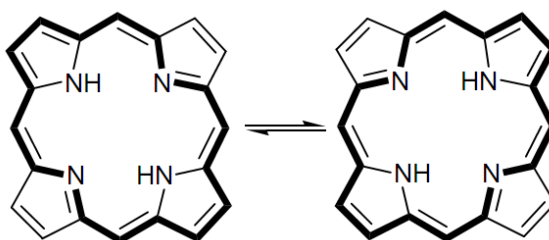


**Fig. 2** Delocalised 18  $\pi$ -electron conjugation pathways of the porphyrin ring system [2]

Porphyrins can be classified into two main categories based on the pattern of substituents attached to the macrocycle namely: *meso*-substituted porphyrins and  $\beta$ -substituted porphyrins, Fig. 3. The  $\beta$ -substituted porphyrins closely resemble naturally occurring porphyrins like heme and chlorophyll [8-10]. The *meso*-substituted porphyrins are not found in nature but have wide applications as biomimetic models and as useful components in material chemistry, photodynamic therapy, molecular recognition, catalysis and electron transfer *etc* [24-27]. Since these can be prepared by simple synthetic methodology, the substituents at the *meso*-positions can be readily adjusted utilizing alkyl, aryl, heterocyclic or organometallic groups as well as other porphyrins.

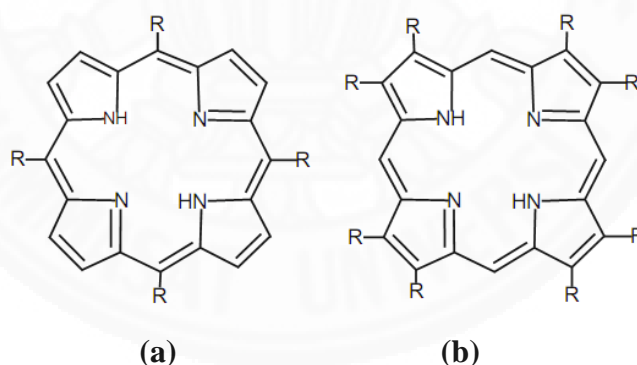


**Fig. 3** Types of porphyrins: (a) *meso*-substituted porphyrin and (b)  $\beta$ -substituted porphyrin

Porphyrins are planar aromatic macrocycles and biochemically important in nature. Porphyrins that occur naturally play a major role in the life sustaining biochemical reactions. The porphyrin ring provides a vacant site at its center hole. The NH protons inside the ring of porphyrins possess acidic character can be deprotonated to give porphyrinato ions. The two inner NH groups lose protons under basic conditions in order to form a dianion species. Such a porphyrin dianion is able

to coordinate may result in the distortion of the planar macrocycle in order to maximize the binding strength towards the metal fragment [3]. The formation of metalloporphyrin is the ability of free base porphyrins to complex almost any known metal ion with the pyrrole nitrogen atoms through the formation of N-metal  $\sigma$ -bonds, as shown in Fig. 4.

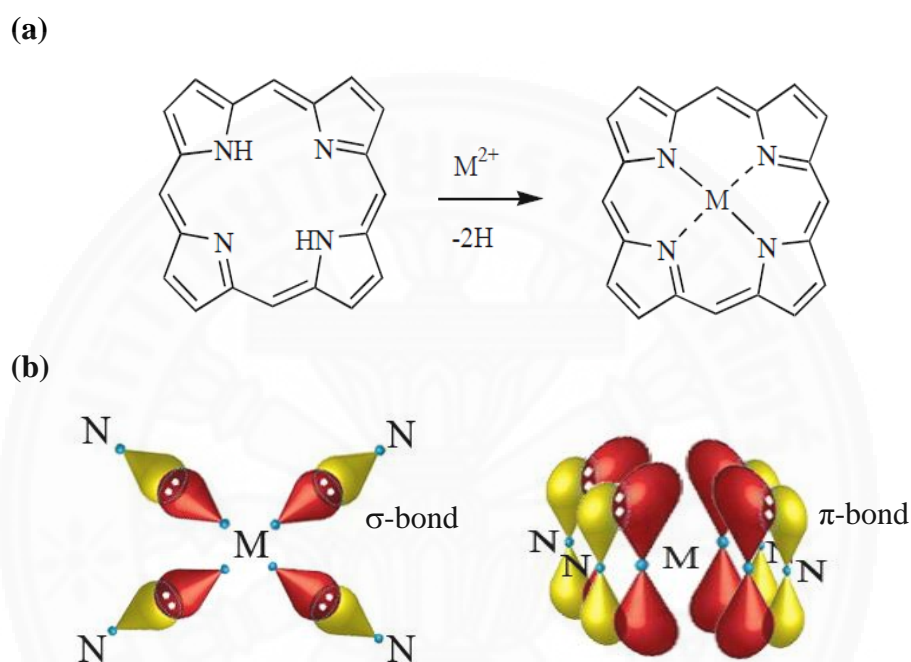


**Fig. 4** (a) Formation of metalloporphyrin (b)  $\sigma$ - and  $\pi$ -bond in metalloporphyrin

The nature of bonding between a central metal and the porphyrin ligand is found to be originating essentially from the following two types of primary interactions:  $\sigma$ -coordination of nitrogen lone pairs directed towards the central metal atoms and  $\pi$ -interaction of metal  $p_\pi$  or  $d_\pi$  orbitals with nitrogen-based  $\pi$  orbitals [4] as shown in Fig. 4.b. Ability to exhibit variable oxidation states of metals in their metalloporphyrins are another important feature in this class of compounds.

## 1.2 Natural Porphyrins

Naturally occurring metalloporphyrins are key components in some of the most important biological processes such as respiration, photosynthesis and solving

transport and other problems in living systems [5-7]. They are ubiquitous class of compounds with many important biological representatives including heme, chlorophyll, vitamin B12, coenzyme F430 and several others (Fig. 5).

### 1.2.1 Heme

The hemoglobin, myoglobin and cytochrome molecules are very large complex proteins, the active site is actually a non-protein group called heme. Hemoglobins are globular proteins that ferry oxygen ( $O_2$ ) molecules and carbon dioxide ( $CO_2$ ) molecules throughout the body. The heme is an asymmetric molecule and consists a porphyrin ring and iron atom in central hole (Fig. 5.a). Heme groups contain positively-charged iron ( $Fe^{2+}$ ) molecules which can reversibly bind to oxygen molecules and transport them to various areas of the body. As the heme groups bind or release their oxygen loads, the overall hemoglobin undergoes conformational changes which alters their affinity for oxygen (Sadava *et al.*, 2008). The ring contains a large number of conjugated double bonds, which allows the molecule to absorb light in the visible part of the spectrum. In spectroscopy, the iron atom modifies the absorption wavelength and gives hemoglobin in red color [8, 9].

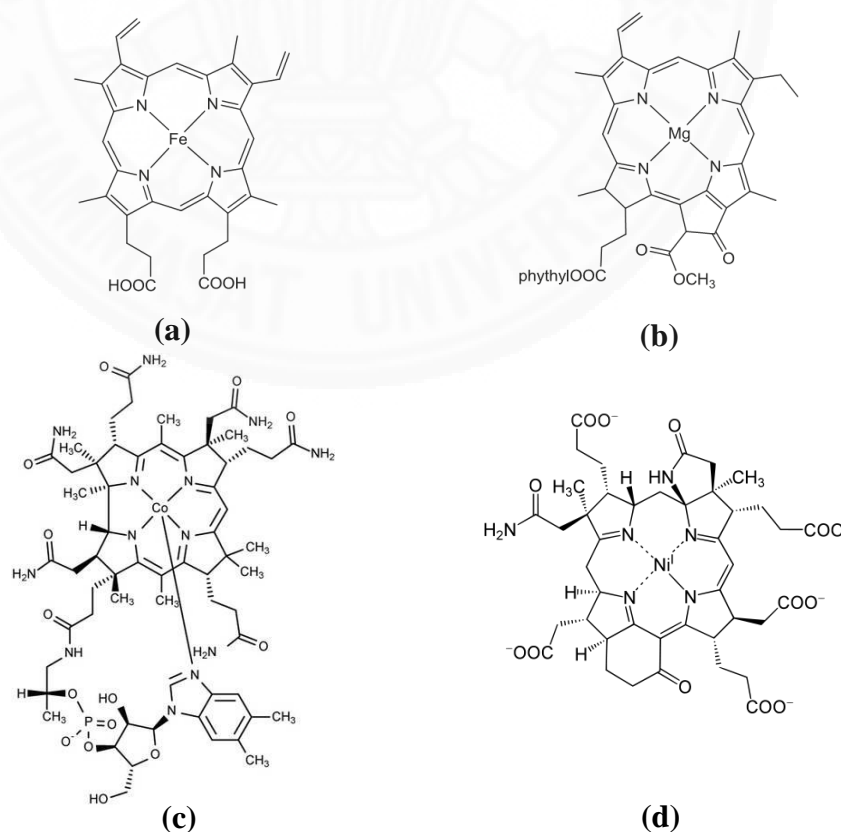


**Fig. 5** Structure of (a) heme [8], (b) chlorophyll [10], (c) vitamin B12 [12] and (d) coenzyme F430 [14]

### 1.2.2 Chlorophyll

Chlorophyll *a* is a large molecule that has a "head" called a porphyrin ring with a magnesium atom at its center. The magnesium-containing porphyrin is a square planar structure. Attached to the porphyrin is a long, insoluble carbon-hydrogen chain which interacts with the proteins of the thylakoids and serves to hold the molecule in the internal membranes of the chloroplast (Fig. 5.b). Chlorophyll *a* is the pigment that participates directly in the light requiring reactions of photosynthesis. Chlorophyll *b* differs from chlorophyll *a* only in one of the functional groups bonded to the porphyrin (a -CHO group in place of a -CH<sub>3</sub> group). It is a necessary pigment and acts indirectly in photosynthesis by transferring the light it absorbs to chlorophyll *a*. Alternating single and double bonds, known as conjugated bonds, such as those in the porphyrin ring of chlorophylls are common among pigments that are responsible for the absorption of visible light by these substances. Both chlorophylls *a* and *b* primarily absorb red and blue light, the most effective colors in photosynthesis. They reflect or transmit green light, which is why leaves appear green [11].

### 1.2.3 Vitamin B12

Vitamin B12, or cobalamin, is the largest and a water-soluble vitamin with a key role in the normal functioning of the brain and nervous system, and for the formation of blood. A slight deficiency of vitamin B12 can lead to anemia, fatigue, mania, and depression, while a long term deficiency causes permanent damage to the brain and central nervous system. Vitamin B12 can only be manufactured by bacteria, plants and can only be found naturally in animal products. However, synthetic forms are widely available and added to many foods like cereals.

The structure of vitamin B12 consists of four pyrroles, joined on methine bridges form three of these links and with the two of the pyrroles joined directly. It is similar to a porphyrin, but with one of the bridging methylene groups removed. The nitrogen of each pyrrole is coordinated to the central cobalt atom (Fig. 5.c). An important aspect of the corrin ring when compared to the porphyrin is the relative flexibility of the corrin system. The corrin ring is also less flat when viewed from the side than is a porphyrin ring. This adds up to some considerable differences between the chemistry of a cobalt porphyrin and a cobalt corrin [13].

### 1.2.4 Coenzyme F430

Coenzyme F430 is the prosthetic group of the enzyme methyl coenzyme reductase. It is found only in methanogenic Archaea. This enzyme catalyzes the release of methane in the final step of methanogenesis. F430 is the most reduced tetrapyrrole in nature with only five double bonds. This particular tetrapyrrole derivative is called a corphin. It is also the only tetrapyrrole derivative found in nature to contain nickel. Ni(II) ion is too small for the four nitrogen atom binding site of the corphin, which causes the macrocycle to adopt a ruffled structure (Fig. 5.d). F430 occurs in particularly high concentrations in bacteria. Organisms that promote this remarkable reaction contain 7% by weight nickel protein [14].

## 1.3 The Synthetic porphyrins

In the past 100 years, porphyrin syntheses have been dramatically developed and modified with in the synthesis of a large class of pyrroles [11]. Most of this early work was accomplished by Fischer and Rothmund [15-17], and were followed by the synthesis of a variety of porphyrins. In general, there are several routes that can be followed to afford porphyrins. Each method has many advantages, which depending on the desired symmetry and later application. Thus, a suitable synthetic approach can be chosen. A general drawback in porphyrin synthesis is obtained low yields in the cyclization reaction, which also explains the demand for improved synthetic strategies. Virtually any porphyrin can be synthesized from known synthetic methodology. For example, tetramerization of pyrroles, [2+2] condensation and [3+1] condensation are common methodologies. The various type of procedure will be explained.

### 1.3.1 Synthesis of porphyrins by Rothmund Method

The first synthetic approaches towards porphyrins started in the 1930s. Rothmund performed the synthesis of *meso*-tetraphenylporphyrin by utilizing the condensation reaction between benzaldehyde and pyrrole in methanol and using pyridine as solvent at high temperature (Fig. 6) for 24 hours. Various aldehydes were utilized to obtain porphyrins by using this methodology [16-17].

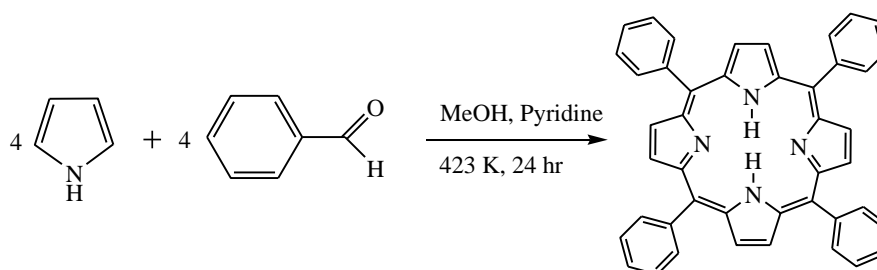


**Fig. 6** Synthesis of TPP using Rothemund conditions

However, these method yields the expected porphyrin only 10%. The product yield is relatively low due to the harshness reaction conditions of the Rothemund reaction and only few benzaldehyde can be used in this reaction. Thus, it is not practical to prepare TPP and the above route becomes rarely used after the development of Adler-Longo conditions.

### 1.3.2 Synthesis of porphyrins by Adler-Longo Method

The Adler-Longo method was developed in 1960, and studied in *meso*-substituted porphyrins synthesis that was achieved by refluxing the mixture of pyrrole and benzaldehyde in propionic acid for 30 minutes under open air conditions at 414 K, as shown in Fig. 7 [18].

Adler and Longo reported many solvent systems with a variety of salts present to enhance the formation of *meso*-substituted porphyrins. At atmospheric pressure, by refluxing pyrrole and benzaldehyde in propionic acid, TPP was obtained in up to 20% yield. The reaction conditions were relatively mild, which afforded higher yield and gave faster reaction rate, when the current condition was compared with Rothemund conditions.

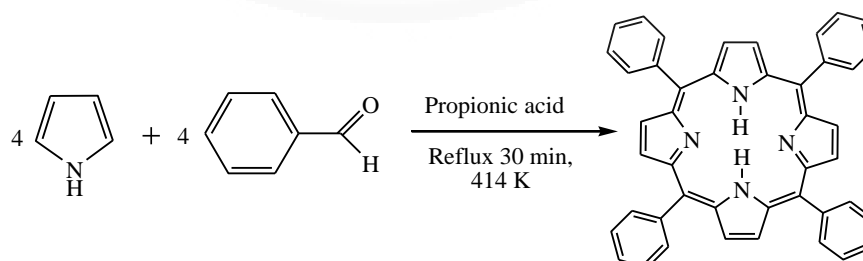


**Fig. 7** Synthesis of TPP using Adler-Longo conditions



### 1.3.3 Synthesis of porphyrins by Lindsey Method

In 1980, Lindsey optimized and developed the synthesis of porphyrins as so called Lindsey conditions (Fig. 8). Under Lindsey conditions, the synthesis of porphyrin is done in two steps through the formation of porphyrinogen from monopyrrole tetramerization and a subsequent separate oxidation. This methodology involved a condensation reaction between benzaldehyde and pyrrole in dichloromethane and added the acid catalyst ( $\text{BF}_3 \cdot \text{Et}_2\text{O}$  or TFA). The yields of porphyrins generated under these conditions were improved to 30-40%. It was found that the use of *p*-chloranil for the oxidation typically gave higher yields than the case of DDQ (oxidation reagent). The efficiency of Lindsey conditions have been proved for both tetra-arylporphyrins and *meso*-tetra-alkylporphyrins, giving good yields [19].

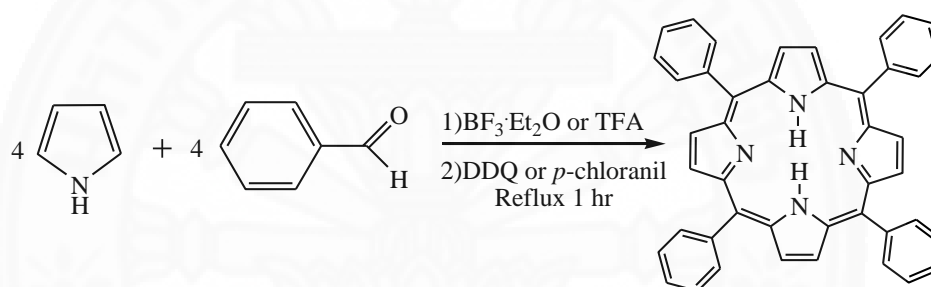


**Fig. 8** Synthesis of TPP using Lindsey conditions

### 1.3.4 Synthesis of porphyrins by MacDonald [2+2] Condensation

In order to synthesize the symmetrical, *meso*-substituted porphyrins (Fig. 9), synthetic pathway based on the MacDonald [2+2] condensation of a dipyrromethane and an aldehyde was designed. The condensation reaction lead to the formation of porphyrinogen reversibly proceeds. The MacDonald [2+2] condensation method achieved by using dipyrromethane and an aldehyde in acid catalyst [20].

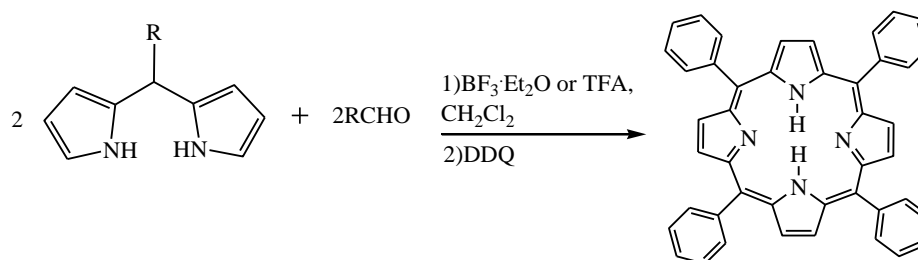


**Fig. 9** Synthesis of TPP using MacDonald [2+2] condensation

### 1.3.5 Synthesis of porphyrins by MacDonald [3+1] Condensation

The Macdonalds approach called [3+1] strategy. Here, the ability to selectively functionalize a porphyrin in one unit is given. Thus, the synthesis of the tripyrrolic building block demanded. The tripyrrane usually carries out carboxylic acid substituents in its  $\alpha$ -positions. Then, it condensed with a monopyrrolic diformylated precursor, as shown in Fig. 10 [21].

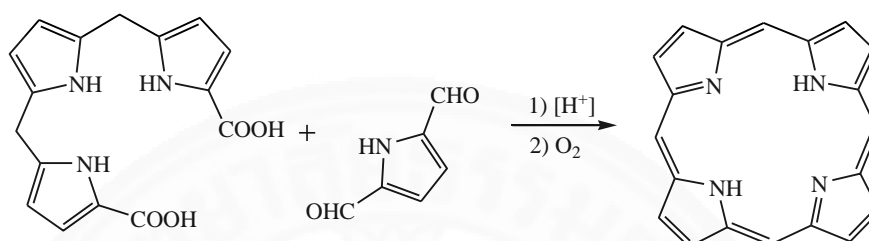


**Fig. 10** Synthesis of TPP using MacDonald [3+1] condensation

### 1.4 Application of porphyrins and metalloporphyrins

Porphyrins and their metal complexes have received much attention. It can be modified in many applications such as catalysis, as materials with novel electrical properties and as biomimetic model systems of primary processes of natural photosynthesis [22-24]. They can be applied for photosensitizing drugs in photodynamic therapy (PDT). Photodynamic therapy is emerging as an important treatment for many diseases. Many applications of PDT involve killing undesirable disease-causing cells such as malignant cancer cells or pathogenic microorganisms [25]. PDT is also used to destroy unwanted tissues such as tumors, new blood vessels, and atherosclerotic plaques [26]. An extra stabilization of the porphyrin occurs by complexation with transition metal ions and which has been explained by the macrocyclic effect [27]. Porphyrins and their derivatives have well-known technological for various applications. The porphyrin can be used as dyes in solar cells to improve the efficiency, due to porphyrin stability [28]. Porphyrins can also be used as biodiesel fluorescent markers [29-30].

## 1.5 Research objectives

1.5.1 To synthesize and characterize various aldehydes with long chain alkane.

1.5.2 To synthesize and characterize the free based porphyrins with long chain alkane ligands from various aldehydes such as 4-hydroxybenzaldehyde, *p*-anisaldehyde, butyloxybenzaldehyde, octyloxybenzaldehyde and decyloxybenzaldehyde by Adler-Longo method.

1.5.3 To synthesize and characterize the metalloporphyrins by adding cobalt ion  $\text{Co}^{2+}$  into the center of free base porphyrin structure.

1.5.4 To study and compare the chemical structure and physical properties of porphyrin long chain, their derivative and metalloporphyrins, which confirmed by using spectroscopy techniques.

## 1.6 Scope and limitations of study

1.6.1 The various aldehyde were prepared by refluxing a mixture of 4-hydroxybenzaldehyde with alkyl bromide such as 1-bromobutane, 1-bromooctane and 1-bromodecane.

1.6.2 The long chain porphyrin and its derivatives with different peripheral substitutions ligands by refluxing pyrrole with various aldehyde such as 4-hydroxybenzaldehyde, *p*-anisaldehyde, butyloxybenzaldehyde, octyloxybenzaldehyde and decyloxybenzaldehyde were synthesized by a modified Adler-Longo method due to its easy procedure with medium yields.

1.6.3 The metalloporphyrin with various porphyrin were prepared by adding metal ion, cobalt acetate ( $\text{Co}^{2+}$ ), in each long chain ligand.

1.6.4 The NMR, IR, mass spectrometry, elemental analysis technique and X-ray diffraction or single crystal X-ray diffraction were applied to confirm the synthesized structure.

1.6.5 The effects of macrocyclic structures with different peripheral substitutions, a group of long chain porphyrins and metalloporphyrins, were characterized by UV-Vis, fluorescence spectrophotometer in different solvent.

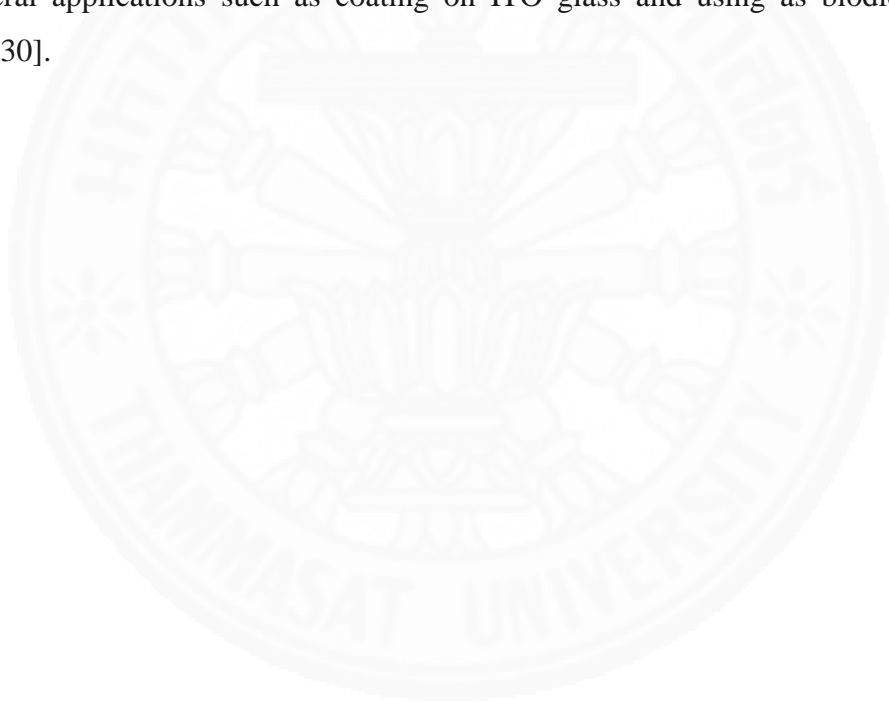
The properties porphyrins were studied by the thermal gravimetric analysis (TGA) and cyclic voltammetry.

### **1.7 Expected results**

1.7.1 The synthesis and characterization of aldehydes, porphyrins and metalloporphyrins were achieved with good yields by a suitable synthesis method.

1.7.2 Porphyrins and metalloporphyrins can be compared by using UV-Vis spectroscopy, fluorescence spectroscopy, TGA and cyclic voltammetric.

1.7.3 Porphyrins long chain and metal complexes were used to apply in several applications such as coating on ITO glass and using as biodiesel markers [29-30].



## CHAPTER 2

### LITERATURE REVIEW

#### 2.1 Synthesis of *meso*-substituted porphyrins and metal complexes

Zhi X. *et al.* (2011) synthesized porphyrins based on condensation (e.g., Rothemund and Lindsey's). Synthesis of tetrakis(4-nitrophenyl)porphyrin **1a** by the reaction of TPP with fuming red HNO<sub>3</sub> at 273 K to chloroform solution of TPP (as shown in Fig. 11). The porphyrin product can be isolated with a great yield of nearly 90% based on an unusual separation technique. Tetrakis (4-nitrophenyl)porphyrin **1a** can be obtained as a major product. The synthesized porphyrins were determined by <sup>1</sup>H NMR, UV-Vis, Fluorescence spectroscopy and mass spectrometry [31].

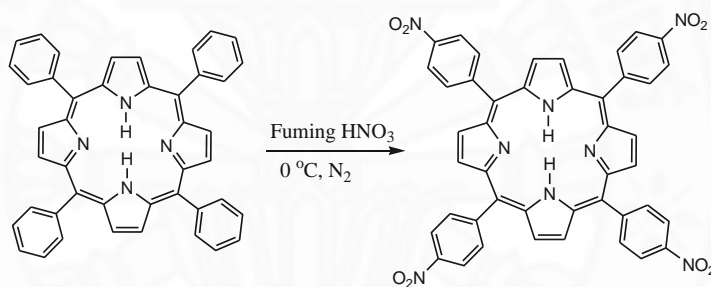


**Fig. 11** Synthesis of tetrakis (4-nitrophenyl)porphyrin **1a**

Temelli B. and Unaleroglu C. (2009) studied the new route synthesis *meso*-tetraphenylporphyrins. Porphyrins and derivatives were prepared by the reaction of dipyrromethanes and *N*-tosyl imines in the presence of a metal triflate catalyst such as Gd(OTf)<sub>3</sub>, Yd(OTf)<sub>3</sub>, Y(OTf)<sub>3</sub>, La(OTf)<sub>3</sub>, Zn(OTf)<sub>2</sub>, Nd(OTf)<sub>3</sub> and Cu(OTf)<sub>2</sub>. The report confirmed that TPP required two steps synthesized reaction. Firstly, the synthesis of porphyrinogen intermediate which has a condensation of diyrromethanes and *N*-tosyl imines. Secondly, the porphyrinogen was oxidized to TPP. This method can be applied to synthesize *trans*-A<sub>2</sub>B<sub>2</sub>-tetraarylporphyrins with other advantages including mild reaction and high yields [32].

Ya-Hong W. *et al.* (2013) synthesized novel *meso*-tetra (schiff-base phenyl) porphyrins **2a**, and their zinc (II) complexes **3a** were also prepared from *meso*-tetra(*p*-aminophenyl)porphyrin with different substituted benzaldehydes

(Fig. 12). These compounds were characterized by UV-Vis, Fluorescence, IR, and EPR determinations. The whole substituted phenyls in the Schiff-base porphyrins should be considered as the secondary substituents. The electron donating effect from all substituted phenyls was stronger than the phenyl groups themselves [33].

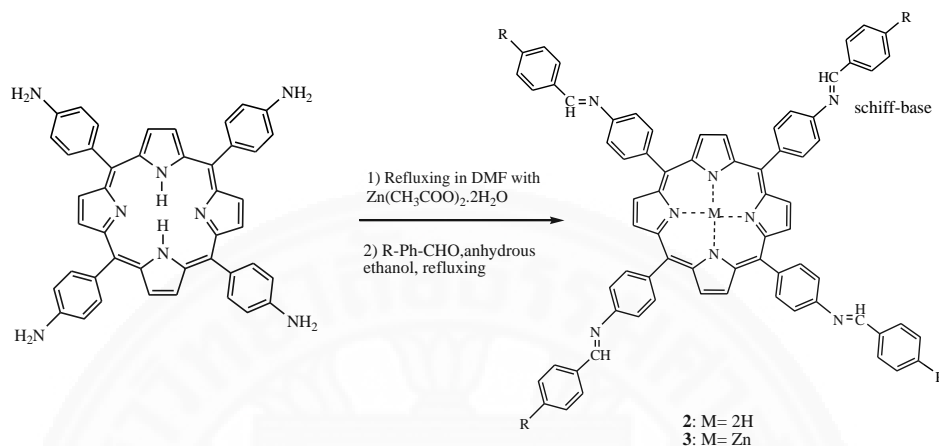


**Fig. 12** Synthesis of Schiff-base phenylporphyrins **2a** and their zinc(II) complexes **3a**

Ana P.J. *et al.* (2004) synthesized hydroxyl nitrophenylporphyrins by Adler's method. The synthesis of tetrakis(2-hydroxy-5-nitrophenyl) porphyrin **4a** are involved the condensation of pyrrole and 2-hydroxy-5-nitrobenzaldehyde in propionic acid, at 414 K. The product yield was 72% and the structure was shown in Fig. 13. These compounds were characterized by  $^1\text{H}$  NMR, UV-Vis absorption and fluorescence spectroscopy. The results obtained demonstrate that these hydroxyl nitrophenyl porphyrins can be considered as promising photosensitizers in PDT [34].

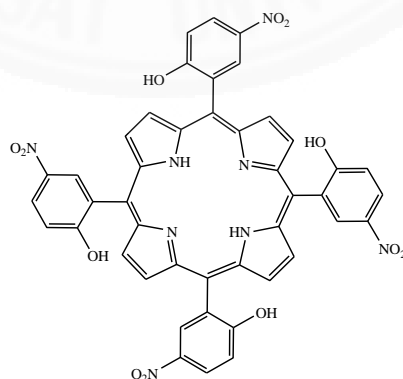


**Fig. 13** Synthesis of tetrakis(2-hydroxy-5-nitrophenyl)porphyrin **4a**

Yuichi T., Brian O.P., and David H.D. (2002) synthesized Zinc(II) complexes of antipodal  $\beta$ -tetrasubstituted *meso*-tetraphenylporphyrin with trifluoromethyl [ $\text{Zn}(\text{TPP}(\text{CF}_3)_4)$ ], bromine [ $\text{Zn}(\text{TPPBr}_4)$ ], and methyl groups [ $\text{Zn}(\text{TPP}(\text{CH}_3)_4)$ ]. Synthesized porphyrins were characterized by UV-Vis, NMR spectroscopy and cyclic voltammetric. The analysis of X-ray crystal structures of the five-coordinate complexes revealed distorted macrocyclic cores where significant differences in the Zn-N distance between the  $\beta$ -substituted and the non- $\beta$ -substituted side were observed [35].

## 2.2 Synthesis of porphyrins long chain and metal complexes

Irina N.F. *et al.* (2007) synthesized symmetrical *meso*-aryl substituted porphyrins with long chain hydrophobic (Fig. 14). The lipoporphyrins can be used to design supramolecular lipid ensembles of nanometer size. The *meso*-aryl substituted dipyrrolylmetanes **7a** and **8a** yield were obtained in 75 and 55% by the condensation of substituted benzaldehydes. The substituted benzaldehydes **5a** and **6a** yield were obtained in 71 and 82% by acylation or alkylation of *p*-hydroxy benzaldehyde with tetradecyl bromide and myristic acid chloride. To prepare porphyrins, the optimal routes were illustrated in figure 15. However, the concentration of both benzaldehyde and pyrrole are gave an optimal yields. The porphyrins long chain were obtained from the substituted benzaldehydes in 33 to 54% yields. Synthesized porphyrins were characterized by IR, MS,  $^1\text{H}$ -NMR spectroscopy, and CHN elemental analysis [36].

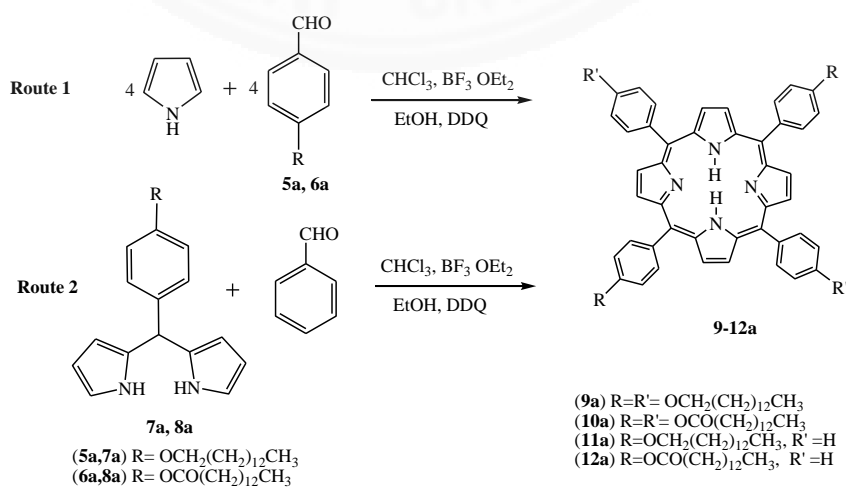
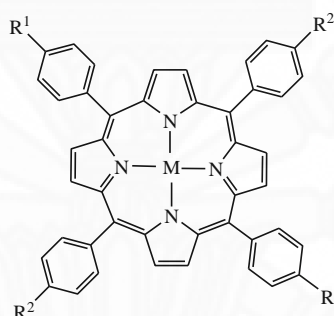


**Fig. 14** Synthesis of *meso*-aryl-substituted porphyrins **9-12a**

The year later, Irina N.F. *et al.* (2008) successfully synthesized *meso*-tetraphenylporphyrins with long chain alkoxy substituents at *para*-positions of 5,15- or 5,10,15,20-phenyl groups (as shown in Table 1). The major method for synthesis of porphyrins with long chain involved the reaction of hydroxybenzaldehyde with alkyl bromides and condensation of pyrrole with various aldehydes. Porphyrins of two structure types were synthesized by monopyrrole condensation (Route 1) and using dipyrrolemethane (Route 2) in 36 to 44% yields. Zinc and cobalt complexes were obtained in 90 to 95% yields by refluxing porphyrin ligand with metal acetate. The synthesized porphyrins were determined by UV-Vis spectroscopy,  $^1\text{H}$  NMR spectroscopy and CHN elemental analysis [37].

**Table 1** Structures of the *meso*-alkoxyphenylporphyrins



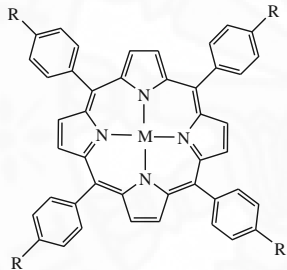
Compound	R <sup>1</sup>	R <sup>2</sup>	M
1	O(CH <sub>2</sub> ) <sub>7</sub> Me	H	2H
2	O(CH <sub>2</sub> ) <sub>13</sub> Me	H	2H
3	O(CH <sub>2</sub> ) <sub>15</sub> Me	H	2H
4	O(CH <sub>2</sub> ) <sub>7</sub> Me	H	Zn
5	O(CH <sub>2</sub> ) <sub>7</sub> Me	H	Co
6	O(CH <sub>2</sub> ) <sub>7</sub> Me	O(CH <sub>2</sub> ) <sub>7</sub> Me	2H
7	O(CH <sub>2</sub> ) <sub>13</sub> Me	O(CH <sub>2</sub> ) <sub>13</sub> Me	2H
8	O(CH <sub>2</sub> ) <sub>15</sub> Me	O(CH <sub>2</sub> ) <sub>15</sub> Me	2H
9	O(CH <sub>2</sub> ) <sub>7</sub> Me	O(CH <sub>2</sub> ) <sub>7</sub> Me	Zn
10	O(CH <sub>2</sub> ) <sub>7</sub> Me	O(CH <sub>2</sub> ) <sub>7</sub> Me	Co
11	O(CH <sub>2</sub> ) <sub>13</sub> Me	O(CH <sub>2</sub> ) <sub>13</sub> Me	Zn

Ref: Irina N. F. *et al.* (2008). *Mendeleev Commun.*, 18, 324–326.



In 2011, Kirill A.F. *et al.* synthesized the novel amphiphilic alkoxyaryl porphyrins bearing long chain substituents terminated with carboxy and carboxymethyl groups. Their metal complexes [Zn(II) and Cu(II)] were shown in Table 2. The 5,10,15,20-tetra substituted porphyrins were obtained by using a method of monopyrrole condensation in which the maximum yields of porphyrins were achieved at the concentrations of benzaldehyde and pyrrole equal to  $10^{-2}$  M. The synthesized symmetrical *meso*-tetrakis [4-(methoxycarbonylalkoxyphenyl porphyrins)] yield and metal complexes yield were obtained in 35 to 40%, and 75 to 90%, respectively. The structure of these compounds was confirmed by TLC, UV-Vis,  $^1\text{H-NMR}$  and mass spectrometry. Their mesomorphic properties have been studied by optical polarizing microscopy [38].

**Table 2** The structures of the porphyrins

Structural formula	Compound	M	R
	1	$2\text{H}^+$	$-\text{O}(\text{CH}_2)_{10}\text{COOH}$
	2	$2\text{H}^+$	$-\text{O}(\text{CH}_2)_5\text{COOMe}$
	3	$2\text{H}^+$	$-\text{O}(\text{CH}_2)_{10}\text{COOMe}$
	4	Zn	$-\text{O}(\text{CH}_2)_{10}\text{COOMe}$
	5	Cu	$-\text{O}(\text{CH}_2)_{10}\text{COOMe}$

Ref: Kirill A. F. *et al.* (2011). *Macroheterocycles*, 4(2), 127-129.

Hua C. *et al.* (2009) prepared *meso*-tetrakis[4-(pentyloxy)phenyl] porphyrin **13a** by the reaction of 4-pentyloxybenzaldehyde with pyrrole refluxing in propionic acid for 1 hour at 383 K. The product gave a 12% yield. The crystal structure of the compound has been determined by single crystal X-ray diffraction methods [39].

Hong B.Z. *et al.* (2013) reported the novel of *meso*-tetrakis[4-(heptyloxy)phenyl]porphyrin **14a**. The mixture was refluxed 4-(heptyloxy)benzaldehyde and pyrrole in propionic for 1 hour at 298 K. The product was obtained in 12% yield (m.p.527-528 K) as shown Fig. 15.1. Single crystals of *meso*-tetrakis [4-(heptyloxy)phenyl] porphyrin suitable for X-ray diffraction were obtained by vapour diffusion of hexane into a dichloromethane solution at room temperature [40].

Jun X.L. *et al.* (2011) reported the crystal data of {*meso*-tetrakis [*p*-(heptyloxy)phenyl]porphyrinato}silver(II) (Fig. 16.2), where the Ag(II) cation are located on a center of symmetry. The compound was synthesized from the condensation of *meso*-tetrakis[*p*-(heptyloxy)phenyl]porphyrin and AgNO<sub>3</sub> in chloroform, refluxed for 6 hours. The product obtained in 23% yield as purple solid. The structure of this compound was characterized by X-ray diffraction. Single crystals were obtained from recrystallization with a dichloromethane solution at room temperature [41].

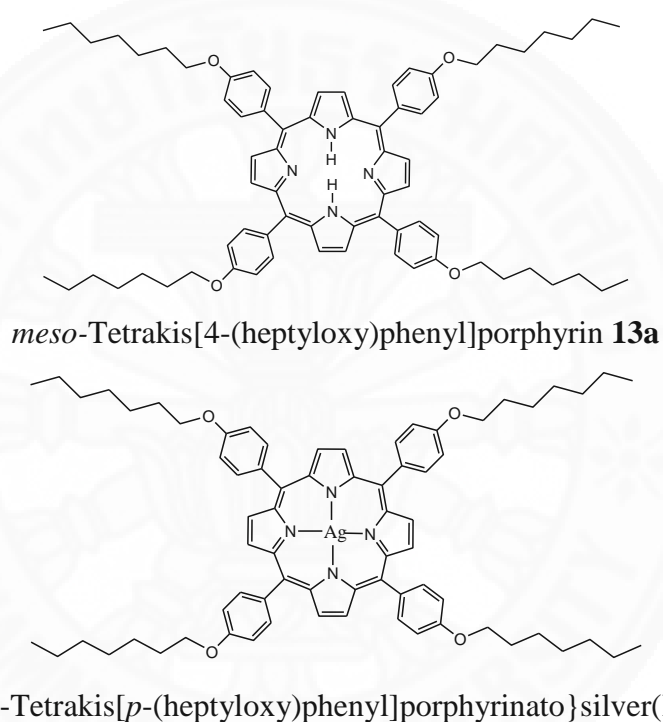


**Fig. 15** The structures of the porphyrin **13a** and silver complex **14a**

Wei L. *et al.* (2013) reported the synthesis liquid crystalline tetraalkanoyloxy phenylporphyrins, free base on tetrakis(4-hydroxyphenyl)porphyrin and Zn complexes. Tetrakis(4-hydroxyphenyl)porphyrin **15a** was synthesized by reacting 4-hydroxybenzaldehyde with pyrrole in propionic acid. Then compound **15a** was further esterified with the appropriate acyl chloride in benzene and triethylamine. The products yield ranged from 86 to 88% (Fig. 16). The free base porphyrin and zinc acetate were heated under reflux in chloroform and *N,N*-dimethylformamide to give the metal porphyrin complex. Zn complexes yield ranged from 82 to 84%. The compounds were investigated their liquid crystalline behaviour and structure [42].

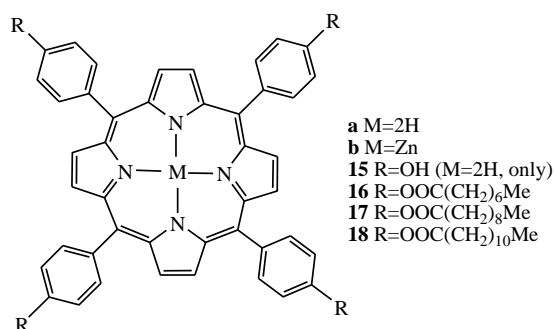


**Fig. 16** The structures of the porphyrin **15-18a** and Zn(II) complex **16-18b**

Amrita G. *et al.* (2007) synthesized tetrakis-[4-(hexadecyloxy)phenyl] porphyrin **19a** and its copper(II) complex **20a**. Alkyl long chain ychloride was prepared from the condensation of alkyl alcohol and thionyl chloride in chloroform, refluxed for 4 hours (72% yield). Long chain aldehyde derivative was synthesized by reacting alkyl chloride with the *p*-hydroxy benzaldehyde in presence of K<sub>2</sub>CO<sub>3</sub> as base. The product was obtained in 74% yield. This aldehyde derivative was allowed to react with equimolar amount of freshly distilled pyrroles for the synthesis of the desired porphyrin **19a**. This was further used for reaction with Cu(II) acetate for synthesis of Cu(II) porphyrin complex, as shown in Fig. 17. The compounds were studied in mix-solvent system at room temperature. Structure of the compound was characterized by scanning electron microscopy (SEM), transmission electron microscopy (TEM), powder X-ray diffraction (XRD), and UV-Vis spectroscopy [43].

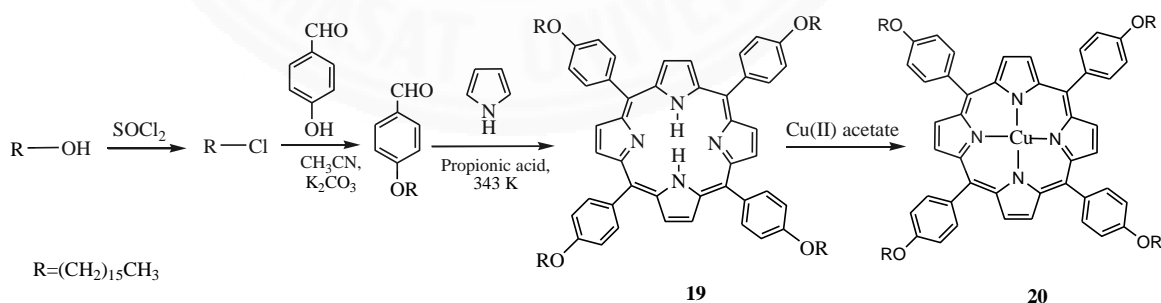


**Fig. 17** Synthesis of tetrakis-[4-(hexadecyloxy)phenyl]porphyrin **19a** and Cu(II) complex **20a**

Renu G. and Chauhan S.M.S. (2014) synthesized *cis* A<sub>2</sub>B<sub>2</sub> porphyrins. It can be carried out by the reaction of tripyrrane with pyrrole dicarbinol. The statistical condensation of corresponding *p*-(alkoxy) benzaldehyde, 4-pyridine carboxaldehyde

and pyrrole in refluxing propionic acid gave the corresponding porphyrins. The products contain different side chain lengths **21-23a** with minor modification in literature method. The required *cis* porphyrins were separated by extensive column chromatography. The zinc derivatives were obtained by refluxing the zinc acetate together with the corresponding porphyrin in DMF (Fig. 18), with subsequent precipitation on cold water and vacuum. Structure of the compound was characterized by NMR and UV-Vis spectroscopy [44].

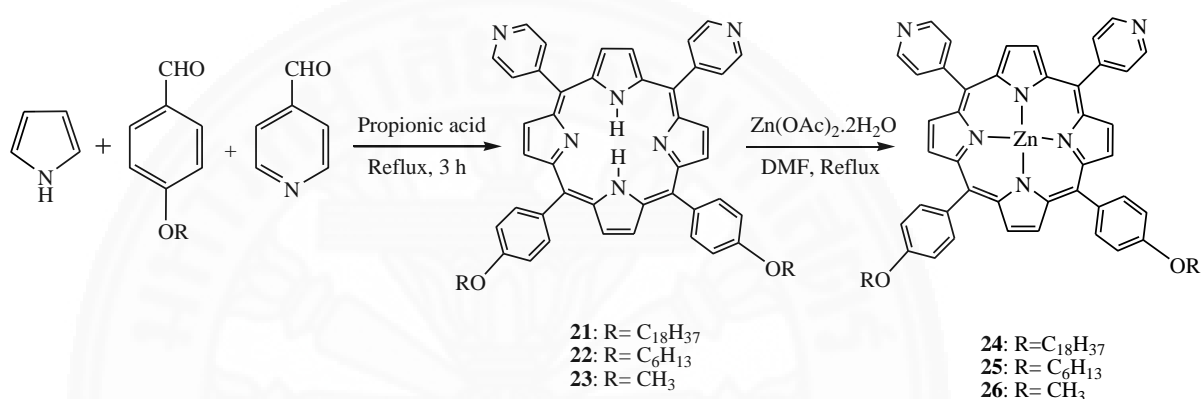


**Fig. 18** Synthesis of porphyrin **21-23a** and Zn(II) complexes **24-26a**

Ekaterina S.Z. *et al.* (2012) studied synthesis of covalent-bound porphyrin-fullerene conjugates based on fullerene C<sub>60</sub> and *meso*-aryl-substituted porphyrins with long chain substituents were used the Prato reaction. The starting *meso*-aryl-substituted porphyrins were obtained in 40% yield by monopyrrole condensation from pyrrole and the corresponding 4-alkoxybenzaldehydes. The copper complexes of porphyrins were obtained in 95% yield. In the case of nickel complexes, the reaction gave lower yield (70%). These metal complexes were performed in CH<sub>2</sub>Cl<sub>2</sub> by heating for 5 to 6 hours. The yields of formylporphyrins were 55 to 60%. The addition of fullerene C<sub>60</sub> to formylporphyrins was carried out by refluxing with *N*-methylglycine in anhydrous toluene for 20 hours under argon. Unlike the original porphyrin, the resulting conjugates were brown as shown in Fig. 19. The products were confirmed by IR, UV-Vis, nuclear magnetic resonance (<sup>1</sup>H and <sup>13</sup>C NMR), and mass spectrometry [45].

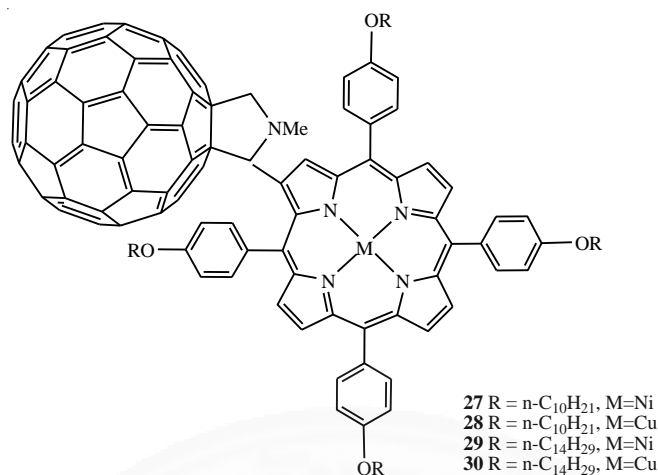


**Fig. 19** The structure of porphyrins, Ni(II) and Cu(II) complexes

Siriorn P. and Patchanita T. *et al.* (2009) synthesized the novel porphyrins fluorescent marker to obtain a long chain aldehyde precursor derived from cardanol and the target porphyrin. The synthesis started with formylation of hydrogenated cardanol by using a reaction with paraformaldehyde in the presence of SnCl<sub>4</sub> and NEt<sub>3</sub>, leading to aldehyde. Then, methylation of phenol was performed, leading to aldehyde in 78% yield. Aldehyde, pyrrole, BF<sub>3</sub>OEt<sub>2</sub> and NaCl was reacted in CHCl<sub>3</sub> at room temperature for 10 min. DDQ was added and the mixture was stirred at room temperature for an additional hour. The *meso*-tetrakis(2-methoxy-4-pentadecylphenyl) porphyrin was obtained in 35% yield [29].

In 2011, Ana C.B.F. *et al.* reported the synthesis and characterization of new porphyrins tailored to become biodiesel fluorescent markers. The compounds were obtained by the synthetic modification of the commercially available porphyrin *meso*-tetrakis(pentafluorophenyl)porphyrin (TPPF<sub>20</sub>) **31a** using ethanol and hexadecan-1-ol (cetylic alcohol) as nucleophilic reagents. The products yield ranged from 95 to 98% (Fig. 20). The synthesized porphyrins were characterized by nuclear magnetic resonance (<sup>1</sup>H and <sup>19</sup>F-NMR), mass spectrometry (MS), UV-Vis absorption spectroscopy and photoluminescence spectroscopy [30].

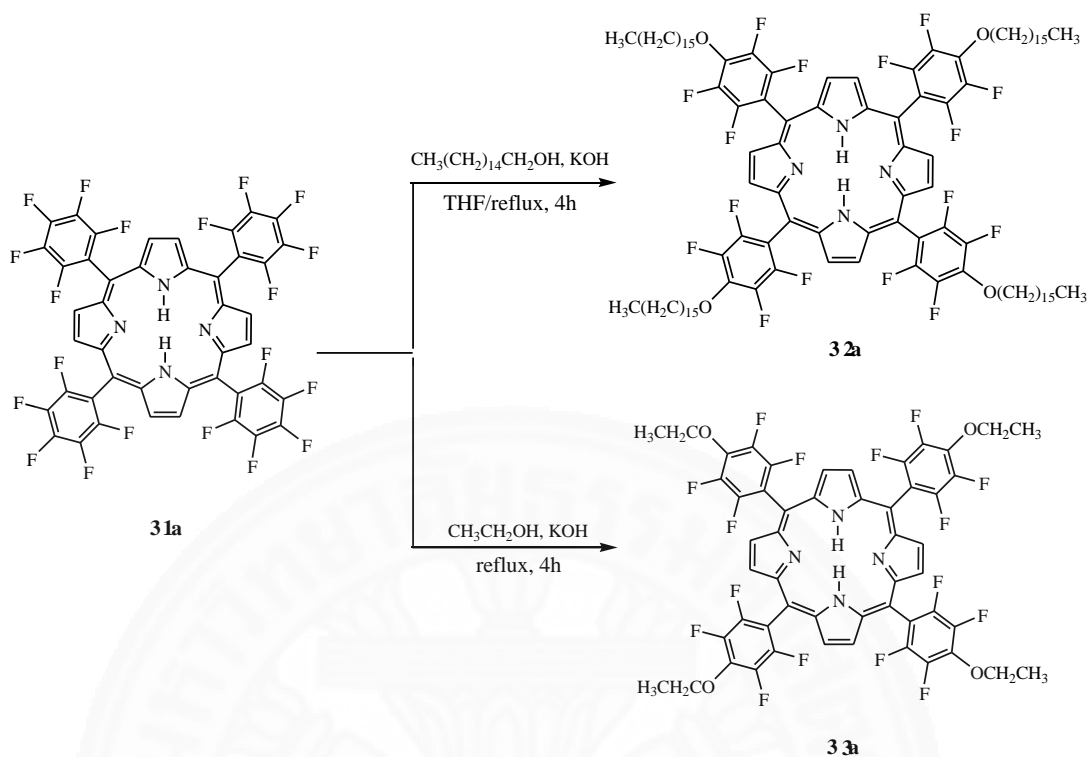


**Fig. 20** Synthesis of porphyrins marker

Ioannis D.K. *et al.* (2007) synthesized the water-soluble palladium porphyrin is outlined in Fig. 21. Functionalized aldehyde was obtained in 95% yield by the alkylation of 4-hydroxybenzaldehyde with ethyl 4-bromobutyrate in the presence of  $\text{K}_2\text{CO}_3$ , in DMF at 353 K. Porphyrin long chain was prepared following the classical method of Adler and Longo. Metalloporphyrin was carried out by the addition of palladium chloride to the free base porphyrin in refluxing benzonitrile. The reaction leads to metal complex in 90% yield. Palladium porphyrin 34a was further dissolved in THF, methanol and KOH to prepare water soluble potassium carboxylate salt with 97% yield. Palladium complex with a porphyrin ligand (Fig. 21) is used as a catalyst precursor for cross-coupling reactions [46].

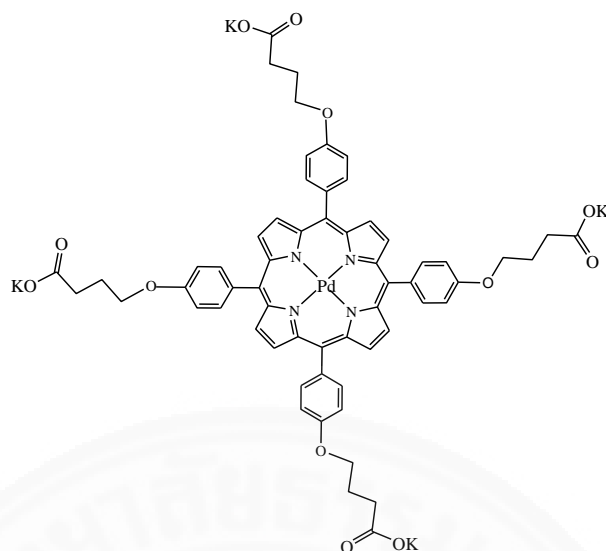


**Fig. 21** The structure of palladium porphyrin **34a**

Nikita V.N. *et al.* (2010) synthesized porphyrins with monopyrrole condensation according to Lindsey followed by using modification of substituents at the aromatic rings. *meso*-Tetrakis[4-(6-bromohexanoyloxyphenyl)] porphyrins and *meso*-tetrakis[4-(11-bromoundecanoyloxyphenyl)]porphyrins obtained from pyrrole and the respective substituted 4-hydroxybenzaldehydes in 35 to 40% yields. Synthesis of lipophilic porphyrins were used as the precursors of metalloporphyrins. Zinc, cobalt, nickel and copper metal complexes were obtained by standard techniques (93 to 95% yields) [47].

In 2011, Beat H. and Reinhard N. synthesized **35a** and **36a** to the *p*-alkyl substituted oxonaphthoporphyrins with two different methods. The compounds **35a** and **36a** were further used for synthesis of metalloporphyrins with Cu(II) and Ni(II) ions, as shown in Fig. 22. [48]

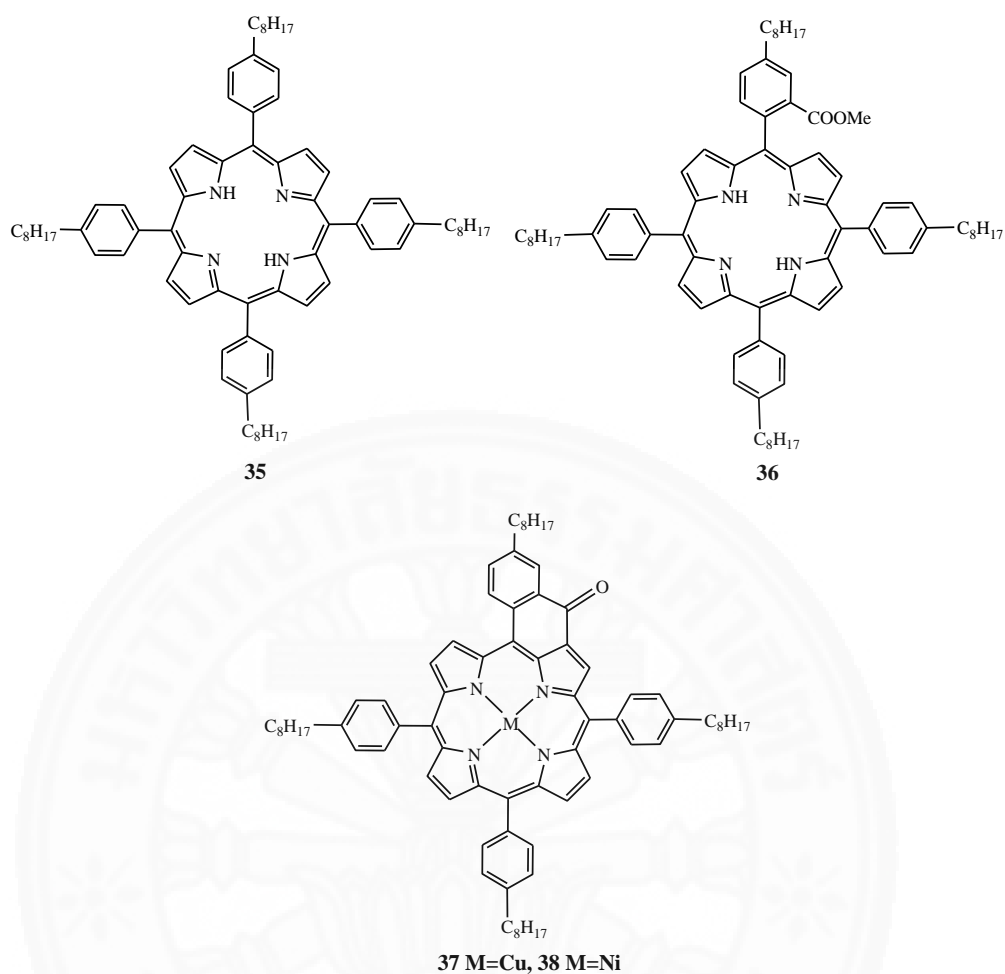


**Fig. 22** The structure of porphyrins and metalloporphyrins

### 2.3 Characterization of porphyrins long chain and metal complexes

Ana V.C.S. *et al.* (2012) reported the synthesis of amphiphilic fluorinated porphyrins appended with sulfonate ester groups. The Soret band was found with an intense band at 410 nm with four broad less intense bands between 500 and 650 nm. The longest-wavelength absorption bands at 641 to 649 nm are used for PDT process, because only red light has sufficient tissue penetration ability [49].

Cecília B.F. *et al.* (2011) studied porphyrins with long chain were largely soluble in nonpolar environments such as  $\text{CH}_2\text{Cl}_2$ , n-hexane, and biodiesel. They are very soluble in ethanol. The porphyrins display the characteristic Soret band (414 nm) with experimental molar extinction coefficients ( $\epsilon$ ) of  $2.67 \times 10^5 \text{ L mol}^{-1} \text{ cm}^{-1}$  and four Q bands (507, 538, 585 and 657 nm) in biodiesel solutions. Figure 23 shows the



typical electronic absorption spectra of long chain porphyrins. The spectrum consists of a strong transition to the second excited state at about 414 nm (Soret band) and four weak transitions to the first excited state from 500-660 nm (Q bands). However, in order to better visualize the four Q bands, solution of porphyrin was prepared at a higher concentration than the initial one. The insets of Fig. 23 show the Q bands for porphyrins with long chain [30].

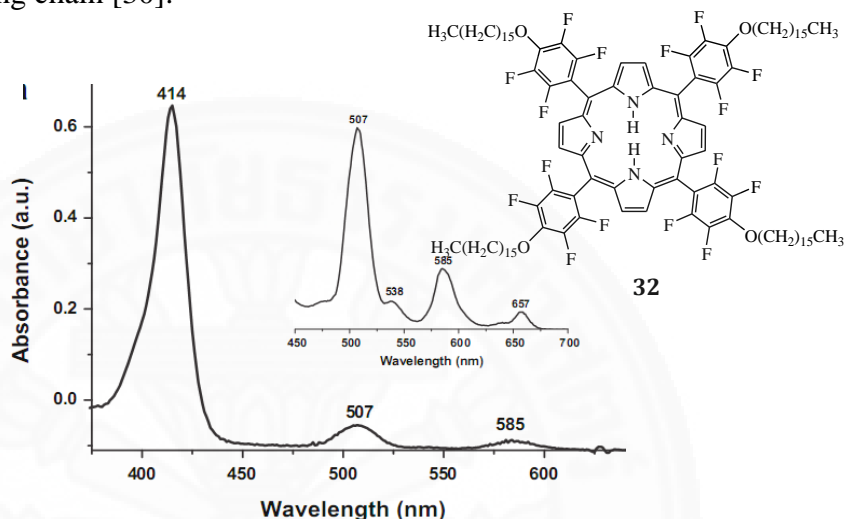


**Fig. 23** UV-Vis absorption spectrum of porphyrin long chain

Irina N.F. *et al.* (2007) carried out preliminary experiments on the porphyrin solubilization in micelles at the porphyrin-detergent ratios of 1: 400 (1), 1: 200(2), and 1: 100 (3), using  $\lambda_{\text{ex}}$  513 nm at 293 K. An analysis of fluorescence spectra at various concentrations within the LPPC micelles showed that increase in the porphyrin content in micelle lead to self-quenching of fluorescence (Fig. 24). They observed the fluorescence decrease, while increasing in porphyrin concentration. [36].

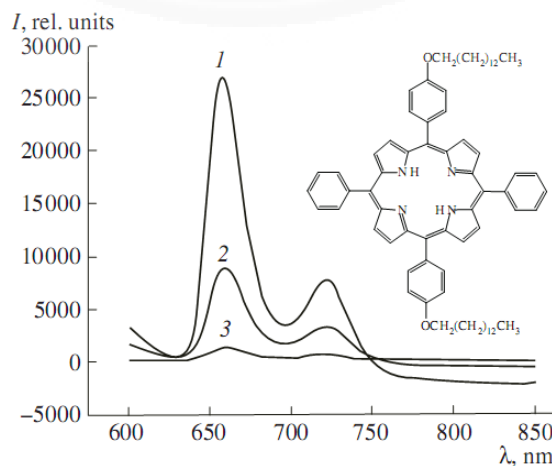


**Fig. 24** Fluorescence spectra of porphyrin long chain

A single crystal of *meso*-tetrakis [4-(pentyloxy)phenyl]porphyrin **39a** with dimensions 0.54x0.50 x0.45 mm was selected and fixed with epoxy cement on a fine glass fibre which was mounted on a Bruker Porphyrin SMART APEX diffraction with graphite-monochromated Mo K $\alpha$  ( $k = 0.71073 \text{ \AA}^{-1}$ ) for cell determination and data collection. The crystal structure is shown in Fig. 25.[39]

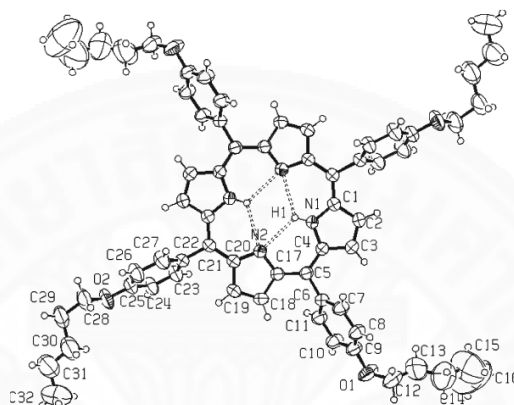


**Fig. 25** The structure of *meso*-tetrakis [4-(pentyloxy)phenyl]porphyrin **39a**

In 2010, Pan M. *et al.* studied electrochemical properties of free base porphyrin of 5,10,15,20-tetrakis(4-pentyloxyphenyl)porphyrin. Electrochemical measurements were carried out with a BAS CV-50W voltammetric analyser. The cell comprised inlets for a glassy carbon disk working electrode of 3.0 mm inner diameter and a silver-wire counter electrode. All potentials were recorded against an Ag/Ag<sup>+</sup> (0.01 mol dm<sup>-3</sup>) reference electrode. The scan rate was 20 and 10 mV s<sup>-1</sup> for CV and DPV, respectively. The electrochemical behavior of H<sub>2</sub>TPOPP was investigated by cyclic voltammetry (CV) and differential pulse voltammetry (DPV) in CH<sub>2</sub>Cl<sub>2</sub> [50].

#### 2.4 Applications of porphyrins long chain and metal complexes

Patchanita T. *et al.* (2009) and Ana C.B.F. *et al.* (2011) have interested porphyrins tailored to become fluorescent markers. The resulting *meso*-tetrakis (2-methoxy-4-pentadecylphenyl)porphyrin exhibits high solubility in diesel fuel and its strong fluorescence was observed. The porphyrin marker was stable in diesel for at least 3 months. The physical properties of the diesel were unaffected by the presence

of the porphyrin marker at a concentration of 2 ppm [29]. While, *meso*-tetrakis(pentafluorophenyl)porphyrin (TPPF<sub>20</sub>) using ethanol and hexadecan-1-ol were studies on a spectrofluorometric detection method for the markers and investigation of the stability of the marked biodiesel fuel. In addition, the marked and unmarked biodiesel fuel physical properties were tested, in order to evaluate the applicability of the synthesized porphyrins as biodiesel markers. The fluorescent markers did not affect the biodiesel physical properties and were stable in storage conditions (at least 3 months and concentration of 4 ppm of the porphyrin marker) [30].

In 2007, Ioannis D.K. *et al.* studied the water-soluble palladium porphyrin. Palladium complex with a porphyrin ligand is used as a catalyst precursor in the Suzuki-Miyaura reaction of phenylboronic acid with representative aryl bromides (electron-rich and electron-poor) at 337 K for 4 hours, using K<sub>2</sub>CO<sub>3</sub> as base, leading to yields of coupling products in the range of 80-100%. This synthesis procedure was shown in Fig. 26. The catalyst can be recycled and reused, but unfortunately, with a less activity [46].

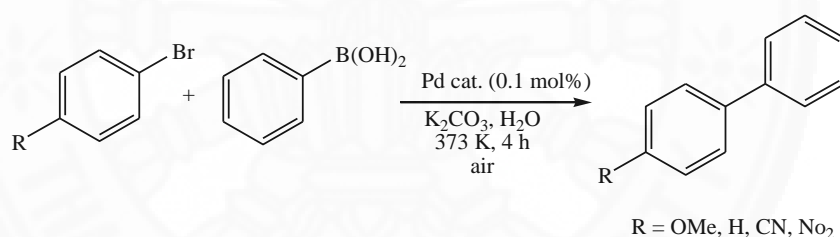


**Fig. 26** Synthesis of the coupling product from palladium catalyst

Bianca S. *et al.* (2013) prepared a nanostructured films with an amphiphilic *meso*-porphyrin whose side chains are derived from cardanol as a byproduct of the cashew industry. The structure is shown in Figure 27. The applicability of the nanostructured ultrathin films as electrochemical sensor for promethazine was demonstrated, with the linear range of that molecule going from 2.00-36.25 μM, a value greater than those obtained by other nanostructured systems [51].

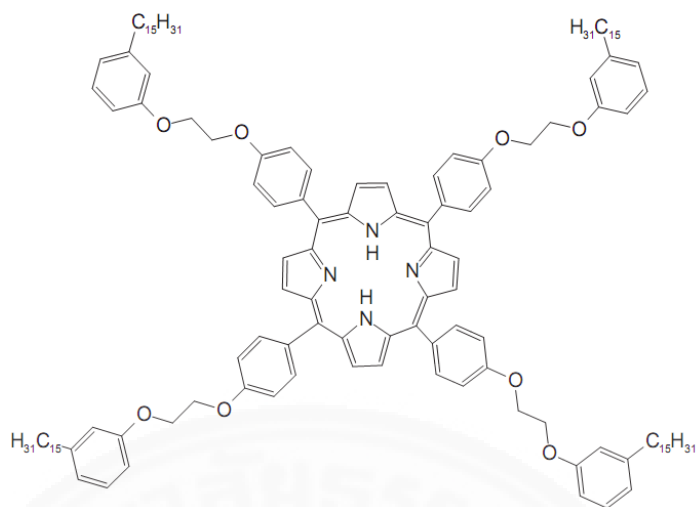


**Fig. 27** Structure of 5,10,15,20-tetrakis-{4-[2-(3-pentadecyl) phenoxy]-ethoxy} phenylporphyrin **40a**

## CHAPTER 3

### RESEARCH METHODOLOGY

#### 3.1 Materials

##### 3.1.1 Reagents

- 1-Bromobutane ( $C_4H_9Br$ , Assay 99%, Sigma-aldrich, USA)
- 1-Bromooctane ( $C_8H_{17}Br$ , Assay 99%, Sigma-aldrich, USA)
- 1-Bromodecane ( $C_{10}H_{21}Br$ , Assay 98%, Sigma-aldrich, USA)
- 4-Hydroxybenzaldehyde ( $C_7H_6O_2$ , Assay 99%, Sigma-aldrich, USA)
- Acetone ( $C_3H_6O$ , Assay 98%, RCI Labscan, Thailand)
- Anisaldehyde ( $C_8H_8O_2$ , Assay 99%, Sigma-aldrich, USA)
- Chloroform ( $CHCl_3$ , Assay 98%, RCI Labscan, Thailand)
- Chloroform-*d* ( $CDCl_3$ -*d*, HPLC grade, Cambridge Isotope, USA)
- Cobalt acetate ( $C_4H_6CoO_4$ , synthesized by Prohmsatit T.)
- Dichloromethane ( $CH_2Cl_2$ , Assay 98%, RCI Labscan, Thailand)
- Dichloromethane ( $CH_2Cl_2$ , HPLC grade, Merck, Germany)
- Dimethyl sulfoxide- $d_6$ , DMSO- $d_6$  ( $C_2D_6OS$ , Assay 99.9%, Sigma-aldrich, USA)
- Distilled water ( $H_2O$ )
- Ethanol ( $C_2H_5OH$ , Assay 98%, RCI Labscan, Thailand)
- Ethyl acetate ( $C_4H_8O_2$ , Assay 98%, RCI Labscan, Thailand)
- Hexane ( $C_6H_{14}$ , Assay 98%, RCI Labscan, Thailand)
- Magnesium sulphate anhydrous ( $MgSO_4$ , QP Panreac Quimica Sa, Barcelona)
- Methanol ( $CH_3OH$ , Assay 98%, RCI Labscan, Thailand)
- Methanol ( $CH_3OH$ , HPLC grade, Merck, Germany)
- *N,N*-Dimethylformamide ( $C_3H_7NO$ , Analytical grade, MAY& BAKER, England)

- Potassium carbonate anhydrous ( $K_2CO_3$ , Assay 99%, Unilab, Australia)
- Propionic acid ( $C_3H_6O_2$ , Assay 95%, Poison, Australia)
- Pyrrole ( $C_4H_5N$ , A.R. grade, Aldrich, Steinheim, Germany)
- Thin layer chromatography (Macherey-nagel, Germany)
- Toluene ( $C_7H_8$ , Assay 98%, RCI Labscan, Thailand)

### 3.1.2 Apparatus

Nuclear magnetic resonance spectra were recorded at 400 MHz for  $^1H$ -NMR and at 100 MHz for  $^{13}C$ -NMR using a Bruker (FT-NMR advance 400 MHz) spectrometer. The FT-IR ( $4000-400\text{ cm}^{-1}$ ) spectra were recorded on Perkin Elmer infrared spectrophotometer (spectrum GX). Mass spectra were obtained on Thermo Finnigan mass spectrometer (LCQ Advantage). The elemental analysis was carried out on Perkin Elmer (2400) elemental analyzer. UV-Vis absorption and fluorescence spectroscopic measurements were carried out on a Shimadzu UV-spectrometer (UV-1700) and a Jasco spectrofluorometer (FP-6200), respectively. Thermal analysis were recorded on Perkin Elmer (TGA7). The X-ray single-crystal data were collected by using a Bruker D8 QUEST CMOS CCD area detector.

#### 3.1.2.1 NMR spectroscopy

For  $^1H$ -NMR and  $^{13}C$ -NMR, 2 mg of free base porphyrins and metalloporphyrins were dissolved in chloroform-*d* while THPP **8** used DMSO- $d_6$  with tetramethylsilane ( $Me_4Si$ ) as an internal standard. The amount of solvent was 1 mL whereas the sample depth was at least 4 cm in the NMR tube.

#### 3.1.2.2 FT-IR spectroscopy

FT-IR spectra of free base porphyrins and cobalt(II) porphyrins were recorded in KBr in the  $4000-400\text{ cm}^{-1}$  region.

#### 3.1.2.3 Mass spectrometry

The solution of free base porphyrins and cobalt(II) porphyrins were prepared by dissolved 10 mg in dichloromethane (HPLC grade) while THPP **8** used methanol (HPLC grade) and made up to 5 mL.

#### **3.1.2.4 The elemental analysis**

The sample under test is weighed in using a tin capsule. The required amount is 5-10 mg of free base porphyrins and cobalt(II) porphyrins. After folding the capsule (looking rather like wrapped tin foil) the sample is placed in the auto sampler.

#### **3.1.2.5 Absorption and fluorescence emission spectroscopy**

For the preparation of 0.1 mM solution, 10 mg of free base porphyrins and cobalt(II) porphyrins were dissolved and made up to 100 mL volumetric flask by dichloromethane while THPP **8** was dissolved in methanol. Properties of free base porphyrins, cobalt(II) complexes and their derivatives characterized by UV-Vis and fluorescence spectroscopy in the wavelength range of 350 to 700 nm and 530 to 700 nm, respectively. For the solid state of UV-Visible spectroscopy were collected ranged from 450 to 700 nm.

#### **3.1.2.6 Thermal analysis**

The thermal behaviors including the possible phase transition of free base porphyrins and cobalt(II) porphyrins were studied during the heating process at temperature of 298 to 873 K. The dye of 10 mg porphyrins were used and heating under nitrogen flow with scan rate 10 K per minute.

#### **3.1.2.7 X-ray crystallography**

The first step, the crystallization of porphyrins and cobalt(II) porphyrins were prepared in the mixture solvent (dichloromethane: hexane, 1:1) which obtain an adequate crystal. In addition, a good single crystal was selected to collect data by using a single crystal X-ray analyzer. A single crystal of TOBPP **5** with dimensions  $0.28 \times 0.28 \times 0.2$  mm was selected and fixed with epoxy cement on a fine glass fibre which was mounted on a Bruker Porphyrin SMART APEX diffraction with graphite-monochromated Mo  $K\alpha$  ( $\lambda = 0.71073 \text{ \AA}$ ) for cell determination and data collection.

## 3.2 Methods

### Part 1: Synthesis of alkyloxybenzaldehydes

#### 3.2.1 Butyloxybenzaldehyde 1, octyloxybenzaldehyde 2 and decyloxy benzaldehyde 3

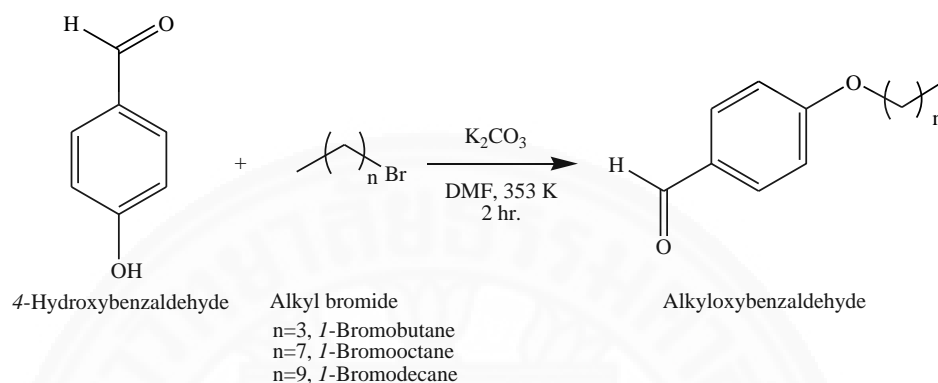


**Fig. 28** Synthesis of alkyloxybenzaldehydes

Following a previously published procedure [46], a mixture of 4-hydroxybenzaldehyde (2.00 g, 17.5 mmol) and  $\text{K}_2\text{CO}_3$  (2.7 g, 18 mmol) was stirred in DMF (15 mL). 1-Bromobutane (2 mL, 18.6 mmol) [various bromoalkane; 1-bromooctane (3.5 mL, 21.4 mmol), 1-bromodecane (4 mL, 19.3 mmol)] was slowly added and the mixture was heated at 353 K for 2 hour. After refluxing, the reaction mixture was cooled to room temperature and then the salts were filtered. Then, DMF solvent was evaporated to dryness. The reaction mixture was re-dissolved in  $\text{CH}_2\text{Cl}_2$  (100 mL) and washed with 4×50 mL distilled water. Magnesium sulfate anhydrous was used for drying. The products as yellow oil were afforded by filtration and evaporation. The reaction products were used without any further purification. Butyloxybenzaldehyde **1** was obtained in 75 % yield (2.24 g).  $^1\text{H-NMR}$  (400 MHz,  $\text{CDCl}_3$ ):  $\delta$  9.87 (1H, CHO), 7.82 (2H,  $J = 8.65$  Hz, Phenyl, *o*-H), 6.99 (2H,  $J = 8.78$  Hz, Phenyl, *m*-H), 4.05 (2H,  $-\text{OCH}_2$ ), 1.79 (2H,  $J = 8.49$  Hz,  $-\text{OCH}_2\text{CH}_2$ ), 1.51 (2H,  $J = 6.71$  Hz,  $-\text{CH}_2\text{CH}_3$ ), 0.99 (3H,  $J = 7.39$  Hz,  $-\text{CH}_3$ ).  $^{13}\text{C-NMR}$  (100 MHz,  $\text{CDCl}_3$ ):  $\delta$  190.55, 166.28, 131.86, 129.85, 114.77, 68.11, 31.06, 19.10, 13.64 ppm. IR (NaCl): 3074, 2957, 2873, 2736, 1689, 1599, 1509, 1467, 1393, 1159, 1024, 883  $\text{cm}^{-1}$ . Mass  $m/z$  (ESI) calcd for  $\text{C}_{11}\text{H}_{14}\text{O}_2$ : 178.23. Found 178.40  $[\text{M}+\text{H}]^+$ .



Octyloxybenzaldehyde **2** and decyloxybenzaldehyde **3** were prepared similarly in butyloxybenzaldehyde **1** with 97 % and 95 % yield, respectively. Octyloxybenzaldehyde **2** was obtained as yellow oil (3.75 g, 97 % yield).  $^1\text{H-NMR}$  (400 MHz,  $\text{CDCl}_3$ ):  $\delta$  9.87 (1H, *CHO*), 7.82 (2H,  $J = 8.81$  Hz, Phenyl, *o*-H), 6.98 (2H,  $J = 8.43$  Hz, Phenyl, *m*-H), 4.03 (2H,  $J = 6.59$  Hz,  $-\text{OCH}_2$ ), 1.81 (2H,  $-\text{OCH}_2\text{CH}_2$ ), 1.46 (2H,  $J = 7.54$  Hz,  $-\text{CH}_2\text{CH}_3$ ), 1.31 (8H,  $-\text{CH}_2\text{CH}_2\text{CH}_2$ ), 0.89 (3H,  $J = 6.54$  Hz,  $-\text{CH}_3$ ).  $^{13}\text{C-NMR}$  (100 MHz,  $\text{CDCl}_3$ ):  $\delta$  190.34, 164.24, 131.77, 129.88, 114.75, 68.41, 31.69, 29.19, 29.08, 29.01, 25.88, 22.51, 13.84 ppm. IR (NaCl): 3073, 2928, 2856, 2734, 1691, 1599, 1509, 1468, 1393, 1159, 1019, 883  $\text{cm}^{-1}$ . Mass  $m/z$  (ESI) calcd for  $\text{C}_{15}\text{H}_{22}\text{O}_2$ : 234.33. Found 236.01  $[\text{M}+\text{H}]^+$ .

Decyloxybenzaldehyde **3** was obtained as yellow oil (4.11 g, 95 % yield).  $^1\text{H-NMR}$  (400 MHz,  $\text{CDCl}_3$ ):  $\delta$  9.87 (1H, *CHO*), 7.82 (2H,  $J = 8.82$  Hz, Phenyl, *o*-H), 6.99 (2H,  $J = 8.67$  Hz, Phenyl, *m*-H), 4.04 (2H,  $J = 6.58$  Hz,  $-\text{OCH}_2$ ), 1.81 (2H,  $-\text{OCH}_2\text{CH}_2$ ), 1.44 (2H,  $-\text{CH}_2\text{CH}_3$ ), 1.28 (12H,  $-\text{CH}_2\text{CH}_2\text{CH}_2$ ), 0.88 (3H,  $J = 6.68$  Hz,  $-\text{CH}_3$ ).  $^{13}\text{C-NMR}$  (100 MHz,  $\text{CDCl}_3$ ):  $\delta$  190.15, 164.30, 131.69, 129.82, 114.76, 68.41, 32.81, 31.73, 29.44, 29.37, 29.18, 29.01, 25.85, 22.45, 13.76 ppm. IR (NaCl): 3073, 2924, 2854, 2732, 1693, 1602, 1509, 1467, 1391, 1159, 1015, 883  $\text{cm}^{-1}$ . Mass  $m/z$  (ESI) calcd for  $\text{C}_{17}\text{H}_{26}\text{O}_2$ : 262.39. Found 269.49  $[\text{M}+\text{H}]^+$ .

## Part 2: Synthesis of porphyrin and its derivatives

**3.2.2 Tetrakis(4-methoxyphenyl)porphyrin (TOMPP 4), tetrakis(4-butyloxyphenyl)porphyrin (TOBPP 5), tetrakis(4-octyloxyphenyl)porphyrin (TOOPP 6), tetrakis(4-decyloxyphenyl)porphyrin (TODPP 7) and tetrakis(4-hydroxyphenyl)porphyrin (THPP 8)**

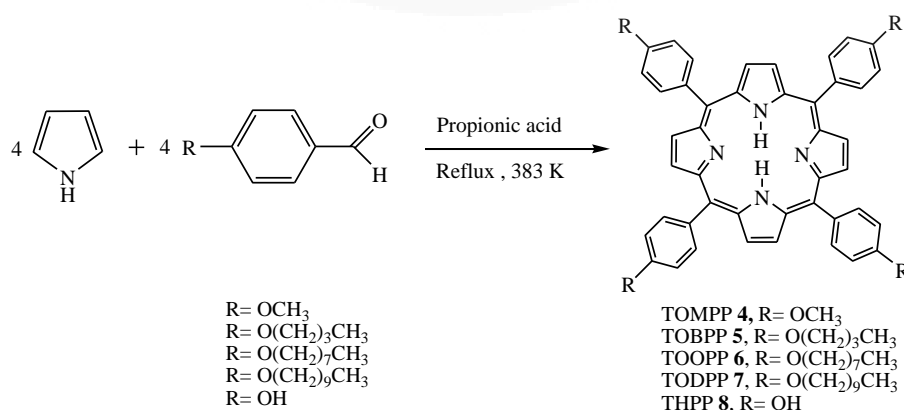


**Fig. 29** Synthesis of porphyrin and their derivatives

Following a published procedure with slight modification [39,40,52], a 100 mL round-bottomed flask equipped with a magnetic stirring bar and a reflux condenser was charged with *p*-anisaldehyde (1.5 mL, 12.4 mmol), and propionic acid (40 mL) and stirred for 15 min at 383 K. Pyrrole (1 mL, 14.3 mmol) was added slowly, and the mixture was refluxed for 2 hour. After refluxing, the reaction mixture was cooled to room temperature and added 40 mL ethanol, kept in the refrigerator overnight. The purple crystals were filtered, washed, and dried by vacuum filtration with cold ethanol to remove traces of propionic acid. The crude products were purified by column chromatography (dichloromethane: hexane solvent) to afford TOMPP **4** as a purple crystals (0.80 g, 26 %). <sup>1</sup>H-NMR (400 MHz, CDCl<sub>3</sub>): δ 8.86 (8H, Pyrrole, β-H), 8.12 (8H, *J* = 8.06 Hz, Phenyl, *o*-H), 7.29 (8H, *J* = 8.10 Hz, Phenyl, *m*-H), 4.10 (12H, -OCH<sub>3</sub>). <sup>13</sup>C-NMR (100 MHz, CDCl<sub>3</sub>): δ 158.75, 134.68, 133.99, 129.97, 127.89, 118.83, 111.44, 54.65 ppm. IR (KBr): 3317, 2928, 2832, 1606, 1509, 1247, 1175, 965, 802 cm<sup>-1</sup>. Elemental analysis; calcd (%) for C<sub>48</sub>H<sub>38</sub>N<sub>4</sub>O<sub>4</sub> (734.84): C 78.45, H 5.21, N 7.62; found: C 76.42, H 5.75, N 7.42. Mass *m/z* (ESI): found 735.23 [M+H]<sup>+</sup>. UV-Vis (CH<sub>2</sub>Cl<sub>2</sub>): (λ<sub>abs</sub>(nm), ε (10<sup>3</sup>M<sup>-1</sup>cm<sup>-1</sup>)): S-band; (421, 115.4), Q-band; (517, 24.0), (556, 16.6), (594, 7.6), (651, 10.2) (Figure ). Fluor: λ<sub>em</sub> (λ<sub>ex</sub>= 530nm) 655 nm.

The tetrakis(4-butyloxyphenyl)porphyrin (TOBPP **5**), tetrakis(4-octyloxyphenyl)porphyrin (TOOPP **6**), tetrakis(4-decyloxyphenyl)porphyrin (TODPP **7**) and tetrakis(4-hydroxyphenyl)porphyrin (THPP **8**) were prepared similarly to TOMPP **4** with 5%, 13%, 14% and 7% yield, respectively. Tetrakis(4-butyloxyphenyl)porphyrin (TOBPP **5**) was obtained as a purple crystals (0.11 g, 5% yield). <sup>1</sup>H-NMR (400 MHz, CDCl<sub>3</sub>): δ 8.86 (8H, Pyrrole, β-H), 8.10 (8H, Phenyl, *o*-H), 7.29 (8H, Phenyl, *m*-H), 4.24 (-OCH<sub>2</sub>), 1.98 (-OCH<sub>2</sub>CH<sub>2</sub>), 1.29 (-CH<sub>2</sub>CH<sub>3</sub>), 0.92 (-CH<sub>3</sub>). <sup>13</sup>C-NMR (100 MHz, CDCl<sub>3</sub>): δ 159.12, 135.50, 134.64, 130.89, 128.75, 119.77, 112.87, 68.17, 31.60, 19.37, 13.78 ppm. IR (KBr): 3318, 2929, 2868, 1605, 1507, 1244, 1173, 965, 800 cm<sup>-1</sup>. Elemental analysis; calcd (%) for C<sub>60</sub>H<sub>62</sub>N<sub>4</sub>O<sub>4</sub> (903.16): C 79.79, H 6.92, N 6.20; found C 79.44, H 6.55, N 5.83. Mass *m/z* (ESI): found 904.16 [M+H]<sup>+</sup>. UV-Vis (CH<sub>2</sub>Cl<sub>2</sub>): (λ<sub>abs</sub>(nm), ε (10<sup>3</sup>M<sup>-1</sup>cm<sup>-1</sup>)): S-band; (422, 115.4), Q-band; (517, 24.0), (556, 16.6), (594, 7.6), (651, 10.2).

Tetrakis(4-octyloxyphenyl)porphyrin (TOOPP **6**) was obtained as a purple crystals (0.46 g, 13 % yield).  $^1\text{H-NMR}$  (400 MHz,  $\text{CDCl}_3$ ):  $\delta$  8.86 (8H, Pyrrole,  $\beta$ -H), 8.10 (8H, Phenyl, *o*-H), 7.26 (8H, Phenyl, *m*-H), 4.24 ( $-\text{OCH}_2$ ), 1.99 ( $-\text{OCH}_2\text{CH}_2$ ), 1.36 ( $-\text{CH}_2\text{CH}_3$ ), 1.26 ( $-\text{CH}_2\text{CH}_2$ ), 0.91 ( $-\text{CH}_3$ ).  $^{13}\text{C-NMR}$  (100 MHz,  $\text{CDCl}_3$ ):  $\delta$  159.16, 135.48, 134.69, 130.80, 128.74, 119.76, 112.93, 68.56, 31.79, 29.57, 29.39, 29.19, 26.19, 22.55, 13.84 ppm. FT-IR (KBr): 3316, 2926, 2850, 1606, 1508, 1242, 1174, 965, 803  $\text{cm}^{-1}$ . Elemental analysis; calcd (%) for  $\text{C}_{76}\text{H}_{94}\text{N}_4\text{O}_4$  (1127.58): C 80.95, H 8.40, N 4.97; found C 81.10, H 8.25, N 4.93. Mass  $m/z$  (ESI): found 1129.47  $[\text{M}+\text{H}]^+$ . UV-Vis ( $\text{CH}_2\text{Cl}_2$ ): ( $\lambda_{\text{abs}}(\text{nm})$ ,  $\epsilon$  ( $10^3\text{M}^{-1}\text{cm}^{-1}$ )): S-band; (422, 120.4), Q-band; (519, 20.0), (556, 14.9), (595, 6.7), (651, 10.1).

Tetrakis(4-decyloxyphenyl)porphyrin (TODPP **7**) was obtained as a purple crystals (0.56 g, 14 % yield).  $^1\text{H-NMR}$  (400 MHz,  $\text{CDCl}_3$ ):  $\delta$  8.86 (8H, Pyrrole,  $\beta$ -H), 8.10 (8H, Phenyl, *o*-H), 7.26 (8H, Phenyl, *m*-H), 4.24 ( $-\text{OCH}_2$ ), 1.98 ( $-\text{OCH}_2\text{CH}_2$ ), 1.33 ( $-\text{CH}_2\text{CH}_3$ ), 1.26 ( $-\text{CH}_2\text{CH}_2$ ), 0.88 ( $-\text{CH}_3$ ).  $^{13}\text{C-NMR}$  (100 MHz,  $\text{CDCl}_3$ ):  $\delta$  159.10, 135.51, 134.51, 130.68, 128.76, 119.77, 112.86, 68.48, 31.88, 29.60, 29.55, 29.53, 29.46, 29.28, 26.20, 22.60, 13.93 ppm. IR (KBr): 3310, 2923, 2852, 1606, 1509, 1243, 1175, 967, 804  $\text{cm}^{-1}$ . Elemental analysis; calcd (%) for  $\text{C}_{84}\text{H}_{110}\text{N}_4\text{O}_4$  (1239.80): C 81.37, H 8.94, N 4.52; found C 81.24, H 8.99, N 4.58. Mass  $m/z$  (ESI): found 1241.55  $[\text{M}+\text{H}]^+$ . UV-Vis ( $\text{CH}_2\text{Cl}_2$ ): ( $\lambda_{\text{abs}}(\text{nm})$ ,  $\epsilon$  ( $10^3\text{M}^{-1}\text{cm}^{-1}$ )): S-band; (422, 122.5), Q-band; (519, 16.7), (556, 12.5), (595, 5.5), (651, 9.2).

Tetrakis(4-hydroxyphenyl)porphyrin (THPP **8**) was obtained as green-purple crystals with small yield of 7 %.  $^1\text{H-NMR}$  (400 MHz,  $\text{CDCl}_3$ , DMSO):  $\delta$  8.88 (8H, Pyrrole,  $\beta$ -H), 8.10 (8H, Phenyl, *o*-H), 7.23 (8H, Phenyl, *m*-H), 9.29 ( $-\text{OH}$ ).  $^{13}\text{C-NMR}$  (100 MHz,  $\text{CDCl}_3$ ):  $\delta$  157.43, 135.68, 133.31, 130.99, 128.80, 120.16, 114.04 ppm. FT-IR (KBr): 3400-3100, 2937, 2869, 1604, 1232, 1170, 967, 802  $\text{cm}^{-1}$ . Elemental analysis; calcd (%) for  $\text{C}_{44}\text{H}_{30}\text{N}_4\text{O}_4$  (678.73): C 77.86, H 4.46, N 8.26; found C 67.63, H 5.13, N 6.55. Mass  $m/z$  (ESI): found 679.33  $[\text{M}+\text{H}]^+$ . UV-Vis (MeOH): ( $\lambda_{\text{abs}}(\text{nm})$ ,  $\epsilon$  ( $10^3\text{M}^{-1}\text{cm}^{-1}$ )): S-band; (414, 118.1), Q-band; (518, 17.2), (555, 13.4), (593, 6.0), (650, 7.2).

### Part 3: Synthesis of metalloporphyrins

#### 3.2.3 Cobalt-methoxyphenyl porphyrin (Co-TOMPP 9), Cobalt-butyloxyphenyl porphyrin (Co-TOBPP 10), Cobalt-octyloxyphenyl porphyrin (Co-TOOPP 11) and Cobalt-decyloxyphenyl porphyrin (Co-TODPP 12)

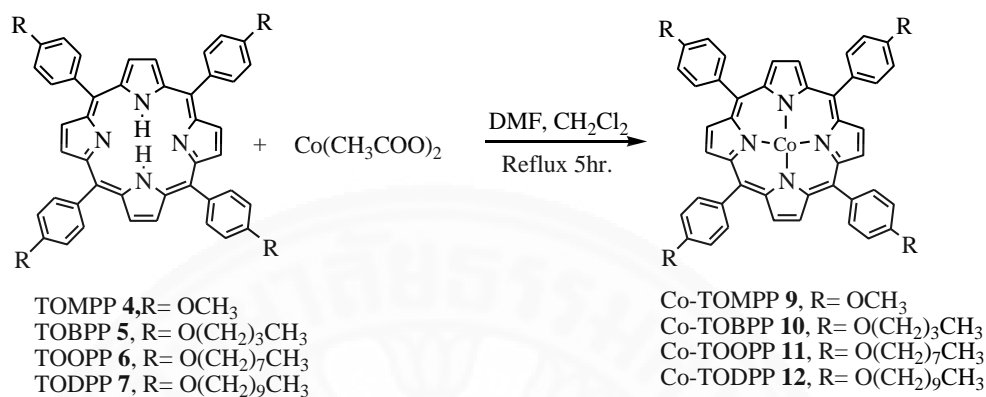


**Fig. 30** Synthesis of cobalt(II) porphyrins

Cobalt-methoxyphenyl porphyrin (Co-TOMPP 9) was synthesized by following the development of a published procedure [45]. Co-TOMPP 9 was used to reflux TOMPP (0.1 g, 0.14 mmol) with cobalt acetate [Co(II)(CH<sub>3</sub>COO)<sub>2</sub>] (0.1 g, 0.56 mmol) in dimethylformamide, DMF (5 mL) and CH<sub>2</sub>Cl<sub>2</sub> (5 mL). The reaction was stirred 363 K for 5 hour. After refluxing, the reaction mixture was cooled to room temperature. The flask is then put in an ice bath before adding distilled water. Finally, the purple crystals were filtered, washed, and dried by vacuum filtration with cold methanol (3×20 mL). The title compound was isolated by column chromatography (hexane: dichloromethane solvent) to afford Co-TOMPP 9 as a purple solid (75 % yield). Co-TOMPP 9 was not identified due to paramagnetic character in <sup>1</sup>H, <sup>13</sup>C NMR data. IR (KBr): 2929, 2829, 1602, 1504, 1248, 1174, 800 cm<sup>-1</sup>. Elemental analysis; calcd (%) for CoC<sub>48</sub>H<sub>36</sub>N<sub>4</sub>O<sub>4</sub> (791.76): C 72.81, H 4.58, N 7.08; found C 73.38, H 4.04, N 7.06. Mass *m/z* (ESI): found 792.44 [M+H]<sup>+</sup>. UV-Vis (CH<sub>2</sub>Cl<sub>2</sub>): (λ<sub>abs</sub>(nm), ε (10<sup>3</sup>M<sup>-1</sup>cm<sup>-1</sup>)): S-band; (414, 133.3), Q-band; (530, 17.3), (611, 1.5).

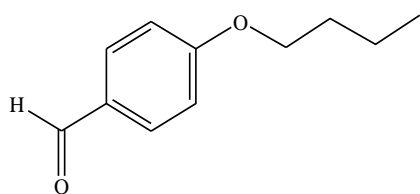
Similarly, reaction of cobalt acetate with TOBPP 5, TOOPP 6 or TODPP 7 gave purple macrocrystalline samples of Co-TOBPP 10 92%, Co-TOOPP 11 81% and Co-TODPP 12 88%. And cobalt-butyloxyphenyl porphyrin (Co-TOBPP 10) was not identified due to paramagnetic character in <sup>1</sup>H, <sup>13</sup>C NMR data. IR (KBr): 2935, 2857, 1605, 1507, 1245, 1174, 794 cm<sup>-1</sup>. Elemental analysis; calcd (%) for

$\text{CoC}_{60}\text{H}_{60}\text{N}_4\text{O}_4$  (960.08): C 75.06, H 6.30, N 5.84; found C 75.24, H 6.09, N 5.78. Mass  $m/z$  (ESI): found 960.96  $[\text{M}+\text{H}]^+$ . UV-Vis ( $\text{CH}_2\text{Cl}_2$ ): ( $\lambda_{\text{abs}}(\text{nm})$ ,  $\epsilon$  ( $10^3\text{M}^{-1}\text{cm}^{-1}$ )): S-band; (415, 133.3), Q-band; (530, 17.3), (611, 1.5).

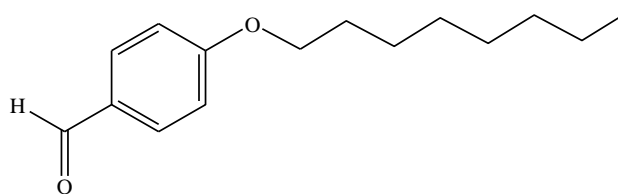
Cobalt-octyloxyphenyl porphyrin (Co-TOOPP **11**) was not identified due to paramagnetic character in  $^1\text{H}$ ,  $^{13}\text{C}$  NMR data. IR (KBr): 2924, 2845, 1607, 1509, 1244, 1174, 797  $\text{cm}^{-1}$ . Elemental analysis; calcd (%) for  $\text{CoC}_{76}\text{H}_{92}\text{N}_4\text{O}_4$  (1184.50): C 77.06, H 7.83, N 4.73; found C 77.11, H 7.67, N 4.73. Mass  $m/z$  (ESI): found 1185.15  $[\text{M}+\text{H}]^+$ . UV-Vis ( $\text{CH}_2\text{Cl}_2$ ): ( $\lambda_{\text{abs}}(\text{nm})$ ,  $\epsilon$  ( $10^3\text{M}^{-1}\text{cm}^{-1}$ )): S-band; (415, 131.7), Q-band; (531, 16.8), (613, 3.1).

Cobalt-decyloxyphenyl porphyrin (Co-TODPP **12**) was not identified due to paramagnetic character in  $^1\text{H}$ ,  $^{13}\text{C}$  NMR data. IR (KBr): 2924, 2853, 1606, 1505, 1241, 1173, 795  $\text{cm}^{-1}$ . Elemental analysis; calcd (%) for  $\text{CoC}_{84}\text{H}_{108}\text{N}_4\text{O}_4$  (1296.71): C 77.81, H 8.40, N 4.32; found C 77.81, H 8.35, N 4.33. Mass  $m/z$  (ESI): found 1297.35  $[\text{M}+\text{H}]^+$ . UV-Vis ( $\text{CH}_2\text{Cl}_2$ ): ( $\lambda_{\text{abs}}(\text{nm})$ ,  $\epsilon$  ( $10^3\text{M}^{-1}\text{cm}^{-1}$ )): S-band; (415, 125.4), Q-band; (531, 12.9), (614, 2.7).

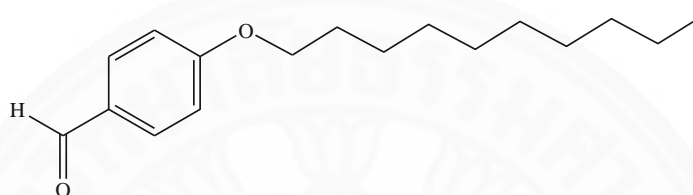




Formula  $C_{11}H_{14}O_2$   
Butyloxybenzaldehyde **1**



Formula  $C_{15}H_{22}O_2$   
Octyloxybenzaldehyde **2**



Formula  $C_{17}H_{26}O_2$   
Decyloxybenzaldehyde **3**

**Fig. 32** The structure of various alkyloxybenzaldehyde **1-3**

#### 4.1.1 Mass spectrometry

The representative example mass spectrum of butyloxybenzaldehyde **1** (without purification, Fig. 33) exhibit very weak molecular ion peaks  $[M+H]^+$  at  $m/z$  178.40. The most important fragmentation reaction for butyloxybenzaldehyde **1** is due to the loss of an alkyl groups, similar results found in the previous reported by Domingues M.R.M. [53-54]. The larger alkyl group, the more readily lost were found. In the butyloxybenzaldehyde **1** spectrum, a methyl group from alkyl long chain loss at 162.28, followed by a series of ions 14 amu apart, related with methylene groups, i.e.  $m/z = 148.26$ , 134.28 and 122.18 (shown in Fig. 33). However, the spectra of octyloxybenzaldehyde **2** and decyloxybenzaldehyde **3** were obtained similarly in butyloxybenzaldehyde **1**, due to the loss of a methyl group and methylene groups from alkyl long chain. Octyloxybenzaldehyde **2** and decyloxybenzaldehyde **3** showed the molecular ion peaks  $[M+H]^+$  at  $m/z = 236.01$  and 269.49 as expected, respectively. The characterization data by mass spectrometry of aldehydes were displayed in Table 3.

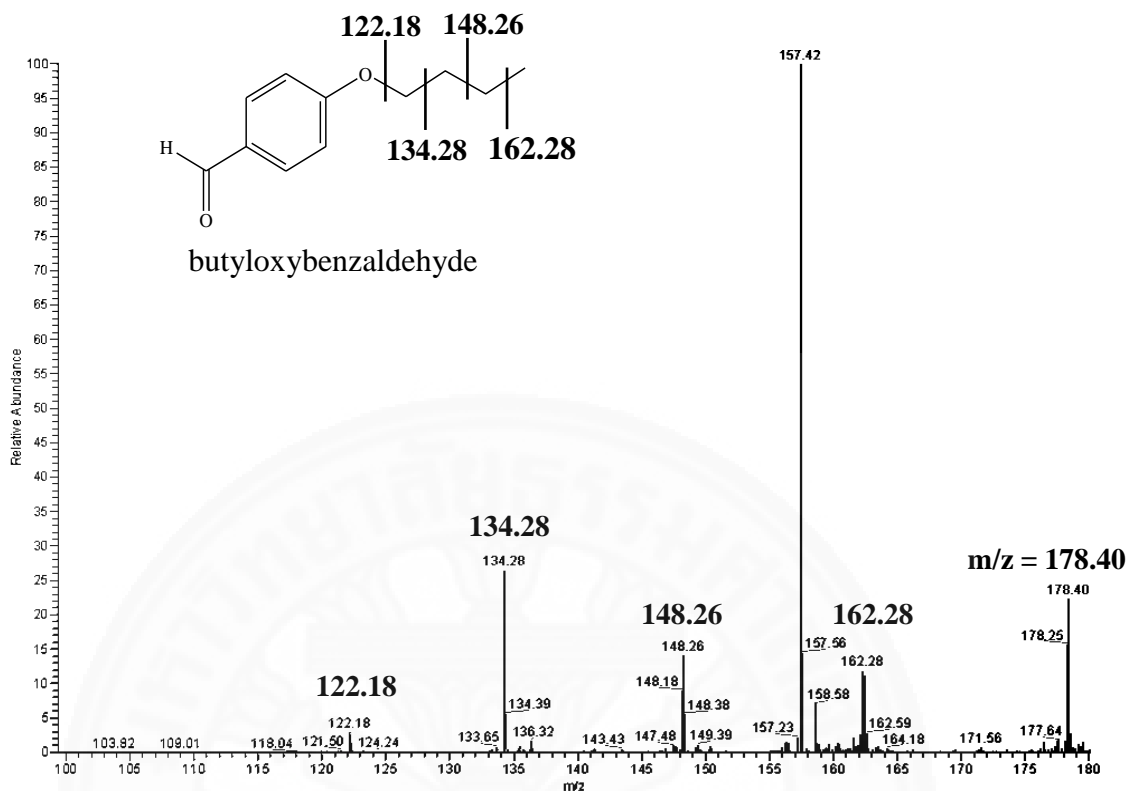


**Fig. 33** Mass spectrum of butyloxybenzaldehyde **1**

#### 4.1.2 NMR spectroscopy

The frequency regions of the  $^1\text{H}$ -NMR and  $^{13}\text{C}$ -NMR showed the chemical shifts for aldehydes with alkyl long chain. The room temperature,  $^1\text{H}$ -NMR and  $^{13}\text{C}$ -NMR spectra of aldehyde (butyloxybenzaldehyde **1**, octyloxybenzaldehyde **2** and decyloxybenzaldehyde **3**) were obtained in  $\text{CDCl}_3$  solvent.



The  $^1\text{H-NMR}$  of butyloxybenzaldehyde **1**, a representative example was shown in Figure 34. The  $^1\text{H-NMR}$  showed sharp single peak of  $\text{CHO}$  at 9.87 ppm, due to the magnetic anisotropy the carbonyl group. The *ortho*- and *meta*-protons of phenyl ring were observed as two doublets ( $J= 8.8$  Hz) at 7.82 and 6.99 ppm (in a 2:2 ratio), respectively. The triplet peak at 4.05 ppm was assigned to the protons of ( $\text{O-CH}_2\text{-R}$ ) of the ether long chain group. Similarly, the highly shield triplet peaks at 0.99 ppm was said to be methyl end group of alkyl long chain. The doublet peaks at 1.51 and 1.79 ppm were corresponded to protons of methylene groups. The alkyl protons in the chain of butyloxybenzaldehyde **1** were found to be greater deshielded than octyloxybenzaldehyde **2** and decyloxybenzaldehyde **3**, due to the inductive effect and the electronegativity of ether group (electron-donating) in side chain.

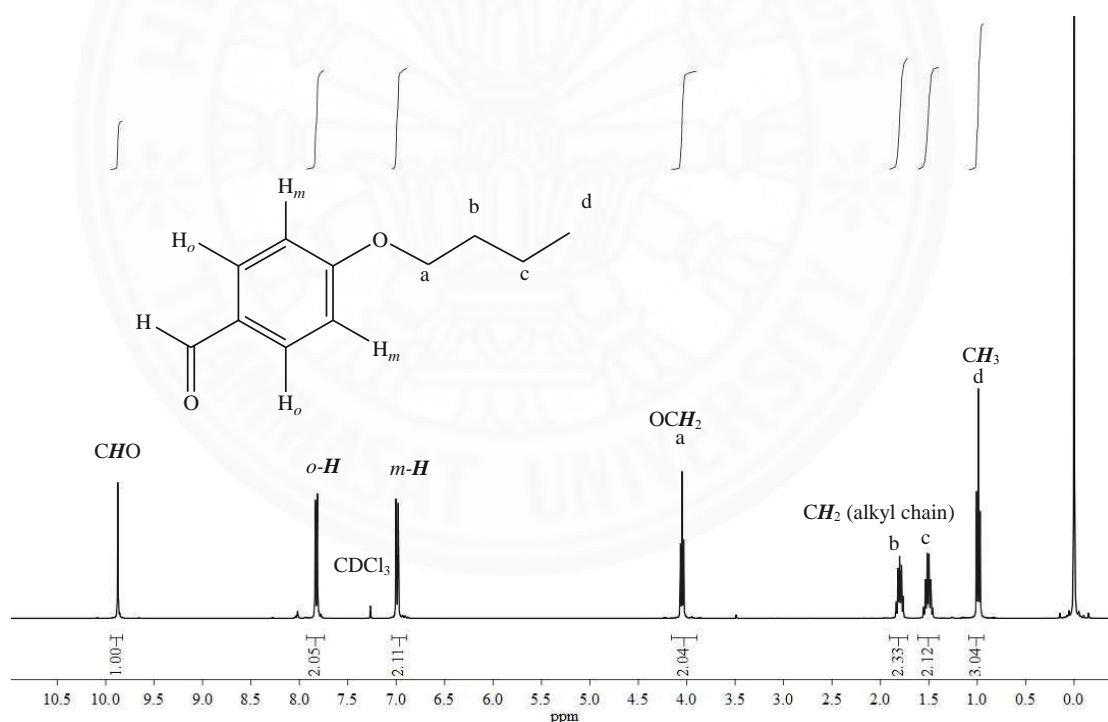


**Fig. 34** The  $^1\text{H-NMR}$  spectrum of butyloxybenzaldehyde **1** in  $\text{CDCl}_3$

The  $^{13}\text{C}$  NMR spectrum of butyloxybenzaldehyde **1** was shown in Figure 35, by using  $\text{CDCl}_3$  as a solvent. The single methyl carbon **d** appeared at the highest field (13.64 ppm), while the methylene carbon **b** and found **c** at 31.06 and 19.10, respectively. The singlet resonance peak at 68.11 ppm was clearly assigned to be  $\text{CH}_2$  carbon at position **a**. The highly deshielded was caused by the attached oxygen atom. Each of the other carbon in phenyl showed four peaks between 114.77 and 166.28 ppm, consistent with disubstituted ring similarly results were reported by Aline T. *et al.* [55,56]. Finally, the downfield peak at 190.55 ppm has already been labeled as arising from the carbonyl carbon. Octyloxybenzaldehyde **2** and decyloxybenzaldehyde **3** were observed similarly in butyloxybenzaldehyde **1** (as shown in Table 4). The results are in agreement with the previous reported by Ioannis D.K. [46]. The proton and carbon chemical shifts were successfully received the expected corresponding aldehydes **1-3**.

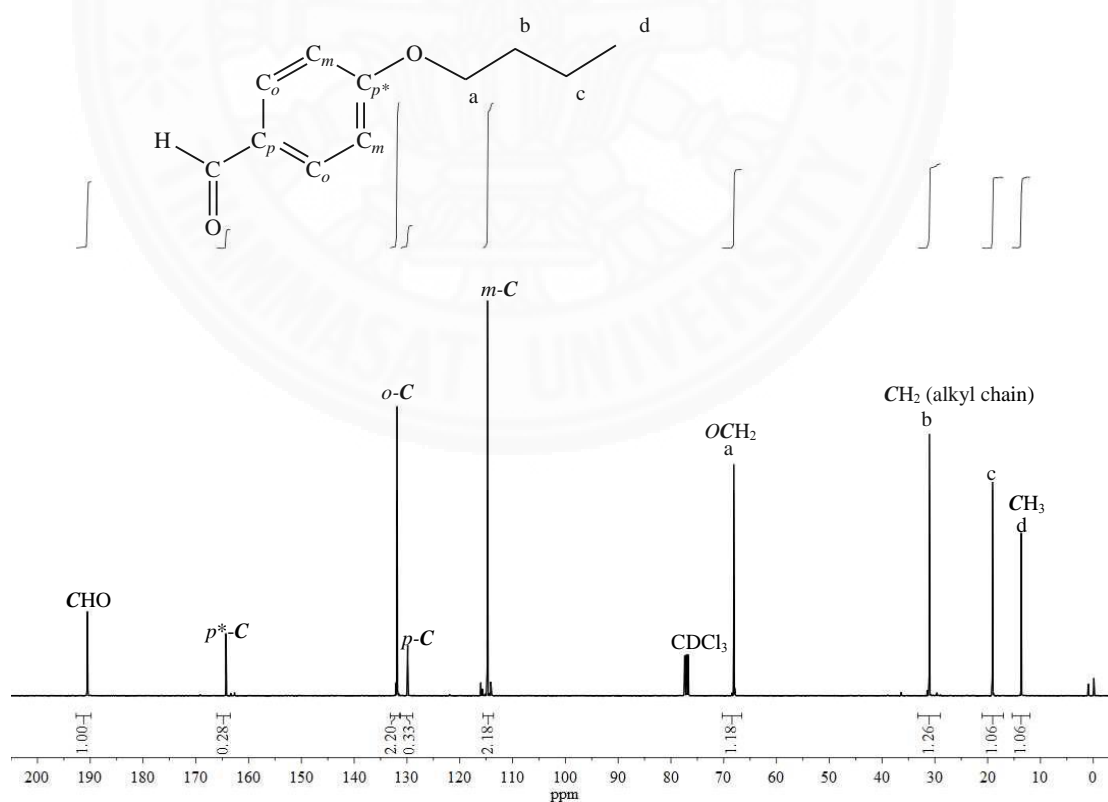


**Fig. 35** The  $^{13}\text{C}$ -NMR spectrum of butyloxybenzaldehyde **1** in  $\text{CDCl}_3$

**Table 4**  $^1\text{H}$  and  $^{13}\text{C}$  NMR spectroscopic data for aldehydes **1-3**

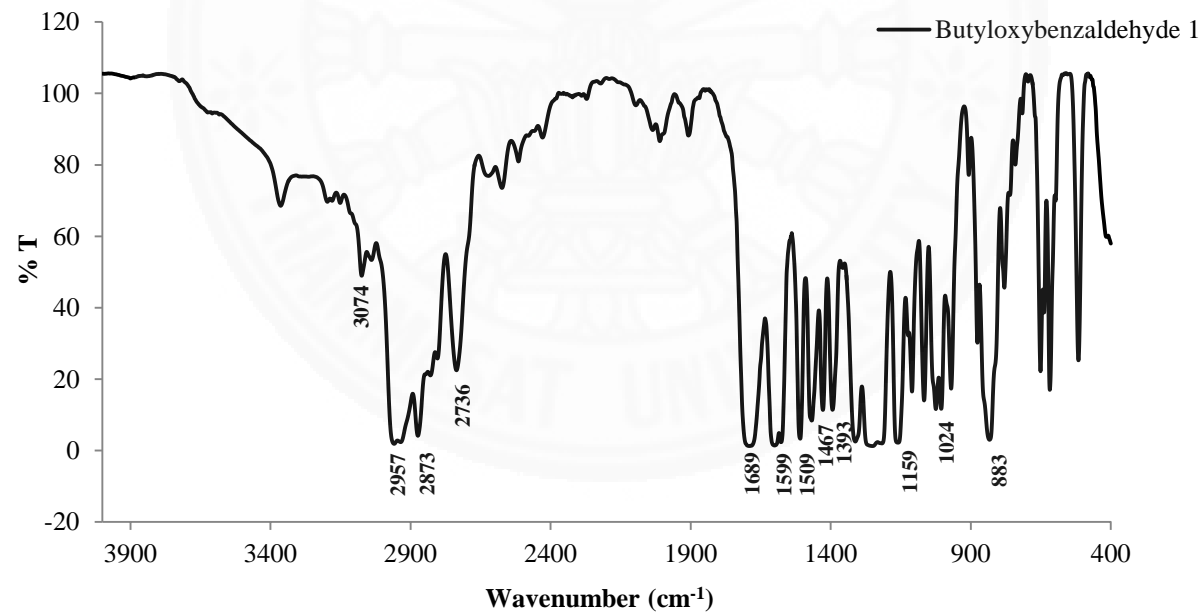
Aldehydes	$^1\text{H-NMR}$ (ppm)							
	CHO	Phenyl, o- <i>H</i>	Phenyl, m- <i>H</i>	OCH <sub>2</sub>	OCH <sub>2</sub> CH <sub>2</sub>	CH <sub>2</sub> CH <sub>3</sub>	CH <sub>2</sub> CH <sub>2</sub> CH <sub>2</sub>	CH <sub>3</sub>
Butyloxybenzaldehyde <b>1</b>	9.87 (1H)	7.82 (2H)	6.99 (2H)	4.05 (2H)	1.79 (2H)	1.51 (2H)	-	0.99 (3H)
Octyloxybenzaldehyde <b>2</b>	9.87 (1H)	7.82 (2H)	6.98 (2H)	4.03 (2H)	1.81 (2H)	1.46 (2H)	1.31 (8H)	0.89 (3H)
Decyloxybenzaldehyde <b>3</b>	9.87 (1H)	7.82 (2H)	6.99 (2H)	4.04 (2H)	1.87 (2H)	1.44 (2H)	1.28 (12H)	0.88 (3H)
Aldehydes	$^{13}\text{C-NMR}$ (ppm)							
	CHO	Phenyl, <i>p</i> *- <i>C</i>	Phenyl, <i>p</i> - <i>C</i>	Phenyl, <i>o</i> - <i>C</i>	Phenyl, <i>m</i> - <i>C</i>	OCH <sub>2</sub>	CH <sub>2</sub> (alkyl long chain)	CH <sub>3</sub>
Butyloxybenzaldehyde <b>1</b>	190.55	166.28	131.86	129.85	114.77	68.11	31.06, 19.10	13.64
Octyloxybenzaldehyde <b>2</b>	190.34	164.24	131.77	129.88	114.75	68.41	31.69, 29.19, 29.08, 29.01, 25.88, 22.51	13.84
Decyloxybenzaldehyde <b>3</b>	190.15	164.30	131.69	129.82	114.76	68.41	32.81, 31.73, 29.44, 29.37, 29.18, 29.01, 25.85, 22.45	13.76

### 4.1.3 Infrared spectroscopy

IR spectra were recorded in NaCl discs. The data were collected in the 4000-400  $\text{cm}^{-1}$  region. The infrared data was assigned in Table 5. The aldehydes **1-3** had similar wave number with a little peak shift, due to the effect of alkyl long chain group were substituted. The intensity bands of each alkyloxybenzaldehyde were unchanged according to the different number of C-H  $sp^2$  stretching in phenyl group, C=C stretching in the conjugated aromatic,  $\text{CH}_3$  bending, and out of plane in the *para* disubstitution. The signal of butyloxybenzaldehyde **1** at 3074  $\text{cm}^{-1}$  were assigned to be C-H  $sp^2$  stretching of phenyl group and the signals at 1599 and 1509  $\text{cm}^{-1}$  were according to stretching vibration of C=C in the conjugated aromatic. The bands at 1467 and 1393  $\text{cm}^{-1}$  were assigned to  $\text{CH}_3$  bend in alkyl chain group and the signals at 883  $\text{cm}^{-1}$  was in agreement with the out of plane in the *para* disubstitution, as shown in Fig. 36. The C-H  $sp^3$  stretching (long chain) and C-H stretching (aldehyde) decrease with increasing the number of carbon in alkyl chain aldehyde. Butyloxybenzaldehyde **1** shows a C-H  $sp^3$  stretching band at 2957  $\text{cm}^{-1}$ , which shifted the wave numbers by 29 and 33  $\text{cm}^{-1}$  in octyloxybenzaldehyde **2**, decyloxybenzaldehyde **3**, respectively. The blue shift of C=O band of carbonyl group was according to number of carbon in each aldehyde. The two bands of ether group observed to decrease wave number with increasing the number of carbon in alkyl chain aldehyde at about 1159 and 1024  $\text{cm}^{-1}$ (Fig. 36). However, the aldehydes **2** and **3** were obtained further identified by their contrastive IR spectra (shown in Table 5). The results are in agreement with the previous reported by Mayank J.M. [57-58].

**Table 5** The IR data of aldehydes **1-3**

Aldehydes	C-H sp <sup>2</sup> str. in phenyl	C-H sp <sup>3</sup> str. in long chain	C-H str. in aldehyde	C=O str. in aldehyde	C=C str. in phenyl	CH <sub>3</sub> bend	C-O-C, ether	oop, para disubst.
Butyloxybenzaldehyde <b>1</b>	3074	2957	2873, 2736	1689	1599, 1509	1467, 1393	1159, 1024	883
Octyloxybenzaldehyde <b>2</b>	3073	2928	2856, 2734	1691	1599, 1509	1468, 1393	1159, 1019	883
Decyloxybenzaldehyde <b>3</b>	3073	2924	2854, 2732	1693	1602, 1509	1467, 1391	1159, 1015	883

Unit = cm<sup>-1</sup>**Fig. 36** The IR spectrum of butyloxybenzaldehyde **1** in NaCl

## 4.2 Porphyrins and cobalt(II)porphyrins synthesis and characterization

The free base porphyrins, including TOMPP **4**, TOBPP **5**, TOOPP **6**, TODPP **7** and THPP **8** (Fig. 37a,b) were synthesized by a modification of the published method for the known TPP, Adler-Longo method [20,39,40,52]. Start with, heating of pyrrole in propionic acid solvent followed by adding of the same amount of aldehydes. Further heated for 2 hours, the reaction mixture was added ethanol, and kept in the refrigerator overnight. The products obtained purple microcrystals in dark solution and then the microcrystals were purified. From this process, the attempt was applied by using longer reaction time, allowed the reaction gave more successful microcrystals. Free base porphyrins were obtained ranged from 5 to 26 %, while TOMPP **4** obtained the highest yield as 26%. However, porphyrins with longer chain were prepared form various type of aldehyde (TOBPP **5**, TOOPP **6** and TODPP **7**) gave the lower yield than TOMPP **4**, due to the steric hindrance and the donating groups on *para*-position of alkyl long chain substituent. The results from Table 6 showed the influence of substituent on phenyl ring and product yield.

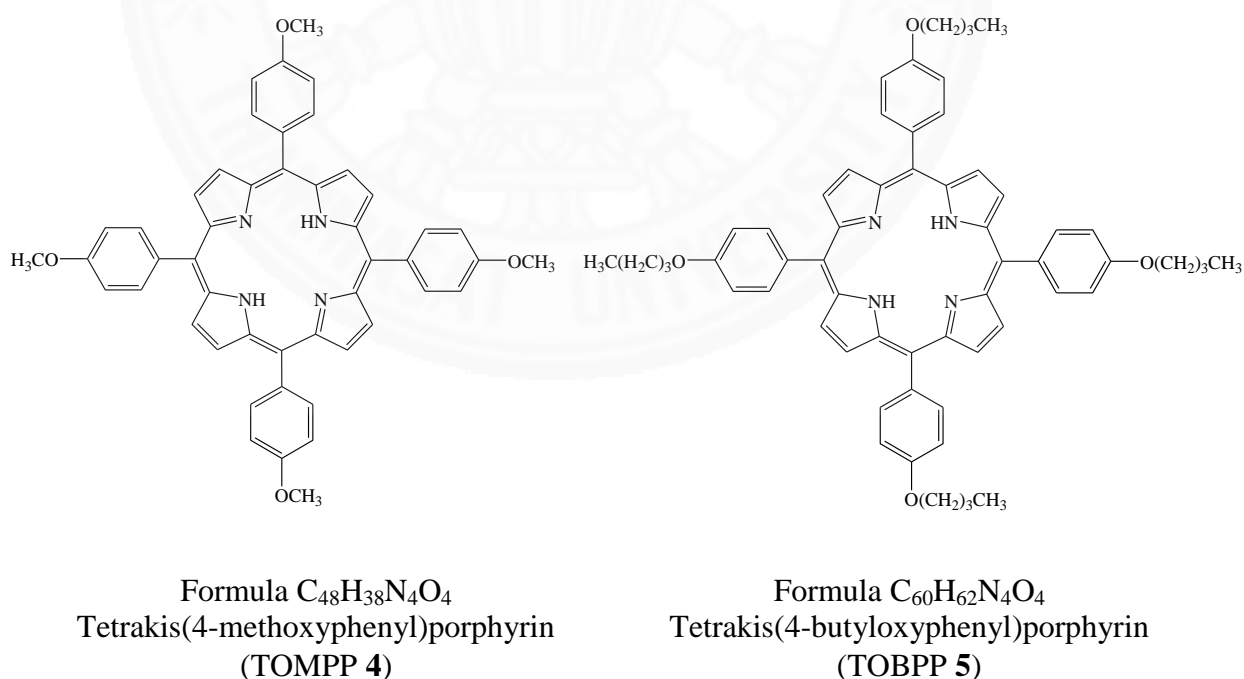
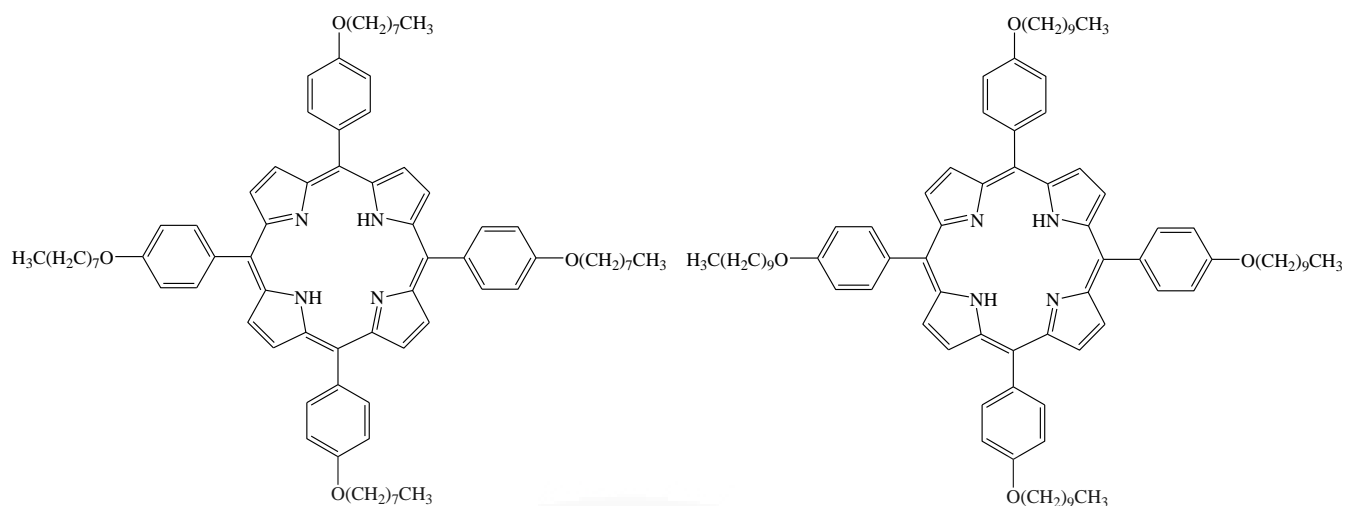
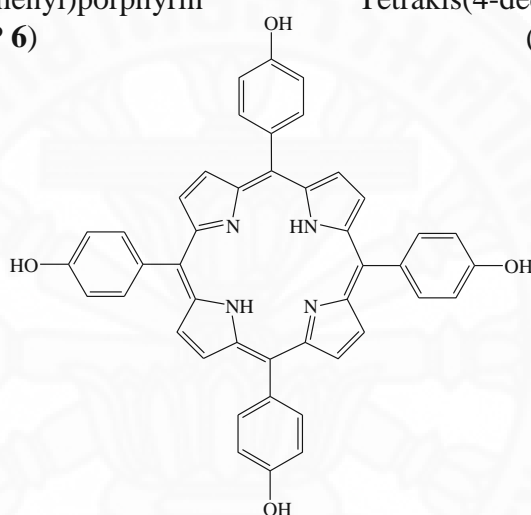


**Fig. 37a** The structure of TOMPP **4** and TOBPP **5**



Formula C<sub>76</sub>H<sub>94</sub>N<sub>4</sub>O<sub>4</sub>  
Tetrakis(4-octyloxyphenyl)porphyrin  
(TOOPP 6)

Formula C<sub>84</sub>H<sub>110</sub>N<sub>4</sub>O<sub>4</sub>  
Tetrakis(4-decyloxyphenyl)porphyrin  
(TODPP 7)



Formula C<sub>44</sub>H<sub>30</sub>N<sub>4</sub>O<sub>4</sub>  
Tetrakis(4-hydroxyphenyl)porphyrin  
(THPP 8)

**Fig. 37b** The structure of TOOPP 6, TODPP 7 and THPP 8

The metalloporphyrins, focusing on cobalt(II) complexes, were prepared by adding cobalt ion into the central position of free base porphyrin (Co-TOMPP 9, Co-TOBPP 10, Co-TOOPP 11, Co-TODPP 12). The products were illustrated in Figure 38. The reaction procedure was started with refluxing porphyrin in *N,N*-dimethylformamide (DMF) mixed with dichloromethane (1:1), followed by adding cobalt(II) acetate, than further refluxing for 5 hours. The reaction mixture was extracted with dichloromethane and removed solvent by evaporator before further purification by column chromatography. The crystals of each cobalt porphyrins were purified.

The cobalt(II) porphyrins had higher yield than the free base porphyrins, due to the metal ionic size of the cobalt(II) ion, that fitted into the central hole ligand as reported by Shu A.Y. for Co-TPP [59]. The long time reaction and the more cobalt(II) acetate, the more successful product was obtained due to the reaction driving forward. The greatest product yield was obtained by Co-TOBPP **10** (92 %), while the lowest yield found in Co-TOMPP **9** (75 %), suggesting the influence of steric hindrance of *para* substituent. The product yield of ligand and complexes were collected in Table 6.

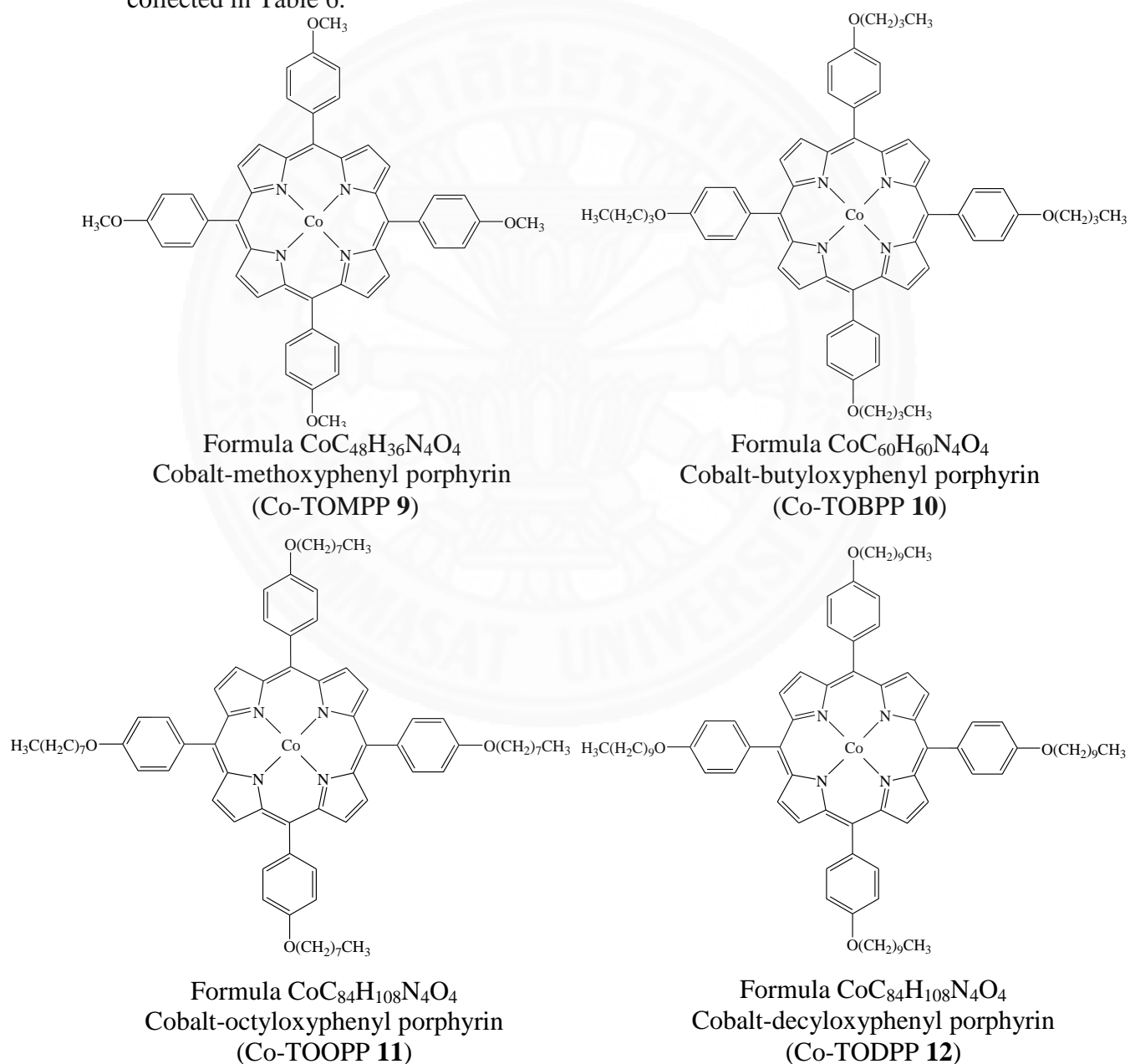


**Fig. 38** The structure of Co-TOBPP **9**, Co-TOBPP **10**, Co-TOOPP **11**, Co-TODPP **12**



However, the amount of free base porphyrins and cobalt(II) porphyrins actually produced from the reaction are usually be less than the theoretical yield due to the impurity by-products. In addition, the reactants were not completely converted to products and the desired product losses during the separation and purification in the purification process. The representative example scheme of TOMPP **4** and Co-TOMPP **9** were shown in Figure 39 and 40, respectively.

The ratio of the reaction compared the theoretical and actual yields. The percentage yield of the products calculated from by using this formula.

$$\% \text{yield} = (\text{actual yield} / \text{theoretical yield}) \times 100$$

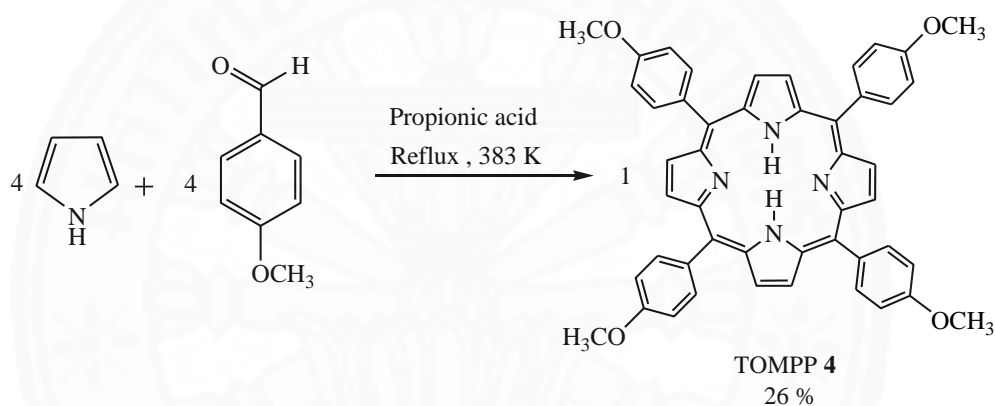


**Fig. 39** Synthesis of tetra-methoxyphenyl porphyrin (TOMPP **4**)

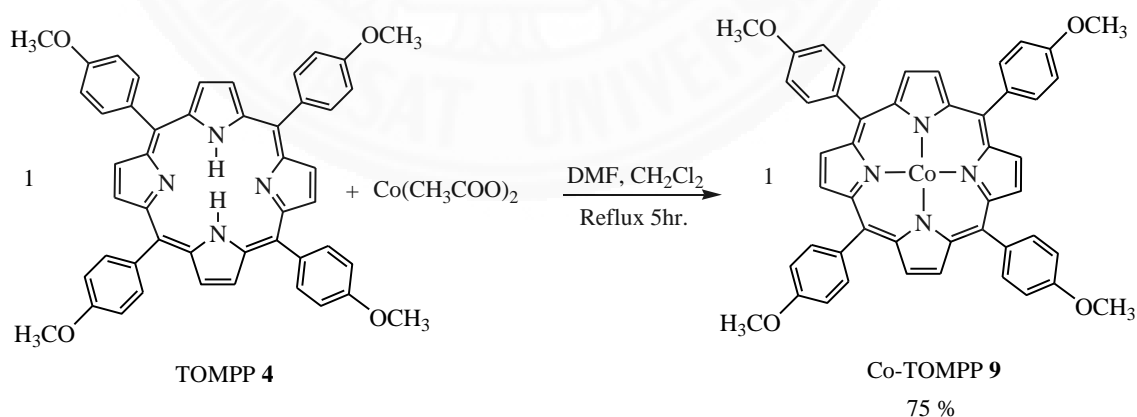


**Fig. 40** Synthesis of cobalt(II)-methoxyphenyl porphyrin (Co-TOMPP **9**)

**Table 6** Characteristic data for porphyrins and cobalt(II) porphyrins

Compounds	Empirical formula	Yield (%)	Elemental analysis ( <sup>a</sup> )%			Formula weight	MS (m/z) [M+H] <sup>+</sup>
			C	H	N		
TOMPP <b>4</b>	C <sub>48</sub> H <sub>38</sub> N <sub>4</sub> O <sub>4</sub>	26	76.42 (78.45)	5.75 (5.21)	7.42 (7.62)	734.84	735.23
TOBPP <b>5</b>	C <sub>60</sub> H <sub>62</sub> N <sub>4</sub> O <sub>4</sub>	5	79.44 (79.79)	6.55 (6.92)	5.83 (6.20)	903.16	904.16
TOOPP <b>6</b>	C <sub>76</sub> H <sub>94</sub> N <sub>4</sub> O <sub>4</sub>	13	81.10 (80.95)	8.25 (8.40)	4.93 (4.97)	1127.58	1129.47
TODPP <b>7</b>	C <sub>84</sub> H <sub>110</sub> N <sub>4</sub> O <sub>4</sub>	14	81.24 (81.37)	8.99 (8.94)	4.58 (4.52)	1239.80	1241.55
THPP <b>8</b>	C <sub>44</sub> H <sub>30</sub> N <sub>4</sub> O <sub>4</sub>	7	67.63 <sup>b</sup> (77.86)	5.13 <sup>b</sup> (4.46)	6.55 <sup>b</sup> (8.26)	678.73	679.33
Co-TOMPP <b>9</b>	CoC <sub>48</sub> H <sub>36</sub> N <sub>4</sub> O <sub>4</sub>	75	73.38 (72.81)	4.04 (4.58)	7.06 (7.08)	791.76	792.44
Co-TOBPP <b>10</b>	CoC <sub>60</sub> H <sub>60</sub> N <sub>4</sub> O <sub>4</sub>	92	75.24 (75.06)	6.09 (6.30)	5.78 (5.84)	960.08	961.05
Co-TOOPP <b>11</b>	CoC <sub>76</sub> H <sub>92</sub> N <sub>4</sub> O <sub>4</sub>	81	77.11 (77.06)	7.67 (7.83)	4.73 (4.73)	1184.50	1185.15
Co-TODPP <b>12</b>	CoC <sub>84</sub> H <sub>108</sub> N <sub>4</sub> O <sub>4</sub>	88	77.81 (77.81)	8.35 (8.40)	4.33 (4.32)	1296.71	1297.35

<sup>a</sup>Theoretical values are given in parentheses. <sup>b</sup>Mixed solvent (3:1, methanol: CH<sub>2</sub>Cl<sub>2</sub>) in THPP **8**.

#### 4.2.1 Elemental analysis

The elemental analysis for porphyrins, their derivatives and cobalt porphyrins were shown in the Table 6. The elemental analysis data for all porphyrins and cobalt porphyrins were confirmed the expected compound and were agreed with theoretical value. However, the THPP **8** was afforded to difference theoretical composition, due to the trace of mixed solvents (methanol: CH<sub>2</sub>Cl<sub>2</sub>, 3:1) in THPP **8** molecule, which was observed the solvent peaks in <sup>1</sup>H-NMR spectroscopy.

#### 4.2.2 Mass spectroscopy

The representative example mass spectrum of TOBPP **5** had the protonated molecule, [M+H]<sup>+</sup> at m/z 904.16 and the mass spectrum was shown in Fig. 41. The important mode fragmentation for TOBPP **5** was the loss of the hydrogen, yielding a strong M-1 peak. This peak appeared as the base peak (m/z 902.06) in the spectrum of TOBPP **5**. However, the spectra of the other free base porphyrins were obtained similarly in TOBPP **5** (shown in Appendix A). The mass spectra of all the porphyrins showed very intense molecular ion peaks because the fragmentation of porphyrins required a great deal of energy from the delocalization in macromolecules. Thus, such fragmentation was not observed to any significant extent. The characterization data of all the porphyrins were displayed in Table 6.

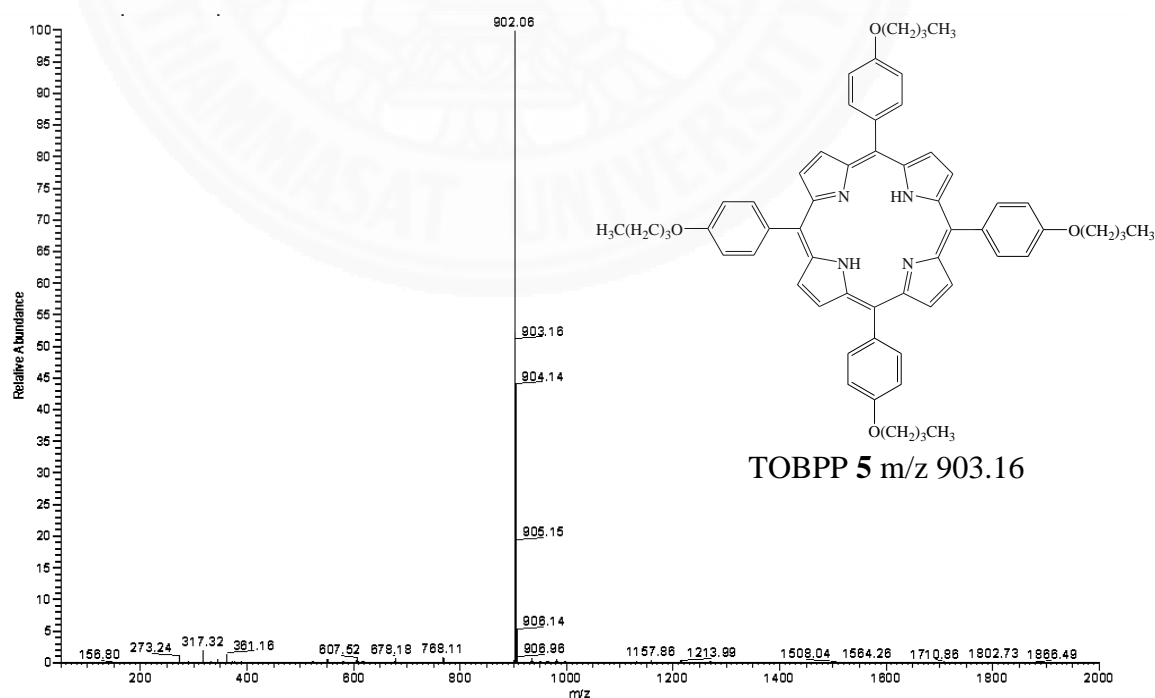


**Fig. 41** The mass spectrum of TOBPP **5**

In addition, the mass spectra of all cobalt(II) porphyrins were shown in Table 6. The representative sample mass spectrum of Co-TOBPP **10** (without purification, Fig. 42) strongly exhibit molecular ion peaks  $[M+H]^+$  at  $m/z$  961.05. This peak appeared as the base peak ( $m/z$  959.83). The mass spectra of all the cobalt(II) porphyrins were obtained similarly in free base porphyrins, showed very intense molecular ion peaks because they had high energy from the delocalization in molecule. The mass spectrum of Co-TOBPP **10** was showed the fragmentation that was related to the elimination of cobalt(II) ion from structure at  $m/z$  903.58. The later fractions were due to the alkyl chain group substituted, ether group and phenyl ring, respectively (Fig. 42). The mass spectra were successfully received to expect corresponding the porphyrins and cobalt porphyrins.

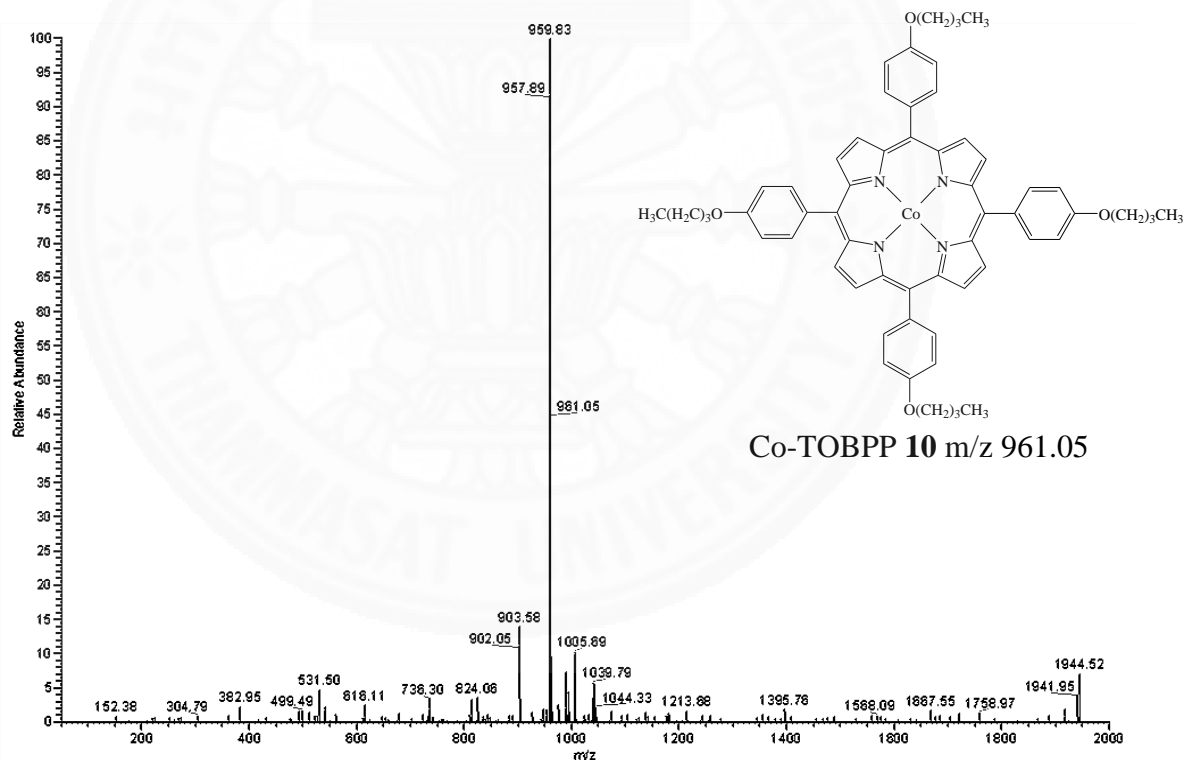
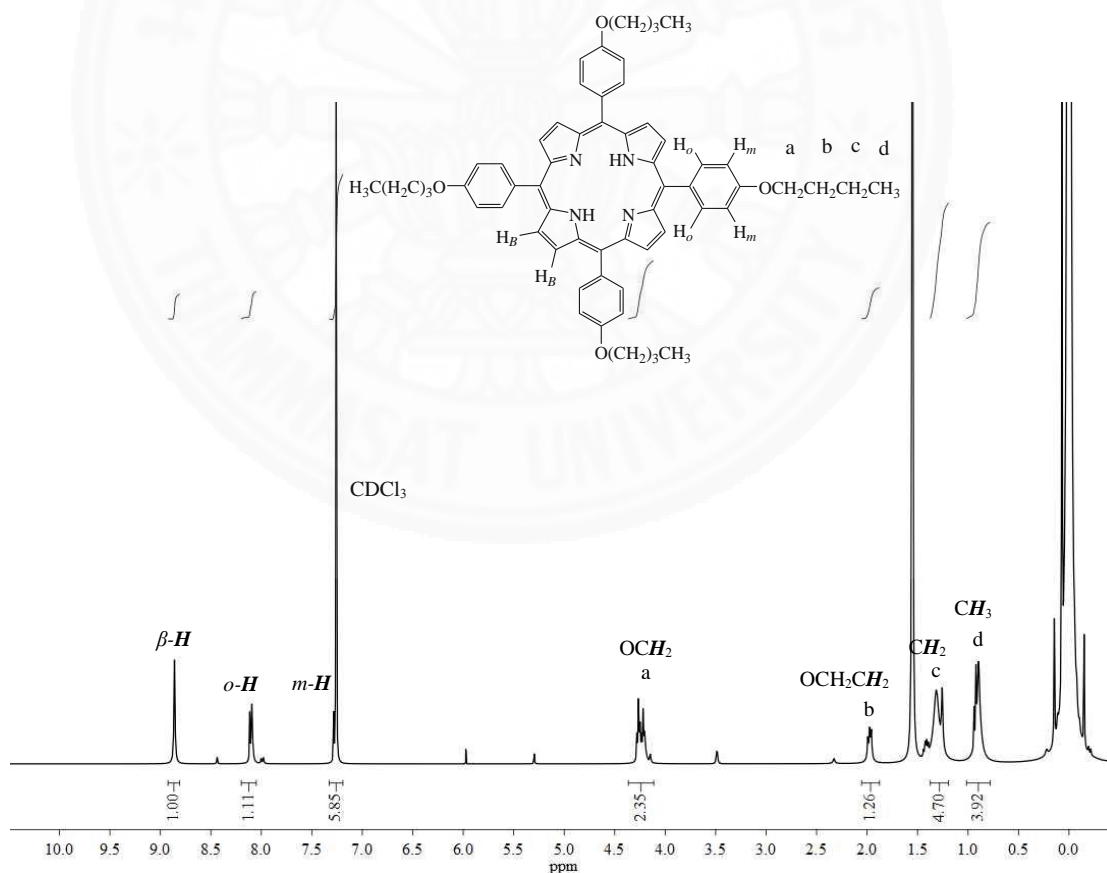


Fig. 42 The mass spectrum of Co-TOBPP **10**

### 4.2.3 NMR spectroscopy

The  $^1\text{H}$ -NMR and  $^{13}\text{C}$ -NMR spectra of all free base porphyrins (TOMPP **4**, TOBPP **5**, TOOPP **6**, TODPP **7** and THPP **8**) have been assigned by a comparison with reported data of TPP, TMPP and TOMPP [60-63]. At room temperature,  $^1\text{H}$ -NMR and  $^{13}\text{C}$ -NMR spectra of all the studied porphyrins were obtained in  $\text{CDCl}_3$  and/or  $\text{DMSO-d}_6$  solvent. The NMR spectral peak ( $^1\text{H}$  and  $^{13}\text{C}$ ), corresponding to the synthesized porphyrins, were selected and the chemical shifts were given in Table 7.

The deprotonation of free base porphyrins, all the  $\beta$ -pyrrole protons had similarly chemical shift at 8.86 ppm, which was slightly downfield shift from TPP [60]. Therefore, the deshielding of the  $\beta$  protons upon protonation of different substituted in porphyrins may related with of the donating electrons from substituent and the relative structurally induced changes in the porphyrin ring (TPP) [61].



**Fig.43** The  $^1\text{H}$ -NMR spectrum of TOBPP **5** in  $\text{CDCl}_3$

**Table 7**  $^1\text{H}$ -NMR and  $^{13}\text{C}$ -NMR spectroscopic data for free base porphyrins and cobalt porphyrins

porphyrins	$^1\text{H}$ -NMR (ppm)										
	Pyrrole, $\beta$ -H	Phenyl, <i>o</i> -H	Phenyl, <i>m</i> -H	OH	OCH <sub>3</sub>	OCH <sub>2</sub>	OCH <sub>2</sub> CH <sub>2</sub>	CH <sub>2</sub> CH <sub>3</sub>	CH <sub>2</sub> CH <sub>2</sub>	CH <sub>3</sub>	
TOMPP 4	8.86	8.12	7.29	-	4.10	-	-	-	-	-	
TOBPP 5	8.86	8.10	7.28	-	-	4.24	1.98	1.29	-	0.92	
TOOPP 6	8.86	8.10	7.26	-	-	4.24	1.99	1.36	1.26	0.91	
TODPP 7	8.86	8.10	7.29	-	-	4.23	1.98	1.33	1.26	0.88	
THPP 8	8.88	8.00	7.23	9.29	-	-	-	-	-	-	
porphyrins	$^{13}\text{C}$ -NMR (ppm)										
	Phenyl, <i>p</i> <sup>*</sup> -C	$\alpha$ -C	Phenyl, <i>o</i> -C	$\beta$ -C	Phenyl, <i>p</i> -C	<i>meso</i> -C	Phenyl, <i>m</i> -C	OCH <sub>3</sub>	OCH <sub>2</sub>	CH <sub>2</sub> (alkyl long chain)	CH <sub>3</sub>
TOMPP 4	158.75	134.68	133.99	129.97	127.89	118.83	111.44	54.65	-	-	-
TOBPP 5	159.12	135.50	134.64	130.89	128.75	119.77	112.87	-	68.17	31.60, 19.37	13.78
TOOPP 6	159.16	135.48	134.69	130.80	128.74	119.76	112.93	-	68.56	31.79, 29.57, 29.39, 29.19, 26.19, 22.55	13.84
TODPP 7	159.10	135.51	134.51	130.68	128.76	119.77	112.86	-	68.48	31.88, 29.60, 29.55, 29.53, 29.46, 29.28, 26.20, 22.60	13.93
THPP 8	157.43	135.68	133.31	130.99	128.80	120.16	114.04	-	-	-	-
Co(II) porphyrin	- <sup>a</sup>										
<b>9-12</b>											

<sup>a</sup>Unable to identify due to paramagnetic character in  $^1\text{H}$  and  $^{13}\text{C}$  NMR data.

The *ortho*- and *meta*- protons of the double bond in the phenyl group had chemical shift in the range from between 8.10 to 8.12 and 7.23 to 7.29 ppm, respectively. The effect of the *para*-alkyl substituted on the phenyl rings were identified with respect to the upfield shifts from TPP [64]. The effects of electron-donating groups were readily apparent within this set of *para*-substituted on phenyl group, found in previous reported [61]. The electron-donating groups, including X = -OH, -OCH<sub>3</sub>, -O(CH<sub>2</sub>)<sub>3</sub>CH<sub>3</sub>, -O(CH<sub>2</sub>)<sub>7</sub>CH<sub>3</sub>, and -O(CH<sub>2</sub>)<sub>9</sub>CH<sub>3</sub>, cause the protons in the phenyl ring to be more shielding (upfield chemical shifts). From the Table 7, the extent of shielding shows that the hydroxyl group had a greater inductive effect than the methoxy group and alkyloxy chain group, causing a greater increase in a  $\sigma$  electron density between the hydrogen bond.

The more shielding effect of singlet N-H peaks (due to the internal protons exchange of the N-H protons) were observed at very high field (-2.90 ppm), which were located within the shielding cone of the porphyrin ring and a higher cyclic consequently to a less twisted porphyrin core, comparing with TPP reported by Rae-Anne E.F. [64]. The results were accordance with the previous reported by Zabardasti A. [65].

The proton at *para*-substituent in TOMPP **4** (X= -OCH<sub>3</sub>) and THPP **8** (X= -OH) were assigned at 4.10 and 9.29 ppm, respectively. The alkyl protons in the short chain (TOBPP **5**) were found to be greater deshielded than the longer chain (TOOPP **6** and TODPP **7**), due to the inductive effect and the electron-donating of ether group in side chain. The similar results found in alkyloxybenzaldehyde. The spectrum of TOBPP **5** showed in Figure 43 as a representative example.

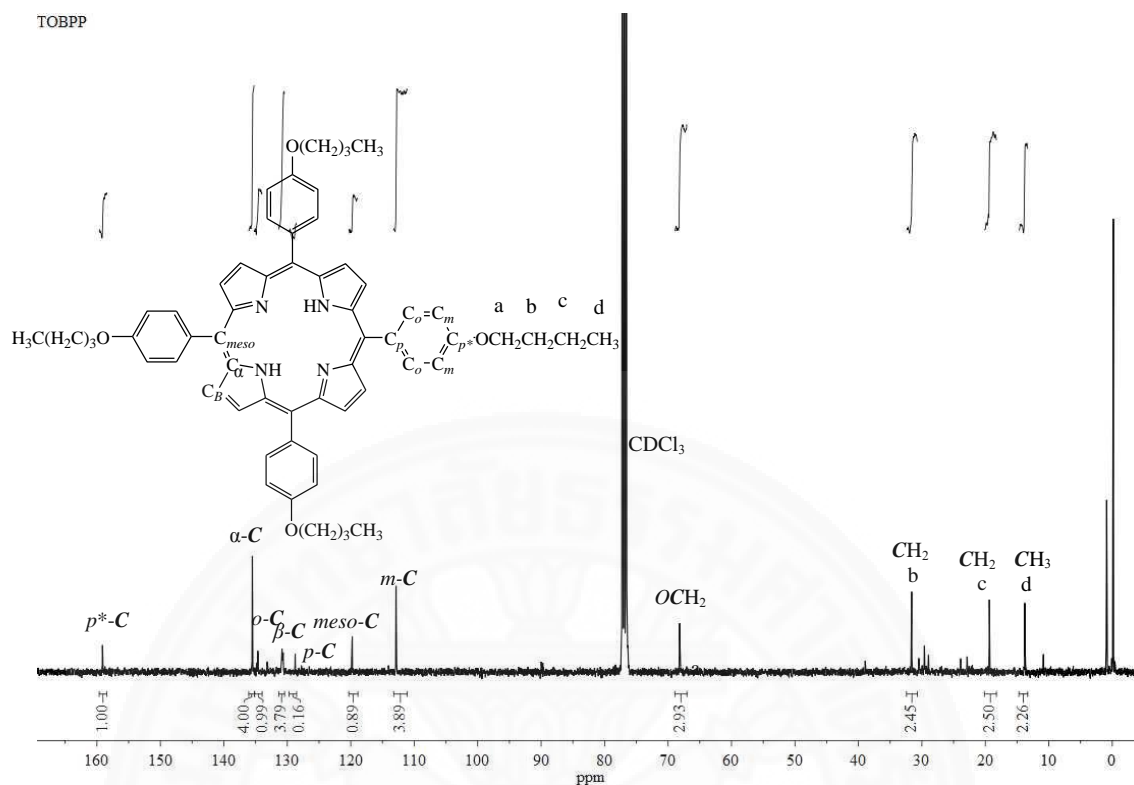


**Fig. 44** The  $^{13}\text{C}$ -NMR spectrum of TOBPP **5** in  $\text{CDCl}_3$

The  $^{13}\text{C}$ -NMR spectrum of TOBPP **5** was shown in Figure 44 as a representative example, by using  $\text{CDCl}_3$  as a solvent. The principal values of the  $^{13}\text{C}$  chemical shift obtained from the experiment were reported in Table 7.  $^{13}\text{C}$ -NMR spectrum of TOBPP **5** was assigned to sharp signals at 135.50 ( $\alpha$ -C, pyrrole), 130.89 ( $\beta$ -C, pyrrole), 119.77 (*meso*-C, methane bridge). The carbon of phenyl group were observed at 159.12 ( $p^*$ -C), 134.64 (*o*-C), 128.75 (*p*-C) and 112.87 ppm (*m*-C) whereas the carbon of alkyl long chain group was similar signals in porphyrins as shown in Table 7. However, the chemical shift of porphyrin ring carbons in pyrrole-C, phenyl-C, or alkyl chain-C were less than 2 ppm compared to other ligands. The  $^{13}\text{C}$  chemical shifts were related with the expected compound especially for TOMPP **4**, which found the same reported by I-chin L. and Jyn-horung C. [66].

In complexes of porphyrins with cobalt(II) ions, the chemical shifts was observed the broad peaks related with ligands information only. Cobalt(II) porphyrins were unsuccessful identified due to the paramagnetic cobalt porphyrin. Further analysis, including ESR spectroscopy, may require studying the information inside into the complexes.



#### 4.2.4 Infrared spectroscopy

IR spectra were recorded in KBr disc. The data were collected in the 4000-400  $\text{cm}^{-1}$  region. The infrared data was assigned in Table 8. The important silence signal of free base porphyrins showed N-H stretching and N-H bending vibrations in the range from 3316 to 3318  $\text{cm}^{-1}$ , and 965 to 967, respectively. While N-H stretching of THPP **8** had disappeared, causing the broadening O-H signal at 3450-3100  $\text{cm}^{-1}$  for the *para*-position substituted. When cobalt(II) ion was inserted into a porphyrin ring, the vibrations patterns changed, the N-H stretching and N-H bending disappeared on the account of replacement of two hydrogens in pyrrole ring by the cobalt(II) ion. From the Figure 45, the IR spectrum of ligand (TOBPP **5**) was compared with those of corresponding complexes (Co-TOBPP **10**). As mention above, the N-H stretching and bending N-H of ligand (TOBPP **5**) was found at 3316 and 695  $\text{cm}^{-1}$ , respectively. However, those two signals disappeared after cobalt(II) ion was inserted into the central hole of TOBPP **5** ligand and formed the Co-TOBPP **10** complex. Similar results found in the previous reported for M-TPP (M = Zn, Ni, Mg) [67].

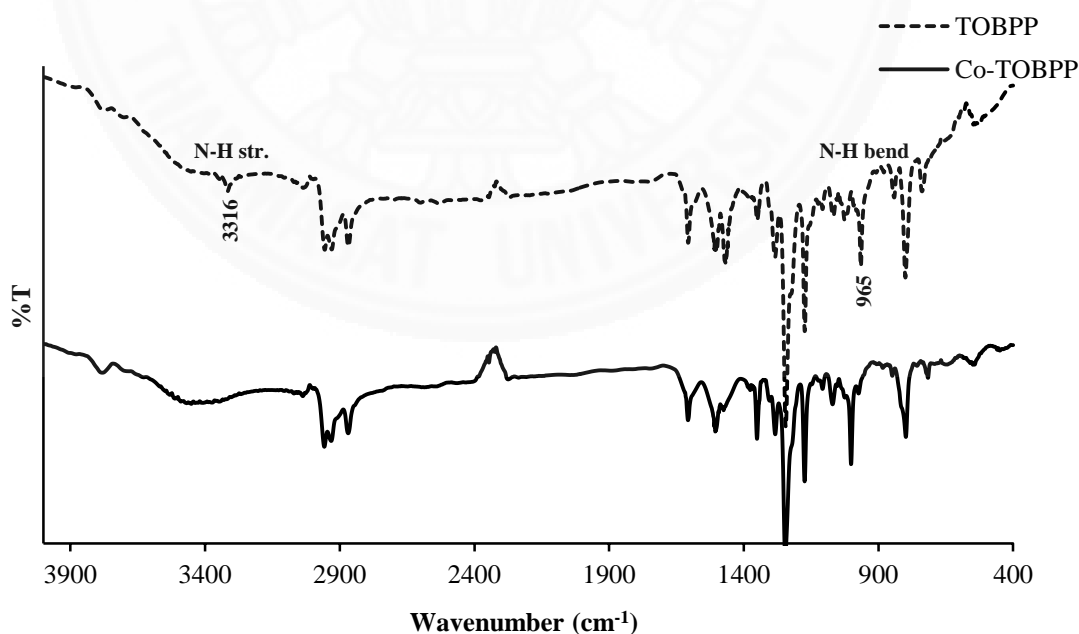


**Fig. 45** The IR spectra of TOBPP **5** and Co-TOBPP **10** in KBr

Furthermore, both ligand and cobalt complexes clearly displayed the C-H stretching (long chain) and C-N stretching in porphyrin ring. When increasing the number of carbon in alkyl chain substituted, those two signals found to slightly decrease due to the electronic effect of long chain substituent. The delocalization of the electrons porphyrin ring only results in the frequency shifts and intensity changes of IR spectra. The substituent saturated alkyl chain group showed electron delocalize from the *para* position of phenyl ring to the electronegativity of the porphyrin. For the ligand and complexes, the frequencies were observed downshifts of carbon in alkyl chain substituted group, which related to the interactions intrinsically decrease the bond strength of the molecule [68-70].

The similar features of the IR spectra between free base porphyrins and cobalt(II) porphyrins displayed with a little peak shift of three bands in the region as the C=C stretching in phenyl, C-O stretching in alkyl chain and C-H bending in porphyrin, respectively. Therefore, the free base ligand porphyrins were similar to those of the cobalt(II) porphyrins. The band observed at 1607 and 1509  $\text{cm}^{-1}$  (TOMPP **4**) were assigned to the vibration of the C=C stretching in phenyl, and the band ranged from 1171 to 1175  $\text{cm}^{-1}$  were assigned to the C-O stretching in alkyl chain group. The vibrations from 796 to 804  $\text{cm}^{-1}$  assigned to (C-H bending in porphyrin). Similar results found in the previous reported by Horng Y. J. [68].

**Table 8** The IR data of free base porphyrins and cobalt(II) porphyrins

Compounds	N-H str. in porphyrin	C-H str. in phenyl and long chain	C=C str. in phenyl	C-N str. in porphyrin	C-O str. in long chain	N-H bend in porphyrin	C-H bend in porphyrin	O-H broad in porphyrin
<b>TOMPP 4</b>	3317	2930, 2834	1607, 1509	1248	1175	967	803	-
<b>TOBPP 5</b>	3316	2930, 2870	1607, 1502	1244	1174	965	800	-
<b>TOOPP 6</b>	3318	2926, 2852	1607, 1501	1243	1174	966	804	-
<b>TODPP 7</b>	3318	2924, 2852	1606, 1509	1244	1175	967	804	-
<b>THPP 8</b>	-	2939, 2868	1604, 1478	1232	1171	967	803	3450-3100
<b>Co-TOMPP 9</b>	-	2933, 2833	1607, 1504	1248	1175	-	800	-
<b>Co-TOBPP 10</b>	-	2932, 2869	1607, 1506	1246	1174	-	798	-
<b>Co-TOOPP 11</b>	-	2928, 2853	1605, 1503	1244	1175	-	804	-
<b>Co-TODPP 12</b>	-	2924, 2853	1607, 1506	1242	1174	-	796	-

Unit =  $\text{cm}^{-1}$

#### 4.2.5 UV-Vis spectroscopy

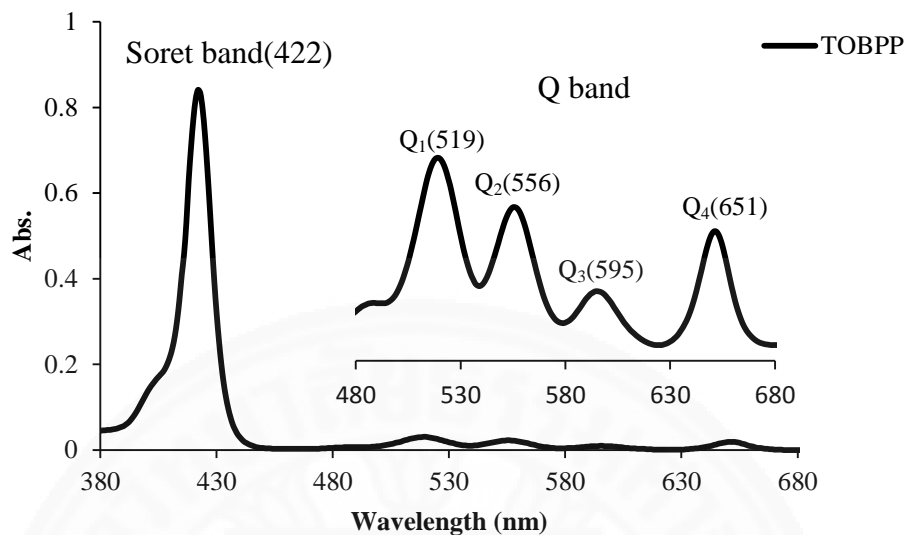


**Fig. 46** UV-Vis absorption spectrum of free base porphyrin (TOBPP **5**) in  $\text{CH}_2\text{Cl}_2$

Absorption spectra were acquired between 350 to 700 nm by using dichloromethane and methanol solvents. Absorption spectra of free base porphyrin (solutions **4-7**) were dissolved in dichloromethane, while THPP **8** was dissolved in methanol. The absorption intensity and the color of porphyrins were derived from the highly conjugated  $\pi$ -electron systems. The most attraction feature of porphyrins was their characteristic UV-Visible spectra that consist of two distinct regions; in the near ultraviolet is called the soret band (380-450 nm) and in the visible region is called Q band (500-700 nm). Both bands from  $\pi \rightarrow \pi^*$  electronic transitions, with the near-UV soret, the soret band with highest coefficient, corresponding to transitions from the ground state to a higher singlet excited state  $S_0 \rightarrow S_2$ . In the Q band region, ranged from 500 to 700 nm, the transitions correspond to  $S_0 \rightarrow S_1$  [71-72]. The example absorption spectra of free base porphyrin (TOBPP **5**) was shown in Fig. 46, with one soret band (S band) and four Q band wavelength and extinction coefficient ( $\epsilon$ ) values were summarized in Table 9. Comparing with the substituent in *para*-position phenyl of absorbance band (soret band and Q bands) of TOBPP **5** had similarly pattern for all free base porphyrins. Moreover, the attempts have been typed on solid state UV-Visible spectroscopy, ranged from 450 to 700 nm. The information revealed a similar pattern of Q band, found in solution.

In cobalt(II) porphyrins, the proton on NH group of porphyrin was deprotonated and then the nitrogen atom binds with cobalt ion to yield the metal-porphyrin. The cobalt ions acting as Lewis acids interact with the lone-pair electrons of porphyrin ligand. These observed intense absorption bands are involving the excitation of electrons from  $\pi$  to  $\pi^*$  porphyrin ring orbital [73], as shown in Figure 47. The absorption band of cobalt complexes displayed only one Q band, which is similar to the result found in solid state study. The results were shown in Table 9.

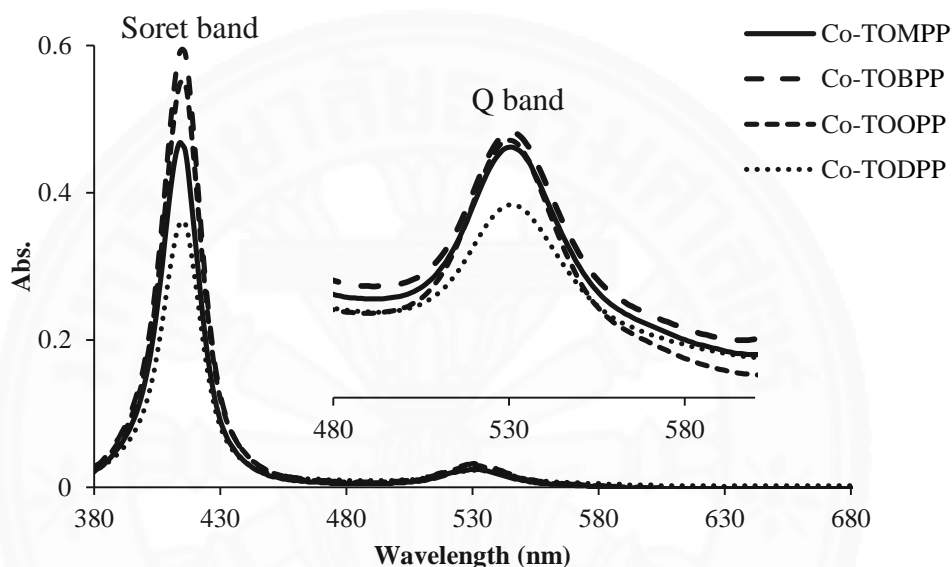


**Fig. 47** UV-Vis absorption spectra of all cobalt(II) complexes in  $\text{CH}_2\text{Cl}_2$

To study the effect of solvent, the absorption spectra of free base porphyrins and cobalt(II) porphyrins were analyzed by comparing solid state and dichloromethane solution. In both free base porphyrins and cobalt(II) porphyrins in dichloromethane, the four Q bands shifted to red. The observation suggested that revealed the influence of solvent, probably caused by hydrogen bonds established between the porphyrins and solvent molecules. The limitation of equipment the Soret band in solid analysis has been unsuccessful. Data were collected from 450 to 700 nm. The different absorption intensity for Q band both solutions and solid state may correspond to the solvent coordination, which influenced the small shift in band energy. As the experimental results, both steric hindrance and electron effects of the functional groups do not affect the changes in the UV-Vis absorption of free base porphyrins and complexes due to the *para*-substituted porphyrin as the similar electronegativity (electron-donating) moved slightly toward short wavelength.

**Table 9** The absorption data of porphyrins and cobalt complexes

Porphyrins	Dichloromethane <sup>a</sup>					Solid <sup>b</sup>			
	S band (nm)	Q band (nm), $\epsilon$ ( $10^3\text{M}^{-1}\text{cm}^{-1}$ )				Q band (nm)			
		Q <sub>1</sub>	Q <sub>2</sub>	Q <sub>3</sub>	Q <sub>4</sub>	Q <sub>1</sub>	Q <sub>2</sub>	Q <sub>3</sub>	Q <sub>4</sub>
TOMPP <b>4</b>	421	517, 24.0	556, 16.6	594, 7.6	651, 10.2	514	553	593	648
TOBPP <b>5</b>	422	519, 21.4	556, 16.2	595, 7.3	651, 13.6	514	551	595	647
TOOPP <b>6</b>	422	519, 20.0	556, 14.9	595, 6.7	651, 10.1	510	548	590	649
TODPP <b>7</b>	422	519, 16.7	556, 12.5	595, 5.5	651, 9.2	513	551	594	650
THPP <b>8</b> <sup>c</sup>	418	517, 17.2	555, 13.4	593, 6.0	650, 7.2	456	526	667	-
Co-TOMPP <b>9</b>	414	530, 17.3	-	-	-	519	-	-	-
Co-TOBPP <b>10</b>	415	531, 17.8	-	-	-	522	-	-	-
Co-TOOPP <b>11</b>	415	531, 16.8	-	-	-	515	-	-	-
Co-TODPP <b>12</b>	415	531, 12.9	-	-	-	525	-	-	-

<sup>a</sup> All solution were prepared in the concentration of  $3 \times 10^{-5}$  mol/L, ( $n=3$ , %RSD  $\leq 1.6$ ) and measured in the wavelength range of 350-700 nm. <sup>b</sup> All compounds were measured in the wavelength range of 450-700 nm. <sup>c</sup> methanol solvent.

#### 4.2.5 Fluorescence spectroscopy

Fluorescence spectroscopy of porphyrin derivatives were characterized in dichloromethane. The spectrum of TOBPP **5** was showed in Fig. 48. All porphyrins exhibited the enlargement of the  $\pi$ -conjugation yields the emission characteristics at the emission from 655 nm when excited at 530 nm as shown in Fig. 48. However, the current work selects the first Q band as the excitation wavelength, the spectra also showed strong fluorescence intensity. The cobalt complexes showed silence signal of emission spectra for all excitation wavelength.

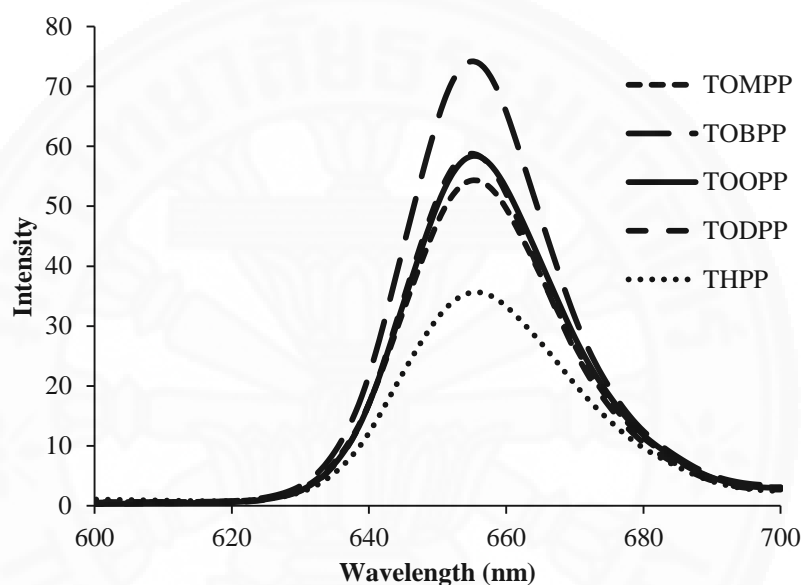


**Fig. 48** The emission spectra of free base ligands in dichloromethane

The term of band gap refers to the energy difference between the top of the valence band to the bottom of the conduction band, electrons are able to jump from one band to another. In order for an electron to jump from a valence band to a conduction band, it requires a specific minimum amount of energy for the transition, the band gap energy [73]. The estimated energy gap determined from an intersection of UV-Vis absorption ( $Q_4$  band) and fluorescence emission spectrum was following the equation [74]. The energy gap of TOBPP was 1.90 eV. The intersection of spectra of TOBPP **5** showed in Figure 49.

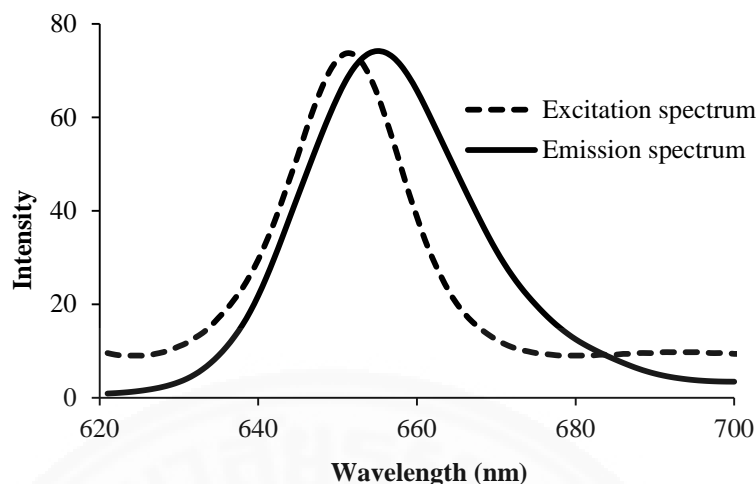


**Fig. 49** Excitation spectrum and emission spectrum of TOBPP **5** in  $\text{CH}_2\text{Cl}_2$

$$\text{Energy gap } (E_{\text{gap}}) = hc / \lambda$$

$$h = \text{Planks constant} = 6.626 \times 10^{-34} \text{ J}\cdot\text{s}$$

$$c = \text{speed of light} = 3.0 \times 10^8 \text{ m/s}$$

$$1 \text{ eV} = 1.602 \times 10^{-19} \text{ J}$$

**Table 10** The absorption-emission wavelength and the estimated energy gap of free base porphyrins in dichloromethane

Porphyrins	Dichloromethane		
	Absorption wavelength (nm)	Emission wavelength (nm)	$E_{\text{gap}}$ (eV)
TOMPP <b>4</b>	651	655	1.90
TOBPP <b>5</b>	651	655	1.90
TOOPP <b>6</b>	651	655	1.90
TODPP <b>7</b>	651	655	1.90
THPP <b>8</b>	650	655	1.90

Table 10 shows absorption-emission wavelength and the estimated energy gap of substituted long chain free base porphyrin **4-8**. The previous work by Barbara V. *et al.* reported the energy gap of TPP at 1.92 eV [74]. The substituted long chain of free base porphyrin, compounds 4-8, provided the lower energy gap at 1.90 eV. The smaller energy gap is related to the donating electrons of long chain



alkyl groups at *para* substituent in the ring. Furthermore, those electrons can delocalized through the ring and caused the smaller HOMO-LUMO gap.

#### 4.2.7 Thermal gravimetric analysis (TGA)

The free base porphyrins and cobalt(II) porphyrins were determined the decomposition temperature by using the thermogravimetric measurements, TGA under a nitrogen flow, in range 305-900 K. The TGA curves of TOBPP **5** and Co-TOBPP **10** were shown in Fig. 50. The first derivative curve showed the initial at temperature weight loss ranged from 680 to 699 K for ligand **4-7** and 373 K for THPP **8**. The second state of the weight loss found only for ligand TOMPP **4** and THPP **8**. The decomposition temperature ( $T_{decomp}$ ) of samples occurred between the initial temperature and temperature at loss a half of the initial weight [75].

Fig. 50 revealed that the process initiated to change curve of TOBPP **5** occurred in the decomposition temperature (stage I) at 688 K, while Co-TOBPP **10** as weight loss at 704 K showed the higher thermal decomposition than free base porphyrin (TOBPP **5**). The results of the decomposition temperature ( $T_{decomp}$ ) and weight loss with corresponding temperature were shown in Table 11.

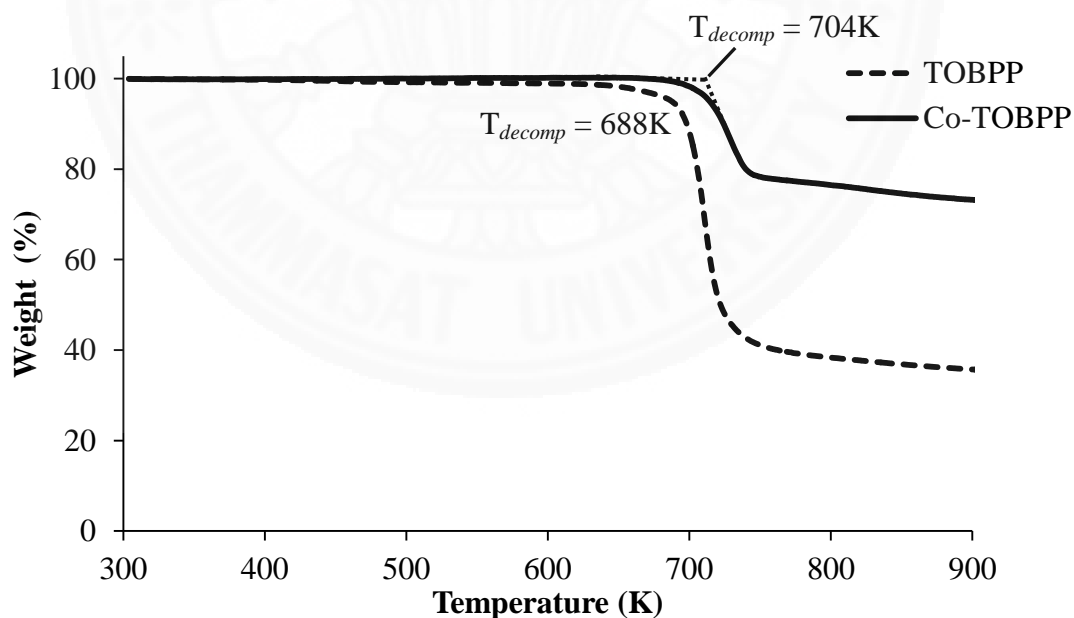


**Fig. 50** Thermogravimetric analysis (TGA) curves of TOBPP **5** and Co-TOBPP **10**

**Table 11** Temperatures of decomposition of free base porphyrins and cobalt(II) porphyrins

Compounds	Stage (I)		Stage (II)	
	T <sub>decomp</sub> /K	Weight loss/% (T <sub>f</sub> /K)	T <sub>decomp</sub> /K	Weight loss/% (T <sub>f</sub> /K)
TOMPP <b>4</b>	680 <sup>a</sup>	18.7 (738) <sup>a</sup>	738 <sup>a</sup>	81.6 (973) <sup>a</sup>
TOBPP <b>5</b>	688	60.1 (763)	-	-
TOOPP <b>6</b>	697	71.5 (783)	-	-
TODPP <b>7</b>	699	72.1 (763)	-	-
THPP <b>8</b> <sup>b</sup>	750	16.5 (873)	-	-
Co-TOMPP <b>9</b>	703	20.0 (873)	-	-
Co-TOBPP <b>10</b>	704	22.0 (755)	-	-
Co-TOOPP <b>11</b>	705	38.0 (752)	-	-
Co-TODPP <b>12</b>	708	45.2 (762)	-	-

T<sub>decomp</sub>: decomposition temperature, T<sub>f</sub>: final decomposition temperature, <sup>a</sup> Ref: Xiuhua W. *et.al.* (2006). *Thermochimica Acta.*, 440, 181-187. <sup>b</sup> THPP **8**; H<sub>2</sub>O loss at 373 K (15.7 %, T<sub>f</sub> = 570 K).

From the Table 11, the compounds **5-7** of free base porphyrins showed one-step weight loss with higher than 60 % weight loss. While the major weight loss of TOMPP **4** and THPP **8** occurred in two steps. The TOMPP **4** showed the initial little weight loss (18.7%) and observed the decomposition temperature at 680 K, attributed to remove the methoxy group. Then the loss weight found again at 738 K with 81.6 %, which was due to the complete disintegration of the porphyrin, the result found in previous reported by Xiuhua W. *et.al.* [76]. The TGA curve of THPP **8**, the weight loss of 15.7% observed at 373 K due to the elimination of small molecular impurity, which related to water or moist in the compound. The later weight loss of 16.3%, the highest thermal stability at 750 K obtained the decomposition of THPP **8** due to hydrogen bonding of the hydroxy group (electron withdrawing group) on *para*-position substituted. TGA curve of compounds **5-7** had the highly weight loss due to remove the decomposition of long chain alkyl group on methane bridges and phenyl group of porphyrin. The cobalt porphyrins **9-12** found to be more thermal stable than the previous free base. However, the small weight loss

(20-40 %) is referred to the only long chain alkane group ( $-C_nH_{2n+2}$ ). In addition, cobalt(II) porphyrins **9-12** exhibited only one step similarly thermal decomposition process to that of compound **5-7** in free base porphyrin as shown in Table 11.

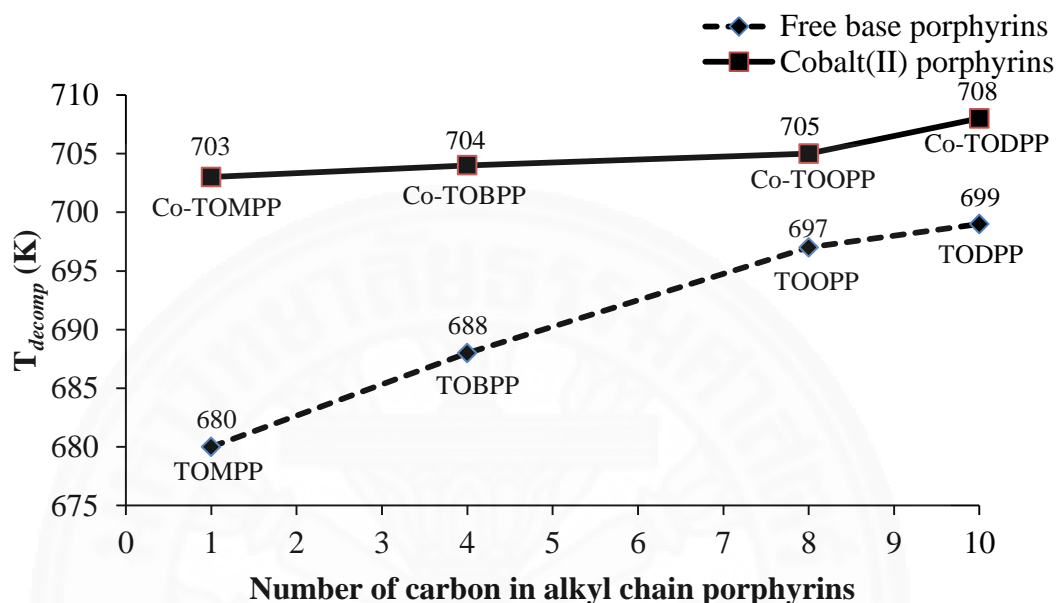


**Fig. 51** Correlation between decomposition temperatures with number of carbon in alkyl chain porphyrins

The first observation decomposition temperature of the free base porphyrins showed the highly thermal stability. The condensation of pyrrole with alkyl chain aldehyde will afford the remarkable stability to porphyrins, which decompose range from 680 to 699 K. The thermal stability trend of porphyrins were found that decomposition temperatures can be ranked as follows: TODPP **7** (699 K) > TOOPP **6** (697 K) > TOBPP **5** (688 K) > TOMPP **4** (680 K), related with the increasing number of carbon in alkyl chain on the *para*-position substituted. However, the decomposition temperature of cobalt(II) porphyrins were relatively higher compared to the free base porphyrins, as shown in Figure 51. The cobalt(II) porphyrins showed the thermal stability can be ranked as follows: Co-TODPP **12** (708 K) > Co-TOOPP **11** (705 K) > Co-TOBPP **10** (704 K) > Co-TOMPP **9** (703 K), which found that the similarly increasing with the number of carbon of free base porphyrin. The relationship was illustrated in Fig. 50. The decomposition temperature value of Co-TOMPP **9** is 23 K higher than the free porphyrin TOMPP **4**.

Co-TOMPP **9** showed the higher thermal stability (703 K) than pure ligand TOMPP **4** (680 K), suggesting the stronger bond in Co-TOMPP **9** due to ligand donate electron to metal ion.

The cobalt complexes showed the greater thermal stability than pure ligands that related to the distance between bonds (Co-N) in metal complexes and the cobalt ion fitted for the free base ligands. Therefore the cobalt ion in porphyrin ring was obtained that a shorter length of the same bonding type was related to stronger bonds in cobalt porphyrins [75]. Consider with TGA, metal complexes were interesting to use in alternative energy in section of solar cell and be a good choice in applications [76].

#### 4.2.8 X-ray crystal structure of tetrakis(4-butyloxyphenyl)porphyrin

The crystal structure of TOBPP **5**,  $C_{60}H_{62}N_4O_4$ , was determined by the single crystal X-ray crystallographic technique. The suitable crystals were obtained by direct method with mixed dichloromethane and hexane (1:1). The crystal data, intensity collection, and structure refinement were summarized in Table 12. The selected bond lengths and angles of porphyrin core were shown in Table 13. This compound was crystallized in the triclinic space group P-1. The porphyrin macrocycle of TOBPP **5** was composed of four pyrrole rings linked through methane carbon bridges and butyloxyphenyl group linked at *meso* position in porphyrin, which showed two disordered alkyl chain. The molecule structure of TOBPP **5** possessed a crystallographic inversion center. The porphyrin core is almost planar and the angle between adjacent pyrrole ring plane (C(4)–N(1)–C(1) and C(6)–N(2)–C(9)) is 5.50 °. The molecular structure of TOBPP **5** was shown in Fig. 52.

The molecular structure of TOBPP **5** is stabilized by intramolecular hydrogen bonds of 2.36 Å (N(2)–H(2)···N(1)) due to the imino H atoms form H-bond with the nearby unprotonated N atoms in porphyrin core as shown hydrogen-bonding geometry in Table 14 and Fig. 52. The molecular packing of TOBPP **5** was shown in Fig. 53. There are four significant C–H··· $\pi$  interactions between adjacent TOBPP **5** molecules in crystallographic *bc* plane leading to 2D network. Three of intermolecular C–H··· $\pi$  interactions between the hydrogen atoms of alkyl chain group and the centroids of pyrrole rings were observed along crystallographic *b* axis including C(25)–H(25)···Cg(2), C(28)–H(28B)···Cg(1) and C(16A)–H(16A)···Cg(1) of 2.80,

2.87 and 2.82 Å, respectively. The latter along *c* axis was observed C(16A)–H(16A)⋯Cg(4) of 2.97 Å between the centroid of phenyl groups at *meso* position porphyrin and hydrogen atom of alkyl chain group. Details of these interactions are shown in Table 14. However, the porphyrin rings have no significant  $\pi\cdots\pi$  interactions between the porphyrin rings due to the steric hindrance of alkyl chains around the porphyrin macrocycle. The packing view of TOBPP **5** in crystallographic *ac* plane is shown in Fig. 54. The steric hindrance of alkyl chains in TOBPP **5** was observed similarly in other porphyrin with alkyl long chain including tetrakis[4-(pentyloxy)phenyl]porphyrin and tetrakis[4-(heptyloxy)phenyl]porphyrin found in the previous reported by Hua C. and Hong-Bin Z., respectively [39,40].

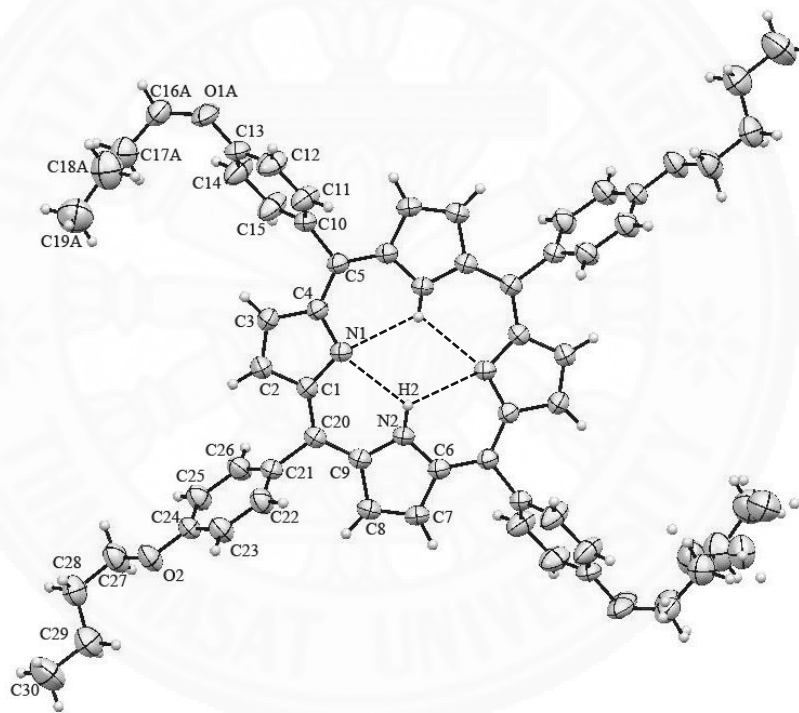


**Fig. 52** The molecular structure of TOBPP **5**, showing 50 % probability displacement ellipsoids and labeling atoms of the asymmetric unit

**Table 12** Crystal data and structure refinement for TOBPP 5

Crystal data	
Compound	Tetrakis(4-butyloxyphenyl)porphyrin
Identification code	TOBPP
Color	Purple
Empirical formula	C <sub>60</sub> H <sub>62</sub> N <sub>4</sub> O <sub>4</sub>
Formula weight	903.16
Temperature/K	296(2)
Crystal system	triclinic
Space group	P-1
a/Å	10.8525(4)
b/Å	11.5883(5)
c/Å	11.8793(5)
α/°	103.2870(13)
β/°	101.6890(13)
γ/°	113.5140(12)
Volume/Å <sup>3</sup>	1258.66(9)
Z	2
ρ <sub>calc</sub> /g/cm <sup>3</sup>	1.110
μ/mm <sup>-1</sup>	0.071
F(000)	421.0
Crystal size/mm <sup>3</sup>	0.28 × 0.28 × 0.2
Radiation	MoKα (λ = 0.71073)
2θ range for data collection/°	6.418 to 50.756
Index ranges	-13 ≤ h ≤ 12, -13 ≤ k ≤ 13, -14 ≤ l ≤ 14
Reflections collected	22911
Independent reflections	4602 [R <sub>int</sub> = 0.0328, R <sub>sigma</sub> = 0.0234]
Data/restraints/parameters	4602/432/356
Goodness-of-fit on F <sup>2</sup>	1.016
Final R indexes [I ≥ 2σ (I)]	R <sub>1</sub> = 0.0500, ωR <sub>2</sub> = 0.1224
Final R indexes [all data]	R <sub>1</sub> = 0.0737, ωR <sub>2</sub> = 0.1376
Largest diff. peak/hole / e Å <sup>-3</sup>	0.37/-0.17

**Table 13** Selected geometric parameters (Å, °) of TOBPP **5**

Bond lengths (Å)			
N(1)–C(1)	1.373(2)	N(2)–C(6)	1.373(2)
N(1)–C(4)	1.373(2)	N(2)–C(9)	1.368(2)
Bond angles (°)			
C(4)–N(1)–C(1)	106.10(14)	C(6)–N(2)–H(2)	125.04
C(6)–N(2)–C(9)	109.90(14)	C(9)–N(2)–H(2)	125.06

**Table 14** Selected intra/intermolecular interactions in TOBPP **5** (Å, °)

Donor–H $\cdots$ Acceptor	D–H (Å)	H $\cdots$ A (Å)	D $\cdots$ A (Å)	D–H $\cdots$ A (°)
N(2)–H(2) $\cdots$ N(1)	0.86	2.36	2.904(2)	121
N(2)–H(2) $\cdots$ N(1) <sup>i</sup>	0.86	2.39	2.925(2)	121
CH $\cdots$ $\pi$ interaction		H $\cdots$ Cg (Å)	X $\cdots$ Cg (Å)	X–H $\cdots$ Cg (°)
C(25)–H(25) $\cdots$ Cg(2)		2.80	3.635(2)	150
C(28)–H(28B) $\cdots$ Cg(1)		2.87	3.672(3)	141
C(16A)–H(16A) $\cdots$ Cg(4)		2.97	3.93(2)	176
C(16A)–H(16A) $\cdots$ Cg(1)		2.82	3.68(2)	147

Symmetry code: (i) -x, -y+1, -z+2

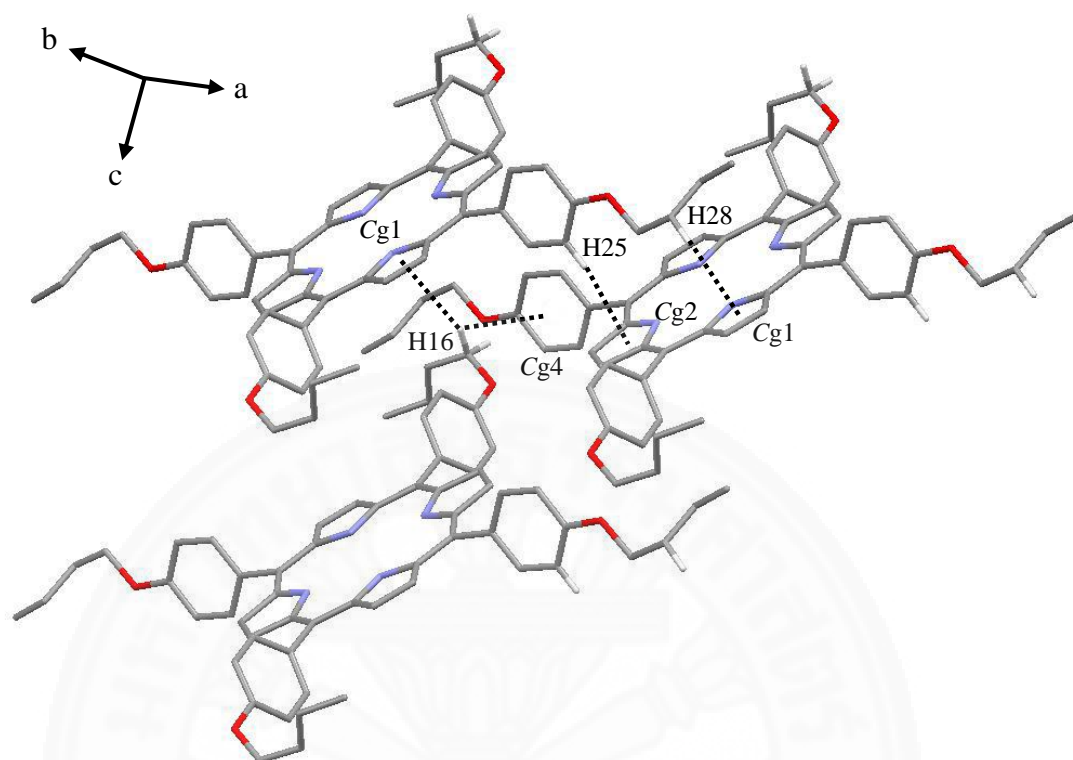


**Fig. 53** View of C-H... $\pi$  interactions in crystallographic *bc* plane, forming the 2D network of TOBPP 5



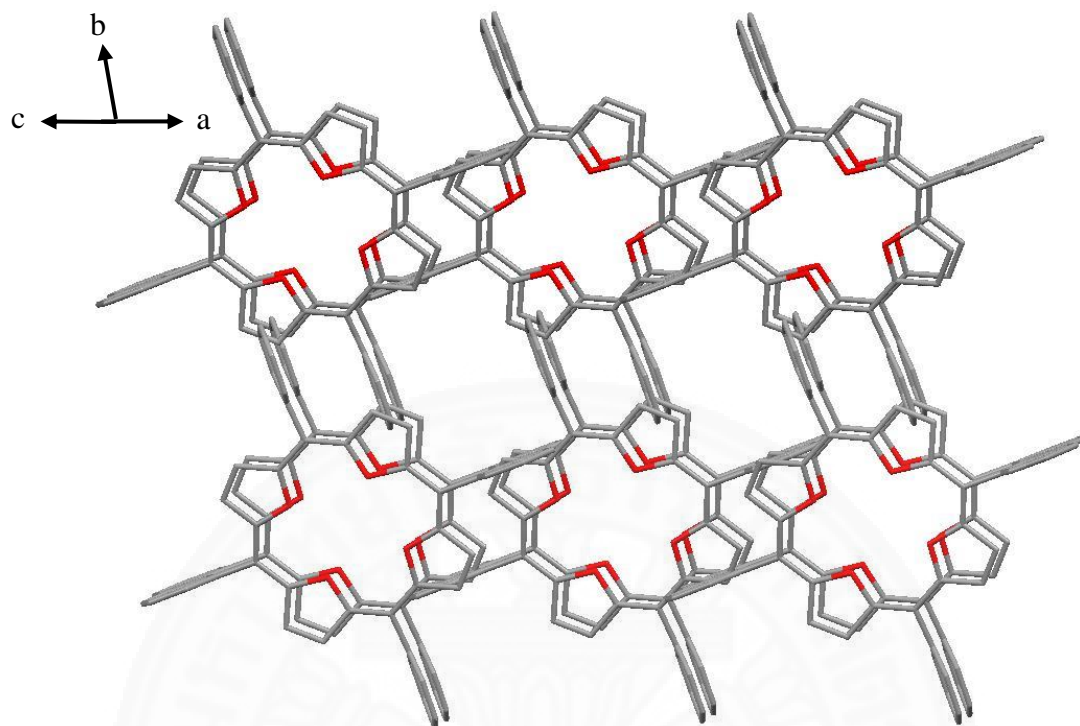


**Fig. 54** The packing view of the porphyrin (TOBPP 5) in crystallographic *ac* plane, showing very weak  $\pi \cdots \pi$  interactions between TOBPP molecules. All H atoms and alkyl chains group have been omitted for clarity.

## CHAPTER 5

### CONCLUSIONS AND RECOMMENDATIONS

The aldehydes with long chain alkane were prepared from a modification previously published works by Ioannis D.K. The purified products were structure confirmed by mass spectrometry (MS),  $^1\text{H}$  and  $^{13}\text{C}$ -NMR, and IR spectroscopy. The alkyloxybenzaldehydes (compounds **1-3**) gave the relatively high reaction yields as over 90 %.

The novel alkyl chain porphyrins were synthesized by a modification of the published Adler-Longo method. The yields of various substituents on *para*-position of phenyl ring in porphyrins (TOMPP **4**, TOBPP **5**, TOOPP **6**, TODPP **7** and THPP **8**) at optimal condition (refluxing in propionic acid) were obtained range 5 to 26%. While TOMPP **4** obtained the highest yield as 26 %. Furthermore, the cobalt(II) porphyrins were prepared by refluxing *N, N*-dimethylformamide with free base porphyrins and followed by adding cobalt(II) acetate. The reactions of ligands with cobalt(II) ions gave Co-TOMPP **9**, Co-TOBPP **10**, Co-TOOPP **11** and Co-TODPP **12** in 75%, 92%, 81% and 88% yields, respectively. The cobalt(II) porphyrins had a greater yield than the free base porphyrins, due to the metal ionic size of the cobalt(II) ion, that fitted into the central hole ligand. The porphyrins and cobalt(II) porphyrins were confirmed the expected synthesized structure by elemental analysis (CHN), mass spectrometry (MS),  $^1\text{H}$  and  $^{13}\text{C}$ -NMR, IR spectroscopy and single crystal X-ray analysis.

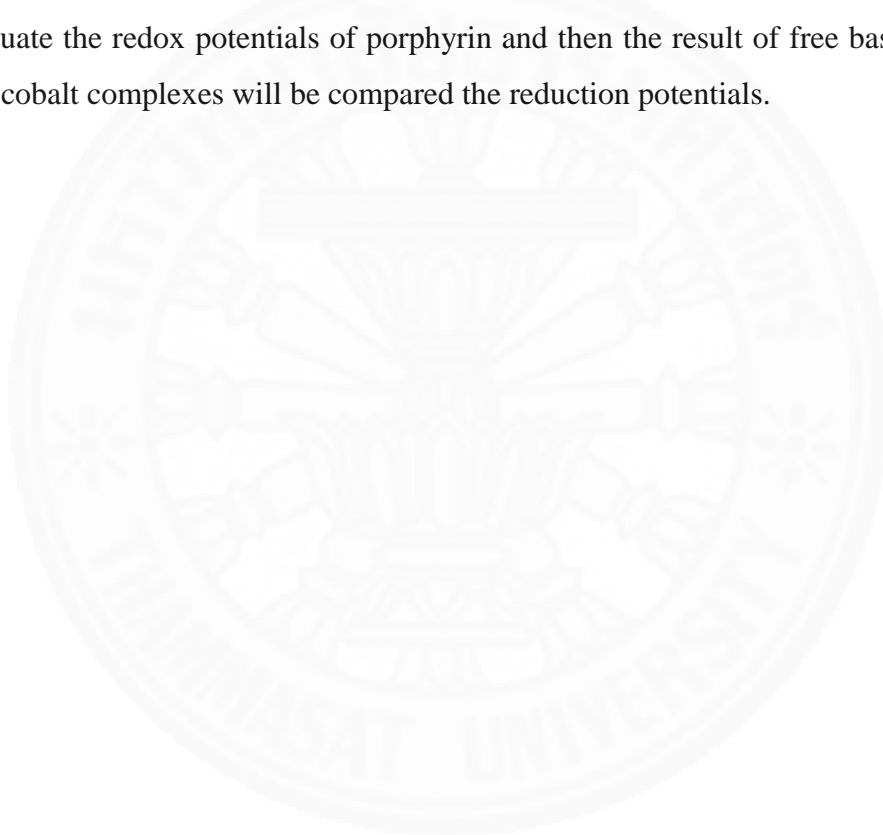
The UV-Vis absorption spectra for porphyrins long chain exhibited a single S band with four Q band, which the cobalt complexes show a single S band couple with only one Q band in the solution and solid state. In the all free base porphyrins and cobalt(II) porphyrins in dichloromethane showed the four Q bands (shifted to red shift compared with solid information). The observation suggested that revealed the influence of solvent, probably caused by hydrogen bonds established between the porphyrins and solvent molecules. When excitation of the porphyrin long chain at 530 nm, the products showed the emitted fluorescence spectra at 655 nm. The energy gap of free base porphyrins was 1.90 eV. The thermal behaviors including the

possible phase transition of porphyrins were studied during the heating process at lower temperature (298-873 K). All porphyrins and cobalt(II) porphyrins were found to be the highly thermal stability as over 680 K (TOMPP 4). The cobalt complexes had greater thermal stability than pure ligands. Therefore, cobalt(II) porphyrins might be interesting to be used in alternative energy technology including solar cell applications.



## **FUTURE WORK**

In view of this, the following points for future work will be determined. First, this complexes of porphyrins with cobalt ions were unsuccessful identified in NMR spectroscopy due to the paramagnetic cobalt porphyrins. Further analysis, including ESR spectroscopy, may require studying the properties inside into the complexes. Second, electrochemical properties of free base porphyrins and metalloporphyrins will be studied by cyclic voltammetric techniques. Therefore, it can evaluate the redox potentials of porphyrin and then the result of free base porphyrins and cobalt complexes will be compared the reduction potentials.



## REFERENCES

1. Milgrom L. R. (1997). The colours of life: an introduction to the chemistry of porphyrins and related compounds. *Oxford University Press, Oxford*.
2. Abraham R. J., Medforth C. J., Mansfield K. E., Simpson D. J. and Smith K.M. (1988). Perkin Transactions 2. *Journal of the Chemical Society*, 1365.
3. Buchler J.W. (1978). The porphyrins. *Dolphin. D. Ed. Academic press, New York*, 389-483.
4. Collman J.P., Hallbert T.R. and Suslick K.S. (1980). Metal ion activation of dioxygen. *In Metal Ions in Biology*, 2.
5. Kaim W., Schwederski B. (2005). *Bioanorganische Chemie*, 4<sup>th</sup>.
6. Messerschmidt A., Huber R., Poulos K. and Wieghardt K. (2001). Handbook of metalloproteins.
7. Bertini I., Gray H.B. (2007). *Biological Inorganic Chemistry* (University Science Books, Sausalito)
8. Heme -<http://en.wikipedia.org>. Retrieved September 10, 2014.
9. Heme -<http://www.bio.davidson.edu>. Retrieved September 10, 2014.
10. Chlorophyll -<http://www.ch.ic.ac.uk>. Retrieved September 10, 2014.
11. Chlorophyll -<http://www.bio.umass.edu>. Retrieved September 10, 2014.
12. Vitamin B12 -<http://en.wikipedia.org>. Retrieved September 10, 2014.
13. Vitamin B12 -<http://www.healthaliciousness.com>. Retrieved September 10, 2014.
14. Farber G., Keller W., Kratky C., Jaun B., Pfaltz A., Spinner C., Kobelt A. and Eschenmoser A. (1991). Coenzyme F<sub>430</sub> from methanogenic bacteria: complete assignment of configuration based on an X-ray analysis of 12,13-diepi-f<sub>430</sub> pentamethyl ester and on NMR Spectroscopy. *Helvetica Chimica Acta*, 74, 697-716.
15. Fischer H. and Gleim W. (1936). Synthese des porphins. *European Journal of Organic Chemistry*, 521, 157-160.
16. Rothmund P. (1935). Formation of porphyrins from pyrrole and aldehydes. *Journal of the American Chemical Society*, 57, 2010-2011.
17. Rothmund P. (1936). A new porphyrin synthesis. The synthesis of porphin. *Journal of the American Chemical Society*, 58(4), 625-627.

18. Adler A.D., Longo F. R. and Shergalis W. (1964). Mechanistic investigations of porphyrin syntheses I. Preliminary studies on me-tetraphenylporphin. *Journal of the American Chemical Society*, 86, 3145.
19. Lindsey J.S., Hsu H.C. and Schreiman I.C. (1986). Synthesis of Tetraphenylporphyrins Under Very Mild Conditions. *Tetrahedron Letters*, 27, 4969.
20. Arsenault G.P., Bullock E. and MacDonald S.F. (1960). Pyrromethanes and porphyrins therefrom<sup>1</sup>. *Journal of the American Chemical Society*, 82, 4384.
21. Boudif A. and Momenteau M. (1994). Synthesis of a porphyrin-2, 3-diacrylic acid using a new "3+1" type procedure. *Journal of the Chemical Society, Chemical Communications*, 2069.
22. Meunier (1992). Metalloporphyrins as versatile catalysts for oxidation reactions and oxidative DNA cleavage. *Chemical Reviews*, 92, 1411.
23. Wagner R. and Lindsey (1994). A molecular photonic wire. *Journal of the American Chemical Society*, 116, 9759.
24. Kurreck H. and Huber M. (1995). Model reactions for photosynthesis- photoinduced charge and energy transfer between covalently linked porphyrin and quinine units. *Angewandte Chemie International Edition*, 34, 849.
25. Dolmans D.E., Fukumura D. and Jain R.K. (2003). Photodynamic therapy for cancer. *Nature Reviews Cancer*, 3, 380-387.
26. Krammer B. (2001). Vascular effects of photodynamic therapy. *Anticancer Research*, 21, 4271-4277.
27. Brumbach M.T., Boal A.K. and Wheeler D.R. (2009). Metalloporphyrin assemblies on pyridine-functionalized titanium dioxide. *Langmuir article*, 25, 10685-10690.
28. Shargh H. and Nejad A.H. (2004). Novel synthesis of meso-tetraarylporphyrins using CF<sub>3</sub>SO<sub>2</sub>Cl under aerobic oxidation. *Tetrahedron*, 60, 1863-1868.
29. Siriorn P., Amorn P. and Patchanita T. (2009). A porphyrin derivative from cardanol as a diesel fluorescent marker. *Dyes and Pigments*, 82, 26-30.
30. Ana C.B.F., Kleber T.O. and Osvaldo A.S. (2011). New porphyrins tailored as biodiesel fluorescent markers. *Dyes and Pigments*, 91, 383-388.

31. Zhi X., Priscilla P.S.L., Yanming W., Daniel W.J.K., Jing L., John H.X., Wai-Kwok W. and Kevin K.L.C. (2011). Further insight into aryl nitration of tetraphenylporphyrin. *Tetrahedron*, *67*, 6030-6035.
32. Temelli B. and Unaleroglu C. (2009). Synthesis of *meso*-tetraphenyl porphyrins via condensation of dipyrromethanes with *N*-tosyl imines. *Tetrahedron*, *65*(10), 2043-2050.
33. Ya-hong W., Lin C., Jian Y., Shan-ling T. and Yan Y. (2013). Synthesis and spectroscopic characterization of *meso*-tetra (Schiff-base substituted phenyl) porphyrins and their zinc complexes. *Dyes and Pigments*, *97*, 423-428.
34. Ana P.J. Antonio C.T., Cláudio R.N., Maria E.F.G., Osvaldo A.S. and Yassuko I. (2004). Synthesis, spectroscopy and photosensitizing properties of hydroxyl nitrophenylporphyrins. *Journal of the Brazilian Chemical Society*, *15*, 708-713.
35. Yuichi T., Brian O. P. and David H.D. (2002). Synthesis, crystal structures, and redox potentials of 2,3,12,13-tetrasubstituted 5,10,15,20-tetraphenylporphyrin zinc(II) complexes. *Inorganic Chemistry*, *41*, 6703-6710.
36. Irina N.F., Bragina N.A., Novikov N.V., Ugol'nikova O.A. and Miron A.F. (2007). Synthesis of lipophilic tetraphenylporphyrins to design lipid-porphyrin ensembles. *Russian Journal of Bioorganic Chemistry*, *33*, 635-639.
37. Irina N.F. Natalya A.B., Nikita V.N., Andrey F.M., Venera V. B., Nadezhda V.U. and Galina A.A. (2008). Synthesis and mesomorphism of tetraphenyl porphyrin derivatives. *Mendeleev Communications*, *18*, 324-326.
38. Kirill A.F., Natal'ya A.B. Andrey F.M., Galina A.A., Venera V.B. and Nadezhda V.U. (2011). Novel alkoxyaryl substituted porphyrins with terminal carboxymethyl and carboxy groups: synthesis and mesomorphic properties. *Macroheterocycles*, *4*(2), 127-129.
39. Hua C., Hong-Bin Z., Fu-Hui Z., Jie-Pin L. and Yan-Li L. (2009). Crystal structure of *meso*-tetrakis [4-(pentyloxy)phenyl] porphyrin. *Journal of Chemical Crystallography*, *39*, 51-54.
40. Hong-Bin Z., Liang C., Bang-Ying W., Jun-Xu L. and Yong-Jun X. (2013). *meso*-Tetrakis[4-(heptyloxy)phenyl]porphyrin. *Acta Crystallographica*, *C69*, 651-653.

41. Jun-Xu L., Hong-Bin Z., De-Liang Y., Liang C. and Bang-Ying W. (2011). {*meso*-Tetrakis[*p*-(heptyloxy)phenyl]porphyrinato}silver(II). *Acta Crystallographica*, *E67*.
42. Wei L., Yuhua S., Tongshun S., Guofa L., Yongxin L., Ce W. and Wangjin Z. (2013). Synthesis and characterization of liquid crystalline 5,10,15,20-tetrakis(4-n-alkanoyloxyphenyl)porphyrins. *Liquid Crystals*, *30*, 1255-1257.
43. Amrita G., Selvamani T., Jose D.A., Amitava D. and Mukhopadhyay I. (2007). Generation of nanostructures by the aggregation of porphyrin derivatives with long alkane chain in mix-solvent. *Journal of Nanomaterials*.
44. Renu G. and Chauhan S.M.S. (2014). Surfactant assisted self-assembly of zinc 5,10-bis (4-pyridyl)-15,20-bis(4-octadecyloxyphenyl) porphyrin into supramolecular nanoarchitectures. *Materials Science and Engineering C*, *43*, 447-457.
45. Ekaterina S.Z., Natalya A.B. and Andrey F.M. (2012). Covalent-bound conjugates of fullerene C<sub>60</sub> and metal complexes of porphyrins with long-chain substituents. *Mendeleev Communications*, *22*, 257-259.
46. Ioannis D.K., Athanassios G.C., Georgios C. and Aggeliki S. (2007). The first use of porphyrins as catalysts in cross-coupling reactions: a water-soluble palladium complex with a porphyrin ligand as an efficient catalyst precursor for the Suzuki-Miyaura reaction in aqueous media under aerobic conditions. *Tetrahedron Letters*, *48*, 6688-6691.
47. Nikita V.N., Kirill A.F., Natalya A.B., Andrey F.M., Galina A.A., Venera V.B. and Nadezhda V.U. (2010). Synthesis and mesomorphism of cationic derivatives of *meso*-aryl-substituted porphyrins and their metal complexes. *Mendeleev Communications*, *20*, 239-241.
48. Beat H. and Reinhard N. Synthesis and characterization of  $\pi$ -extended porphyrins as potential precursors for the formation of columnar mesophases: Design principles for columnar mesophases need revision?. *Archive for Organic Chemistry*, *6*, 29-44.
49. Ana V.C.S., Agnieszka A., Janusz M.D., Mario J.F.C., Artur R.A., Grazyna S., Luis G.A. and Mariette M.P. (2012). Amphiphilic *meso*(sulfonate ester fluoroaryl) porphyrins: refining the substituents of porphyrin derivatives for phototherapy and diagnostics. *Tetrahedron*, *68*, 8767-8772.



50. Pan M., Yanli C., Xue C., Hailong W., Yuexing Z., Yingning G. and Jianzhuang J. (2010). Organic field effect transistors based on 5,10,15,20-tetrakis(4-pentyloxyphenyl)porphyrin single crystal. *Synthetic Metals*, 160, 510-515.
51. Bianca S., Claudenilson S.C., Thiago M.B.F.O., Francisco W.P.R., Felipe J.P., Selma E.M., Pedro L., Adriana N.C., Christiana A.P. and Karen W. (2013). Amphiphilic porphyrin-cardanol derivatives in Langmuir and Langmuir-Blodgett films applied for sensing. *Colloids and Surfaces A: Physicochemical and Engineering Aspects*, 425, 68-75.
52. Xiliang G., Wenting A., Shaomin S., Fangqin C. and Chuan D. (2005). Study on spectroscopic characterization of *meso*-tetrakis (4-hydroxyphenyl) porphyrin (THPP) in  $\beta$ -cyclodextrin and its derivatives. *Journal of Photochemistry and Photobiology A: Chemistry*, 173, 258-263.
53. Domingues M.R.M., S.-Marques M.G.O., Carla A.M.V., Neves M.G., Cavaleiro J.A.S. and Ferrer-Correia A.J. (1999). Do charge-remote fragmentations occur under matrix-assisted laser desorption ionization post-source decompositions and matrix-assisted laser desorption ionization collisionally activated decompositions?. *Journal of The American Society for Mass Spectrometry*, 10, 217-223.
54. Reis A., Domingues P. and Domingues M.R.M. (2013). Structural motifs in primary oxidation products of palmitoyl-arachidonoyl-phosphatidylcholines by LC-MS/MS. *Journal of Mass Spectrometry*, 48, 1207-1216.
55. Aline T., Paulo H.S. and Aloir A.M. (2009). 3,5-Disubstituted isoxazolines as potential molecular kits for liquid-crystalline materials. *European Journal of Organic Chemistry*, 889-897.
56. Aline T., Paolo R.L., Paulo F.B.G. and Aloir A.M. (2009). 3-arylisoxazolyl-5-carboxylic acid and 5-(hydroxymethyl)-3-aryl-2-isoxazoline as molecular platforms for liquid-crystalline materials. *Journal of the Brazilian Chemical Society*, 20, 1742-1752.
57. Mayank J.M., Javed G.M., Juvansinh J.J., Rohit B.M., Manish K.S. (2015). An efficient suzuki reaction using a new benzothiazole/Pd(II) species as catalyst in aqueous media. *World Journal of Pharmaceutical Research*, 4, 1046-1052.

58. IR spectrum of aldehyde-<http://orgchem.colorado.edu/Spectroscopy/irtutor/aldehydesir.html>. Retrieved June 1, 2015.
59. Shu A.Y., Christopher B.H. and John F.B. (2013). A convenient, high-yielding, chromatography-free method for the insertion of transition metal acetates into porphyrins. *Polyhedron*, 58, 2-6.
60. Hossein D. and Mohammad R.M. (2009). Synthesis and spectroscopic characterization of the new sitting-atop complexes from reaction of zirconyl nitrate and free base *meso*-tetraarylporphyrins in mild conditions. *Bulletin of the Korean Chemical Society*, 30, 1715-1718.
61. Hossein D. and Maryam S. (2009). New cationic sandwich-type intermediate sitting-atop complexation between *meso*-tetraarylporphyrins and tantalum(v) chloride: synthesis, spectroscopic characterization and photoluminescence study. *Bulletin of the Korean Chemical Society*, 30, 2792- 2794
62. Hossein D., Ali R.A.S. (2007). Molecular complexation of free base *meso*-tetraarylporphyrins with antimony(III) chloride in free solvent media. *Polyhedron*, 26, 4263-4268.
63. Chang-Hee L., Joo-Yeon P. and Han-Je K. (2000). Studies of porphyrin synthesis through 3+1 condensation. *Bulletin of the Korean Chemical Society*, 21, 97-100.
64. Rae-anne E.F. and Larry M.M. (1999). Microscale synthesis and <sup>1</sup>H NMR analysis of tetraphenylporphyrins. *Journal of Chemical Education*, 76, 237-239.
65. Zabardasti A. (2012). Molecular interactions of some free base porphyrins with  $\sigma$ - and  $\pi$ -acceptor molecules, molecular interactions, Prof. Aurelia Meghea (Ed.), ISBN: 978-953-51-0079-9. In Tech, Available from:  
<http://www.intechopen.com/books/molecular-interactions/molecular-interactions-of-some-free-basesporphyrins-with-sigma-and-pi-acceptor-molecules>.
66. I-Chin L. and Jyh-Horung C. (1996). Synthesis and characterization of antimony complexes of *meso*-tetraphenylporphyrin (TPP) and *meso*-tetra(4-methoxyphenyl)porphyrin (TMPP), and the X-ray crystal structure of [Sb(TMPP)Cl<sub>2</sub>]<sup>+</sup> OH<sup>-</sup>. *Polyhedron*, 15, 3947-3954.

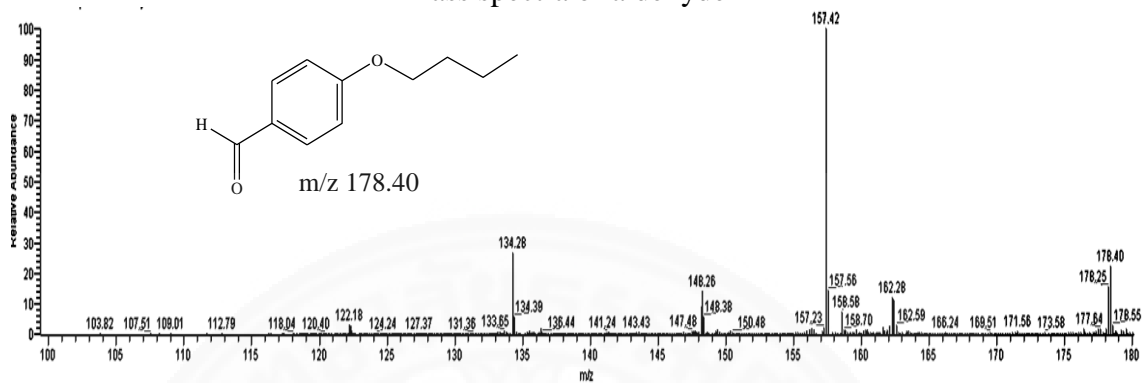
67. Danuta W., Aleksandra S. and Przemyslaw S. (2010). Photovoltaic and spectroscopic studies of selected halogenated porphyrins for their application inorganic solar cells. *Solar Energy Materials & Solar Cells*, 94, 492-500.
68. Horng Y.J., Wang C.L., Ya L.W. and Jing-Huei P. (2008). Substituent effects in porphyrin dimer complexes studied by IR spectroscopy. *Polyhedron*, 27, 3377-3382.
69. Kewei X., Graham R. and Timothy D.L. (1998). Infrared spectroscopy of geoporphyryns analysis of geochemically significant nickel(II) porphyrins. *Vibrational Spectroscopy*, 18, 157-174
70. Alexander V.U., Anastasia V.B. and Johannes G.V. (2014). Highly ordered surface structure of large-scale porphyrin aggregates assembled from protonated TPP and water. *Journal of Molecular Structure*, 1065-1066, 170–178.
71. Alexandra B.O. and Harold S.F. (2013). Effects of substituents on the photophysical properties of symmetrical porphyrins. *Dyes and Pigments*, 96, 440-448.
72. Saeed Z. *et al.* (2011). Substitution effects on the UV-Vis and <sup>1</sup>H NMR spectra of the dications of *meso* and/or  $\beta$  substituted porphyrins with trifluoroacetic acid: Electron-deficient porphyrins compared to the electron-rich ones. *Inorganic Chemistry Communications*, 14, 1827-1832.
73. Bandgar B. and Gujarathi P. (2008). Synthesis and characterization of new *meso*-substituted unsymmetrical metalloporphyrins. *Journal of Chemical Sciences*, 120, 259-266.
74. Barbara V., Lucia F.G.M., Fabio L. and David L.O. (2008). Extending the porphyrin core: synthesis and photophysical characterization of porphyrins with *p*-conjugated  $\beta$ -substituents. *New Journal of Chemistry*, 32, 166-178.
75. Gamboa M. and Campos M. (2010). Study of the stability of 5,10,15,20-tetraphenylporphine (TPP) and metalloporphyrins NiTPP, CoTPP, CuTPP, and ZnTPP by differential scanning calorimetry and thermogravimetry. *The Journal of Chemical Thermodynamics*, 42, 666-674.
76. Xiuhua W., Xiuhong D., Donghua C. and Zhangping C. (2006). Thermal analysis study of 5,10,15,20-tetrakis (methoxyphenyl) porphyrins and their nickel complexes. *Thermochimica Acta*, 440, 181-187.

The image features a large, faint watermark of the Thammasat University seal in the background. The seal is circular and contains a central emblem with a crown and a lotus flower, surrounded by Thai script and the English text "THAMMASAT UNIVERSITY".

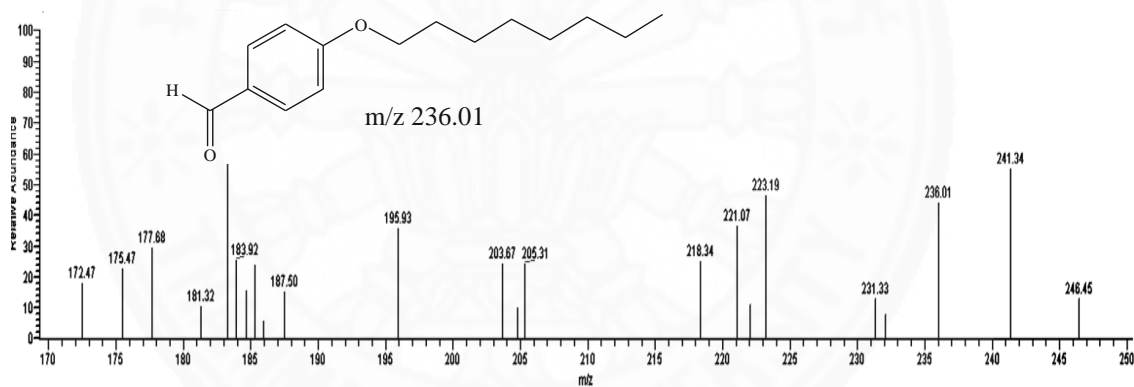
**APPENDICES**

## APPENDIX A MASS SPECTRA

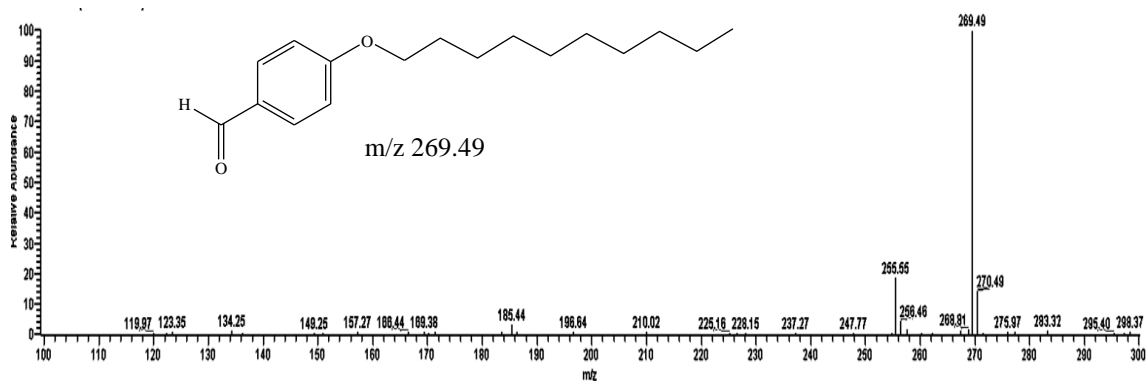
### Mass spectra of aldehyde



**Fig. A1** The mass spectrum of butyloxybenzaldehyde **1** in  $\text{CH}_2\text{Cl}_2$

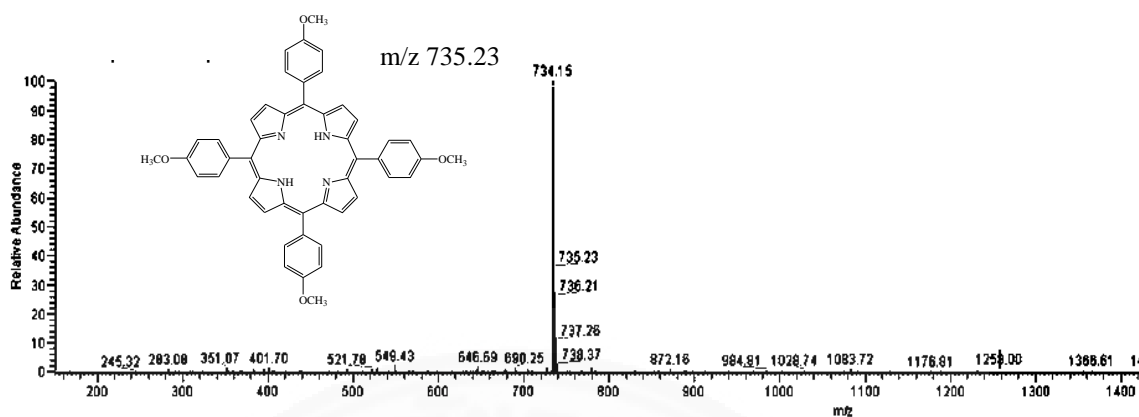
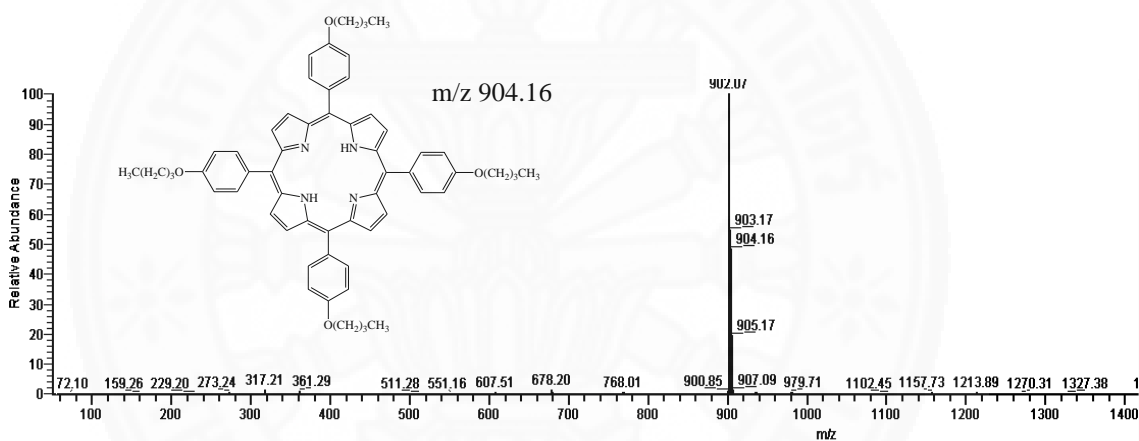
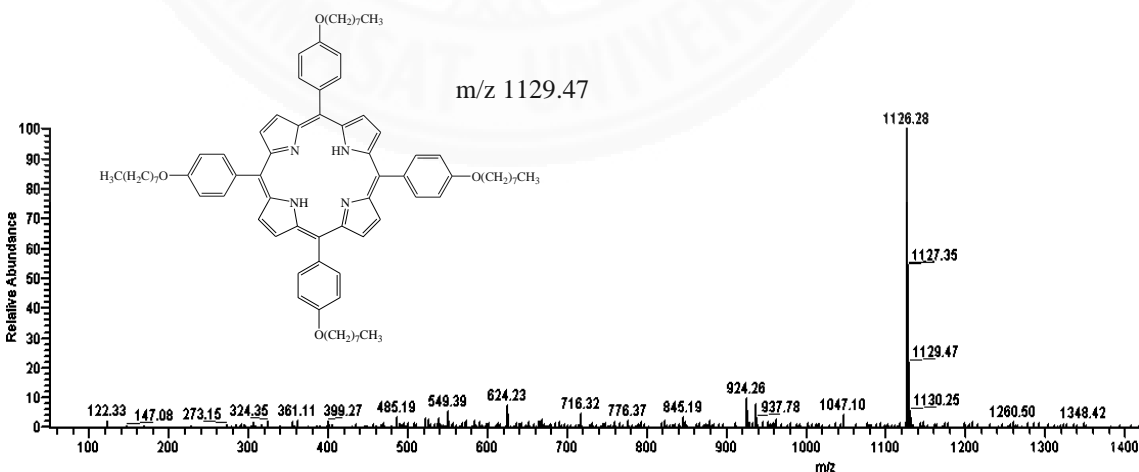


**Fig. A2** The mass spectrum of octyloxybenzaldehyde **2** in  $\text{CH}_2\text{Cl}_2$



**Fig. A3** The mass spectrum of decyloxybenzaldehyde **3** in  $\text{CH}_2\text{Cl}_2$

## Mass spectra of free base porphyrins

Fig. A4 The mass spectrum of TOMPP 4 in  $\text{CH}_2\text{Cl}_2$ Fig. A5 The mass spectrum of TOBPP 5 in  $\text{CH}_2\text{Cl}_2$ Fig. A6 The mass spectrum of TOOPP 6 in  $\text{CH}_2\text{Cl}_2$

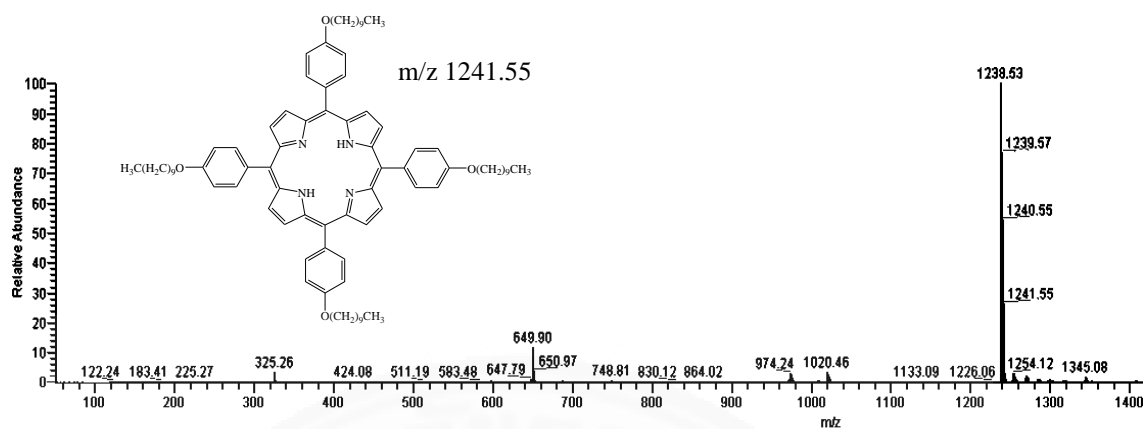


**Fig. A7** The mass spectrum of TODPP 7 in  $\text{CH}_2\text{Cl}_2$

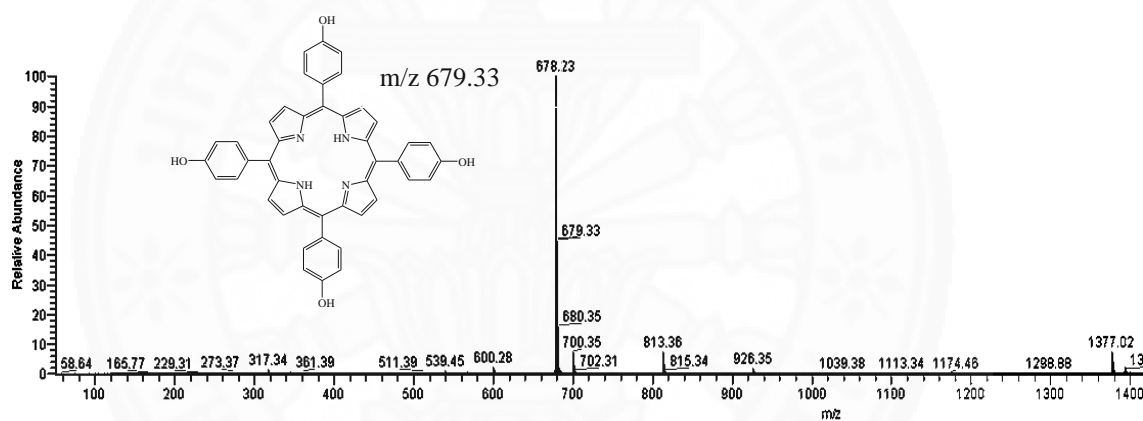


**Fig. A8** The mass spectrum of THPP 8 in methanol

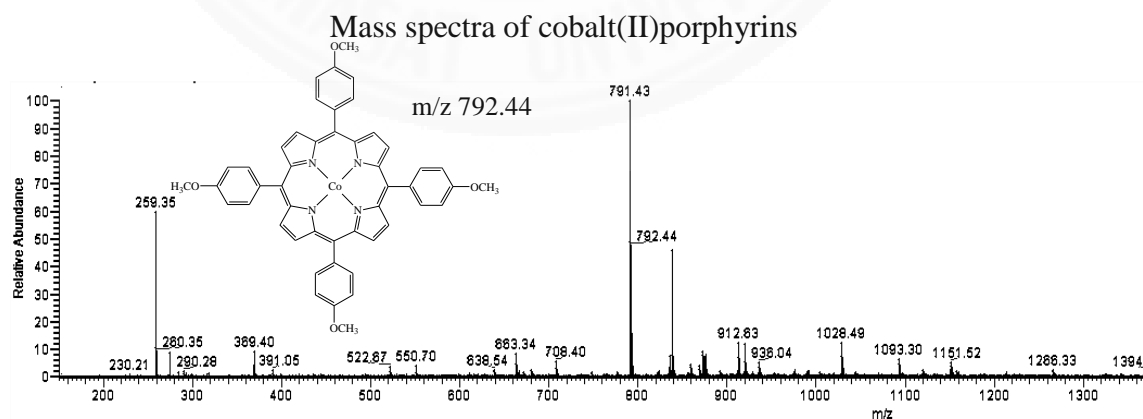


**Fig. A9** The mass spectrum of Co-TOMPP 9 in  $\text{CH}_2\text{Cl}_2$

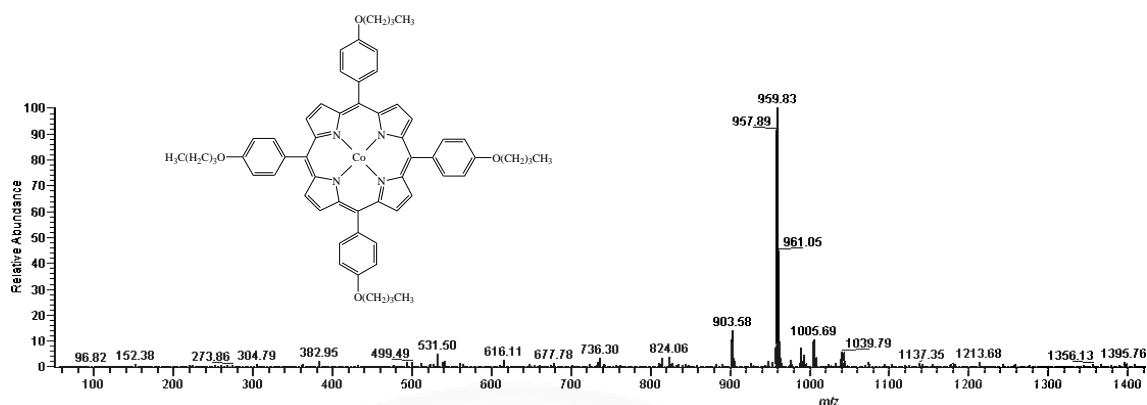


**Fig. A10** The mass spectrum of Co-TOBPP 10 in CH<sub>2</sub>Cl<sub>2</sub>

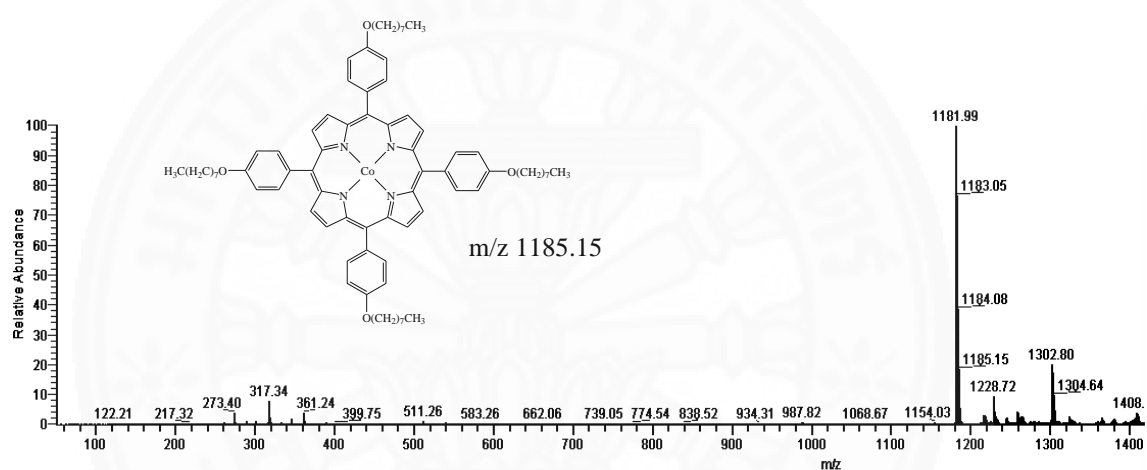


**Fig. A11** The mass spectrum of Co-TOOPP 11 in CH<sub>2</sub>Cl<sub>2</sub>

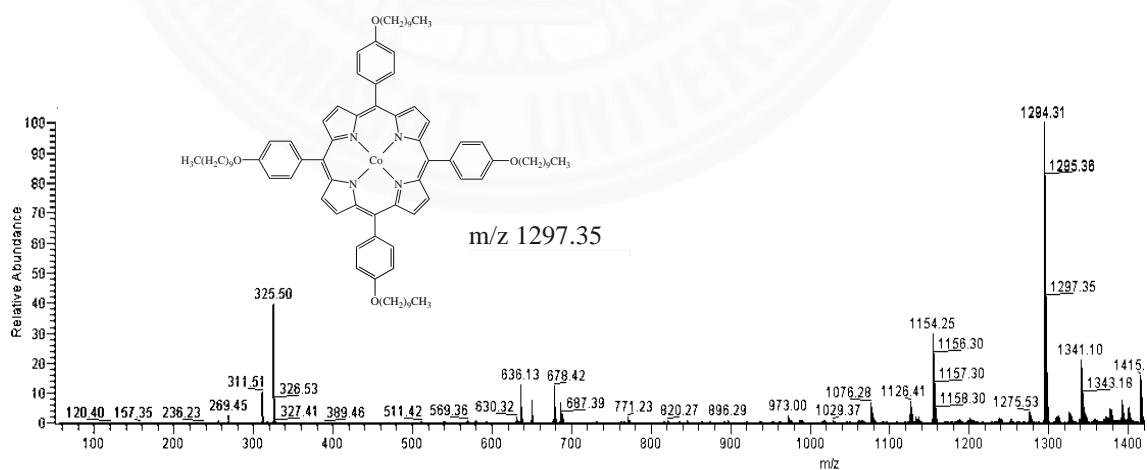


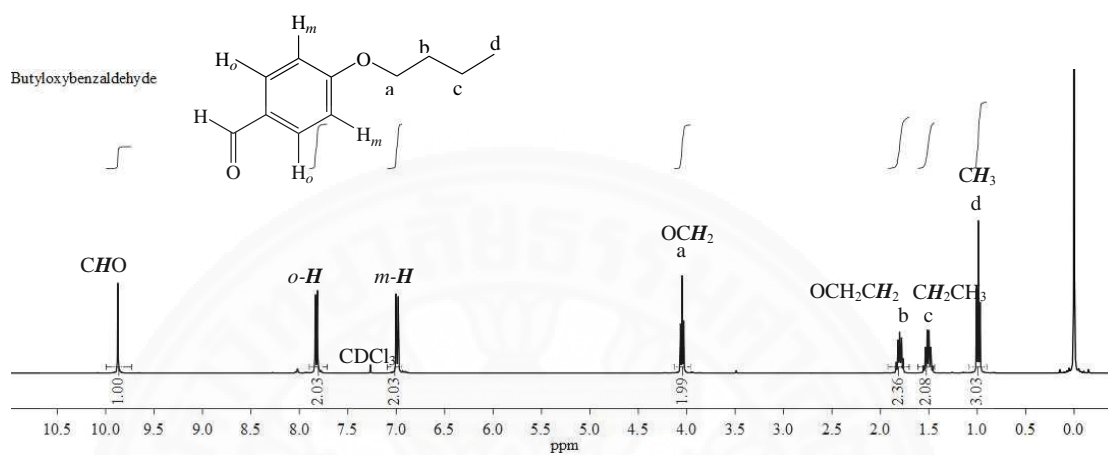
**Fig. A12** The mass spectrum of Co-TODPP 12 in CH<sub>2</sub>Cl<sub>2</sub>



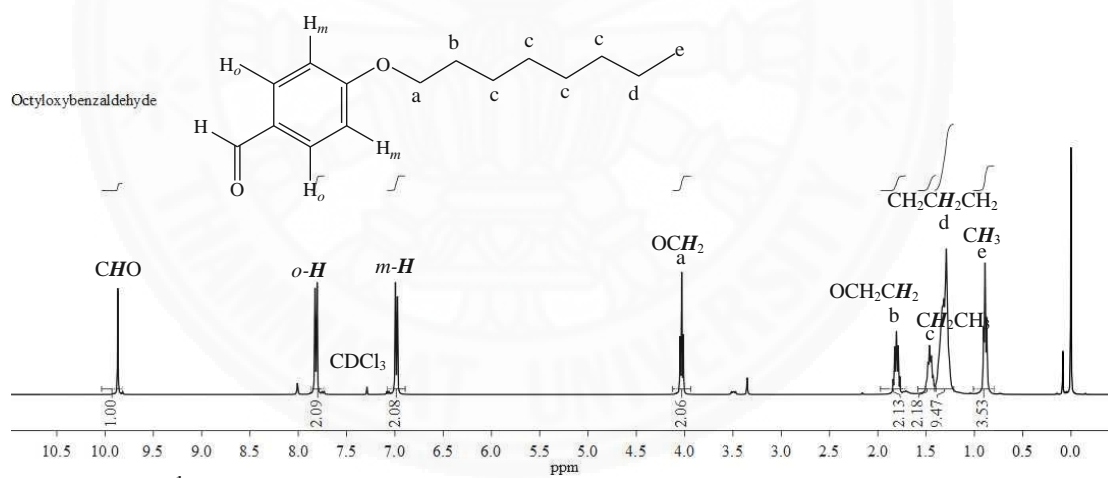
## APPENDIX B

### NMR SPECTRA

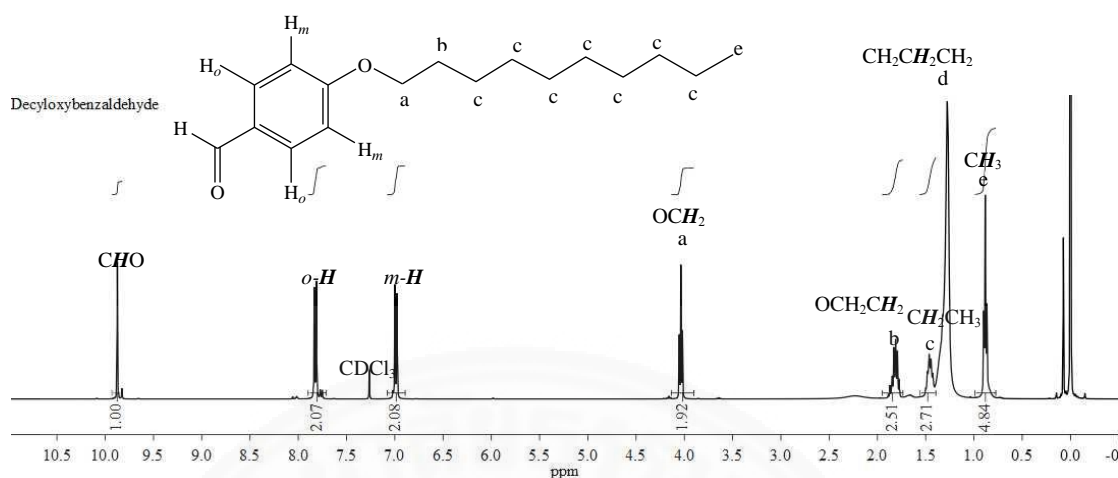
$^1\text{H}$ -NMR of aldehydes



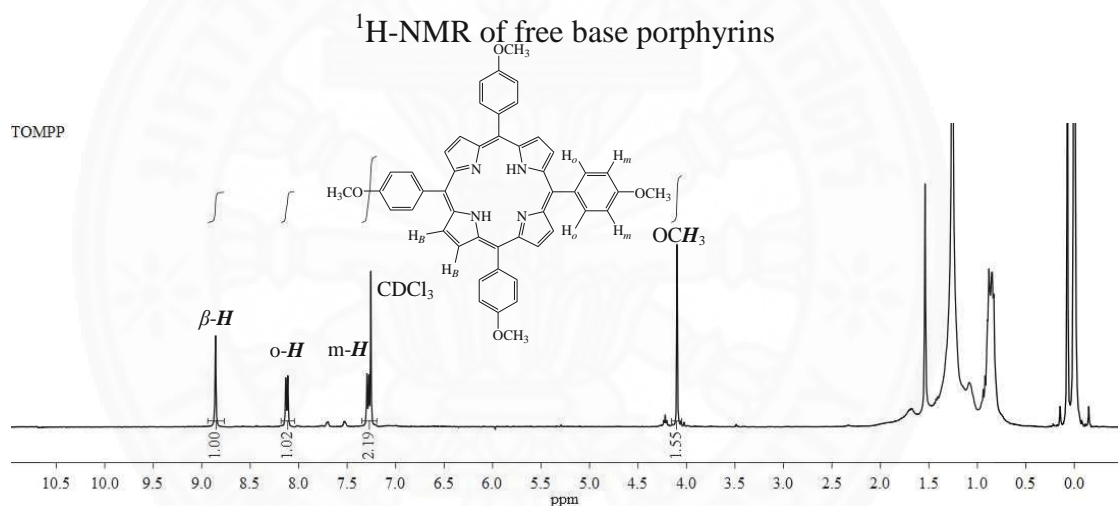
**Fig. B1** The  $^1\text{H}$ -NMR spectrum of butyloxybenzaldehyde **1** in chloroform-d ( $\text{CDCl}_3$ )



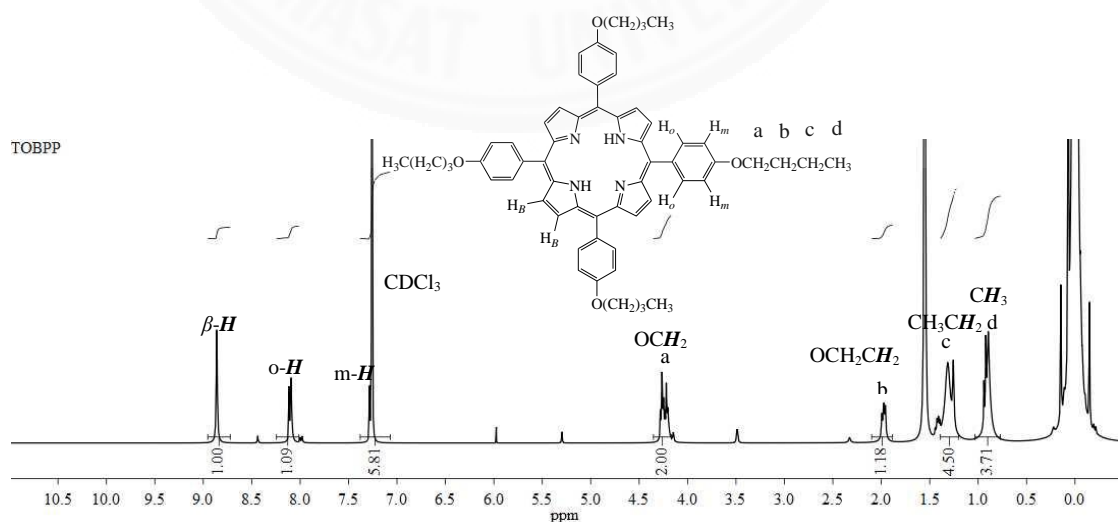
**Fig. B2** The  $^1\text{H}$ -NMR spectrum of octyloxybenzaldehyde **2** in chloroform-d ( $\text{CDCl}_3$ )



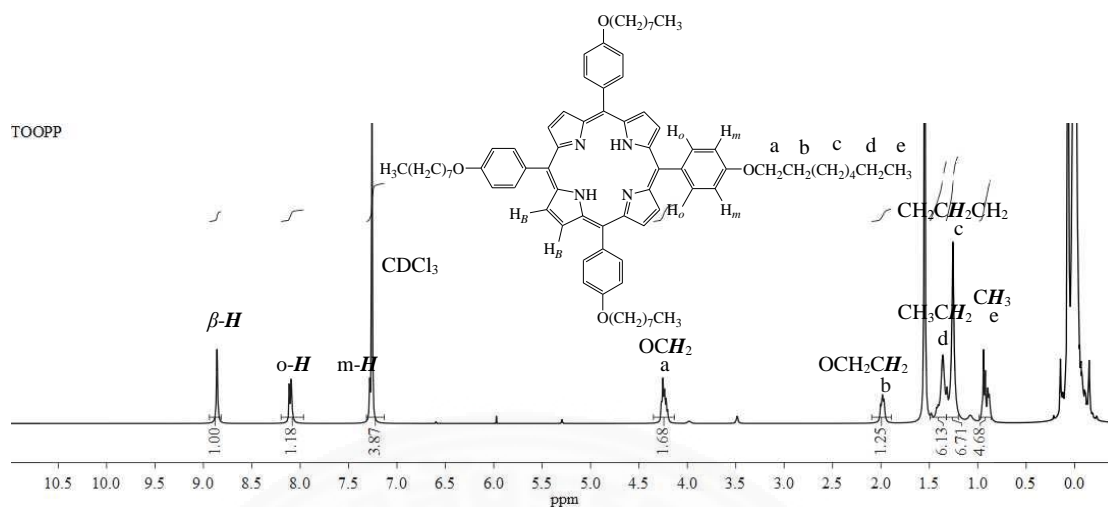
**Fig. B3** The  $^1\text{H-NMR}$  spectrum of decyloxybenzaldehyde **3** in chloroform-d ( $\text{CDCl}_3$ )



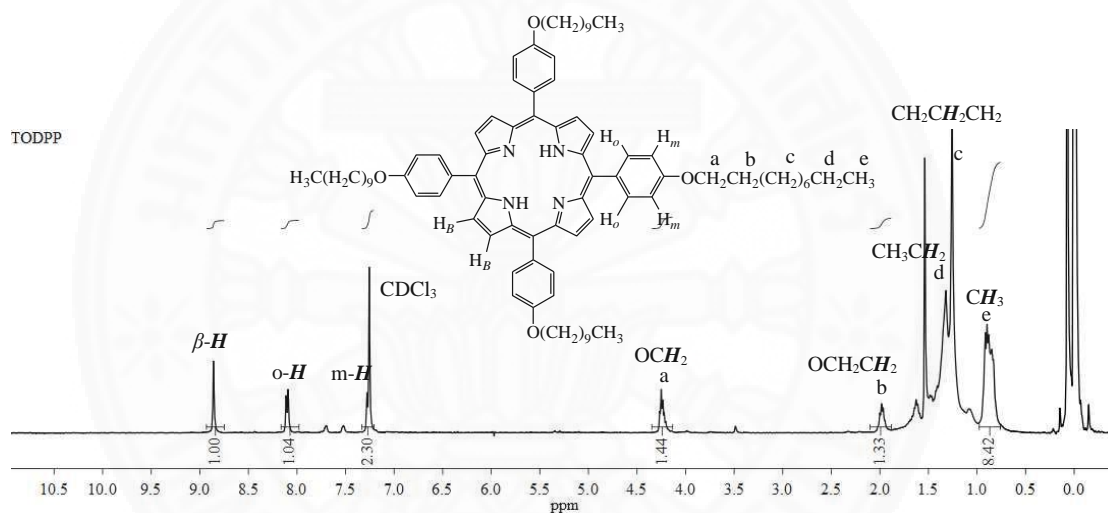
**Fig. B4** The  $^1\text{H-NMR}$  spectrum of TOMPP **4** in chloroform-d ( $\text{CDCl}_3$ )



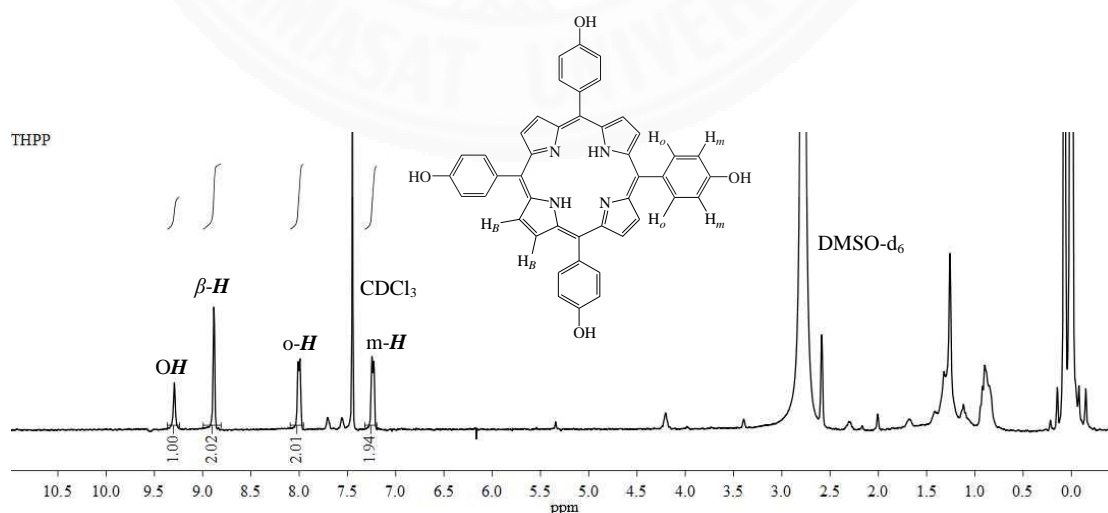
**Fig. B5** The  $^1\text{H-NMR}$  spectrum of TOBPP **5** in chloroform-d ( $\text{CDCl}_3$ )



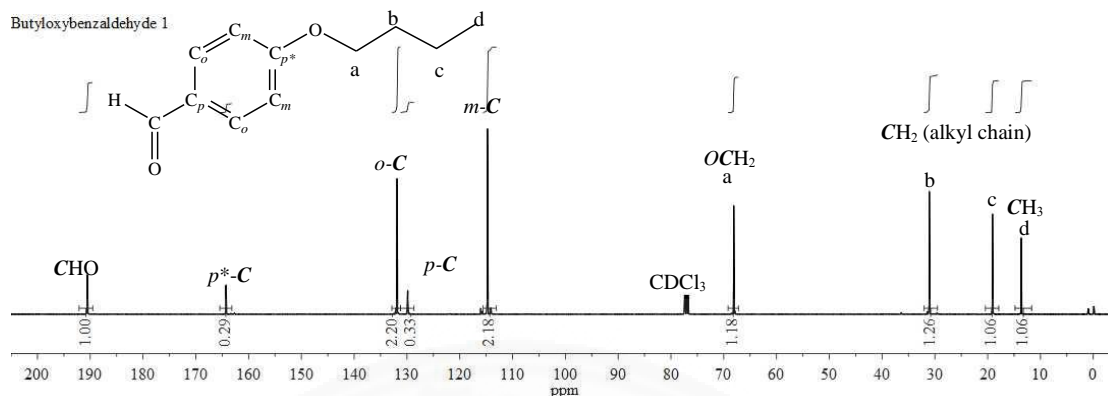
**Fig. B6** The <sup>1</sup>H-NMR spectrum of TOOPP **6** in chloroform-d (CDCl<sub>3</sub>)



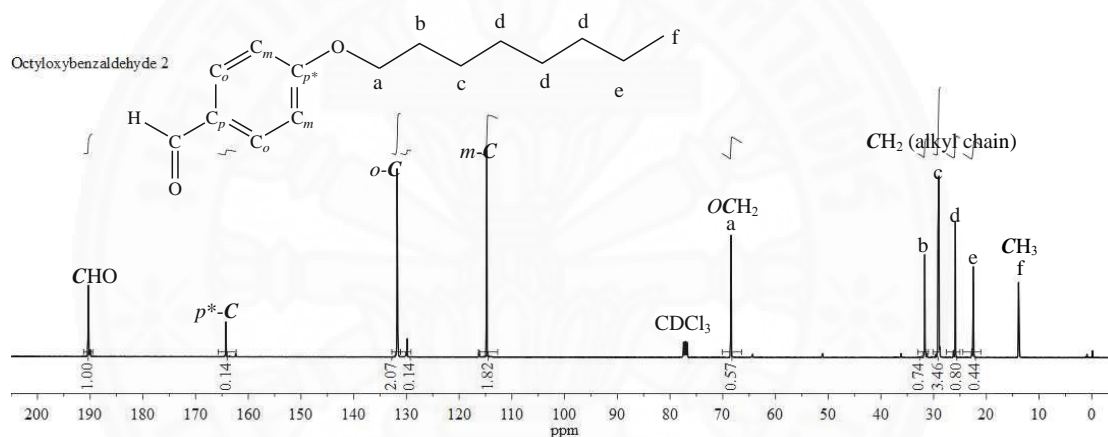
**Fig. B7** The <sup>1</sup>H-NMR spectrum of TODPP **7** in chloroform-d (CDCl<sub>3</sub>)



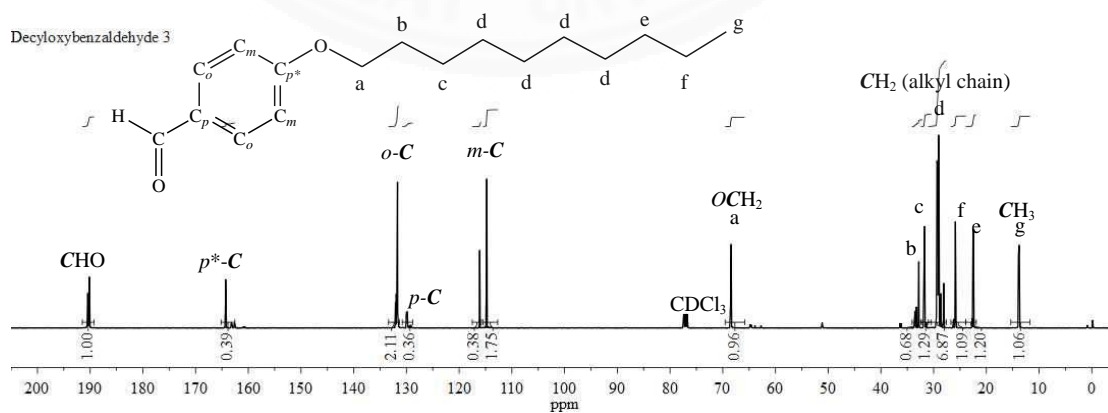
**Fig. B8** The <sup>1</sup>H-NMR spectrum of THPP **8** in chloroform-d (CDCl<sub>3</sub>) and DMSO-d<sub>6</sub>

$^{13}\text{C-NMR}$  of aldehydes

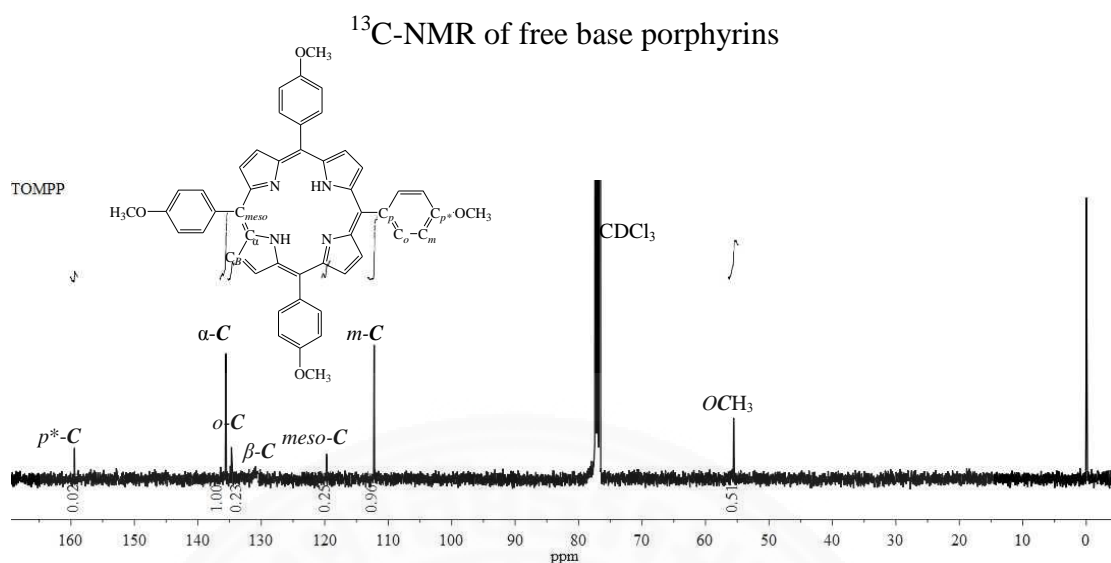
**Fig. B9** The  $^{13}\text{C-NMR}$  spectrum of butyloxybenzaldehyde 1 in chloroform-d ( $\text{CDCl}_3$ )



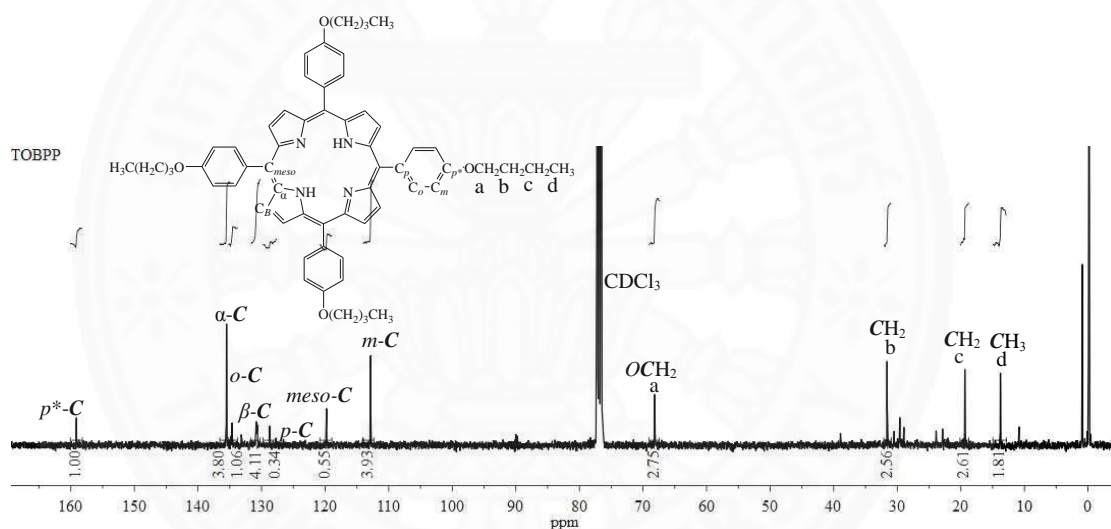
**Fig. B10** The  $^{13}\text{C-NMR}$  spectrum of octyloxybenzaldehyde 2 in chloroform-d ( $\text{CDCl}_3$ )



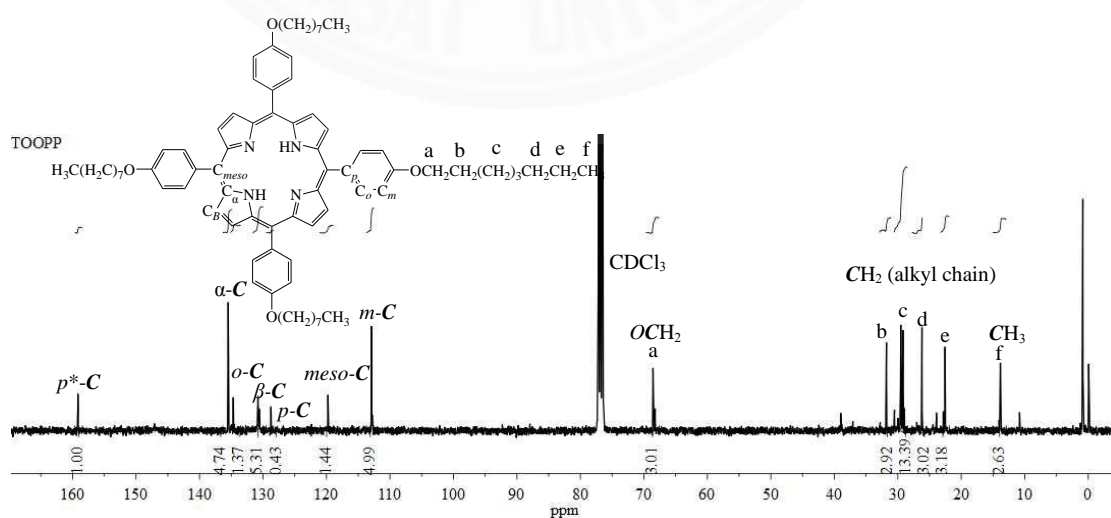
**Fig. B11** The  $^{13}\text{C-NMR}$  spectrum of decyloxybenzaldehyde 3 in chloroform-d ( $\text{CDCl}_3$ )



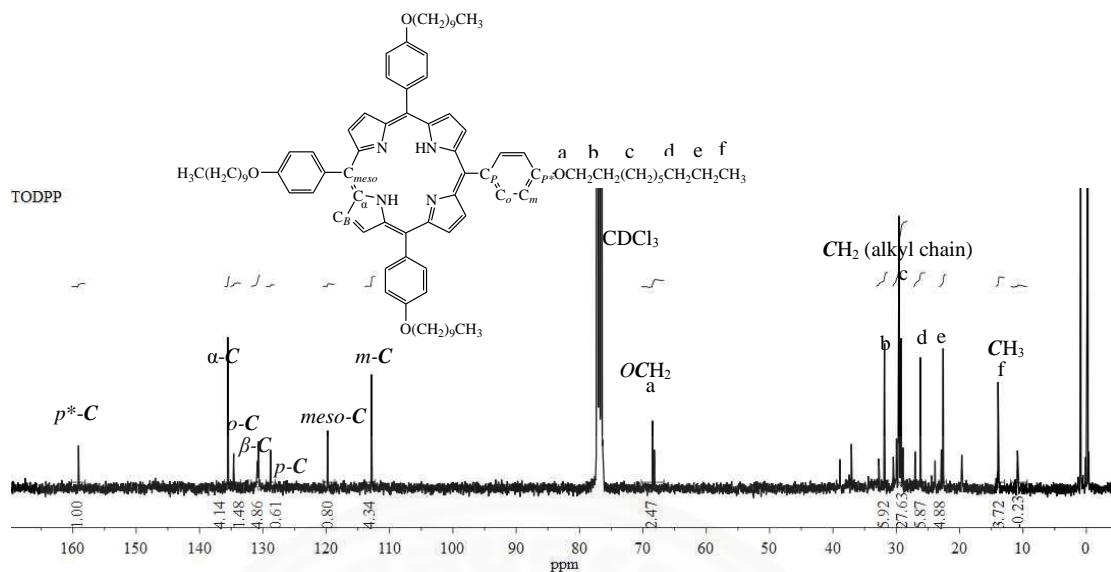
**Fig. B12** The  $^{13}\text{C-NMR}$  spectrum of TOMPP **4** in chloroform-d ( $\text{CDCl}_3$ )



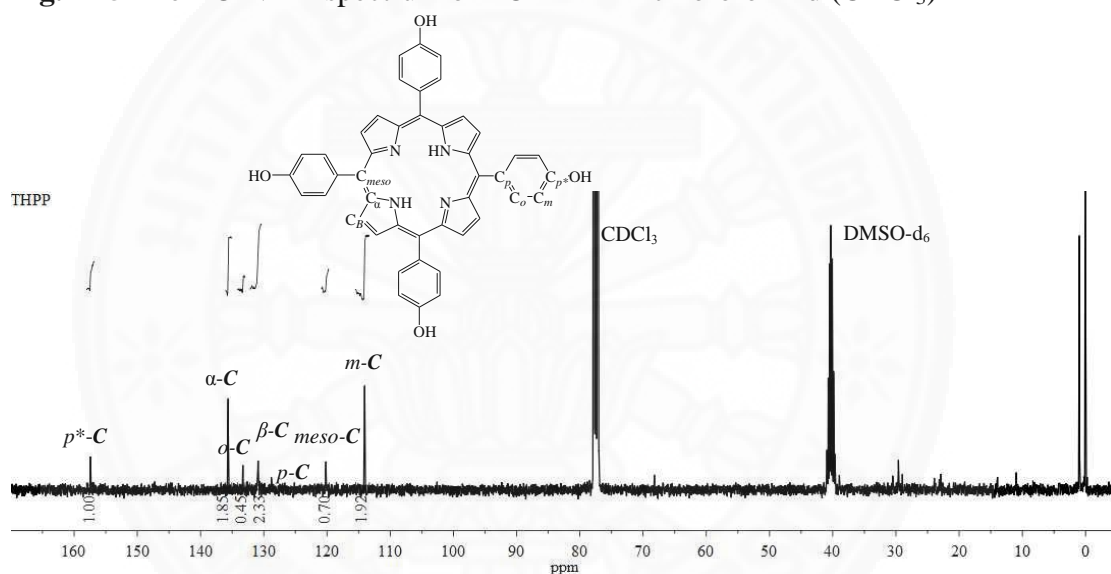
**Fig. B13** The  $^{13}\text{C-NMR}$  spectrum of TOBPP **5** in chloroform-d ( $\text{CDCl}_3$ )



**Fig. B14** The  $^{13}\text{C-NMR}$  spectrum of TOOPP **6** in chloroform-d ( $\text{CDCl}_3$ )



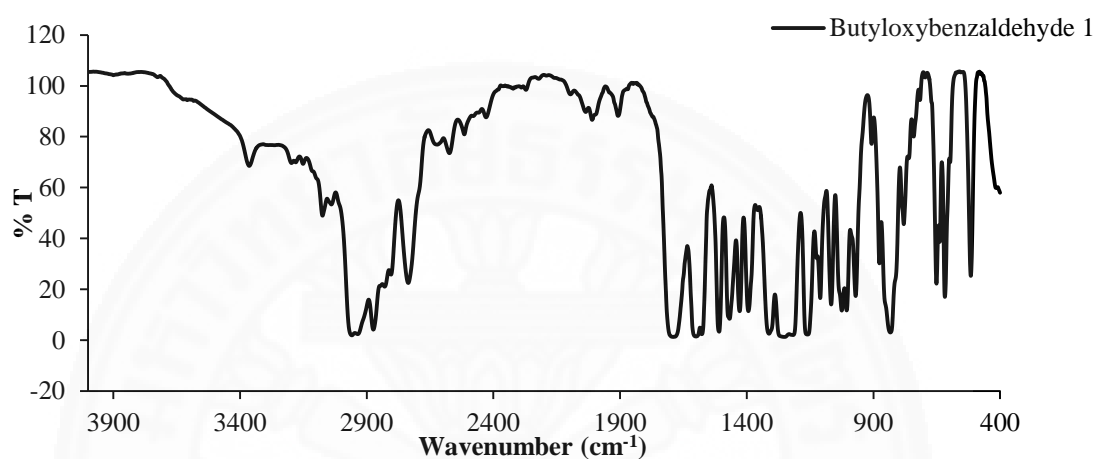
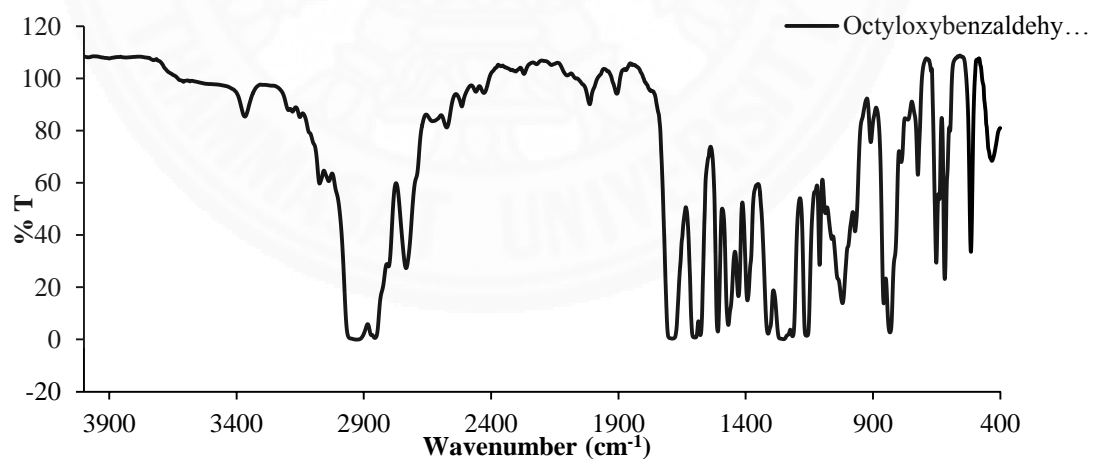
**Fig. B15** The  $^{13}\text{C}$ -NMR spectrum of TODPP **7** in chloroform-d ( $\text{CDCl}_3$ )



**Fig. B16** The  $^{13}\text{C}$ -NMR spectrum of THPP **8** in chloroform-d ( $\text{CDCl}_3$ ) and  $\text{DMSO}-d_6$

**APPENDIX C****IR SPECTRA**

IR spectra of aldehydes

**Fig. C1** The IR spectrum of butyloxybenzaldehyde **1** in NaCl**Fig. C2** The IR spectrum of octyloxybenzaldehyde **2** in NaCl

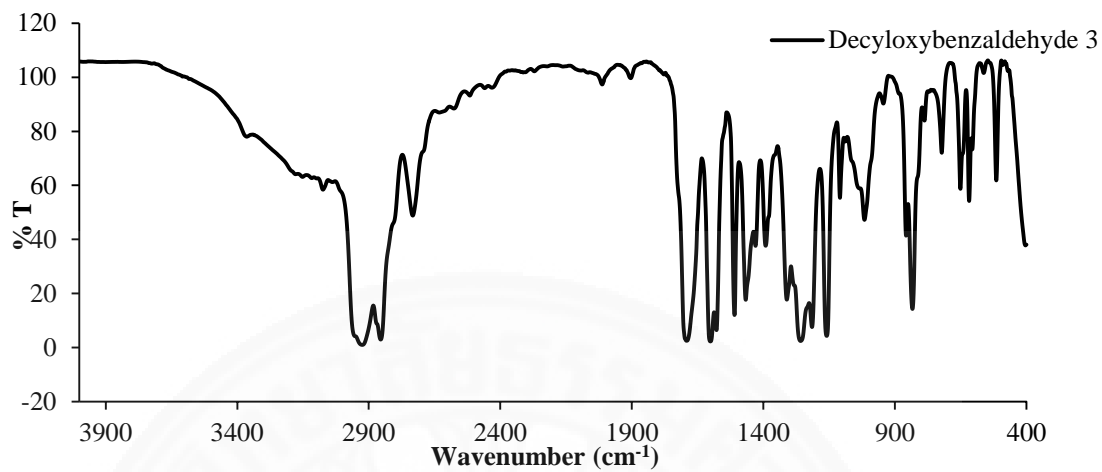


**Fig. C3** The IR spectrum of decyloxybenzaldehyde **3** in NaCl

### IR spectra of porphyrins and cobalt(II)porphyrins

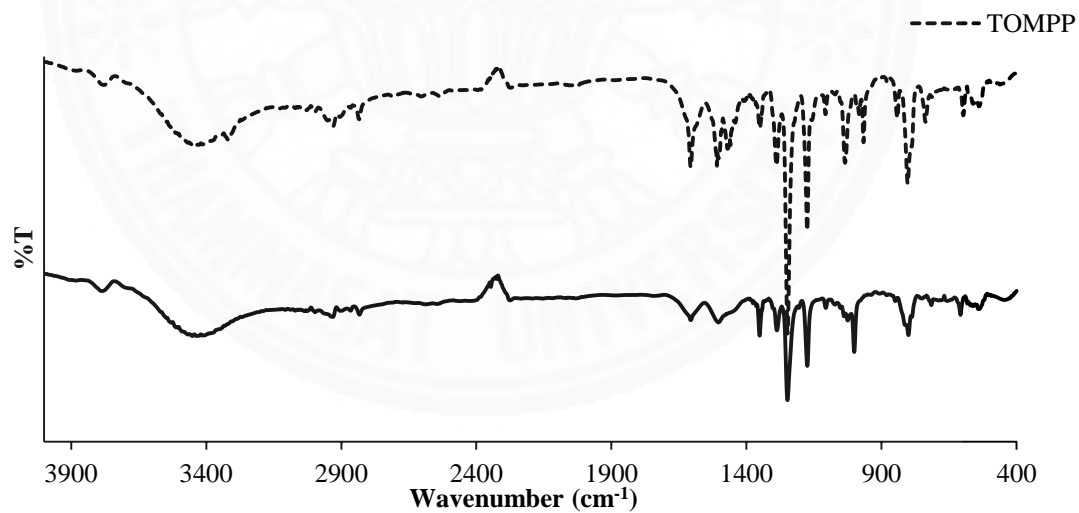


**Fig. C4** The IR spectra of TOMPP **4** and Co-TOMPP **9** in KBr



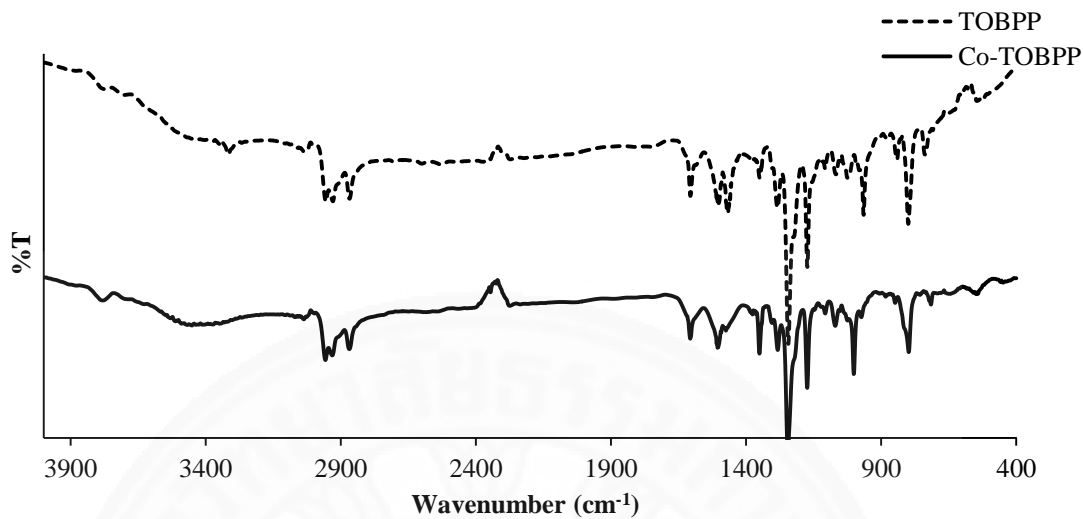


**Fig. C5** The IR spectra of TOBPP **5** and Co-TOBPP **10** in KBr

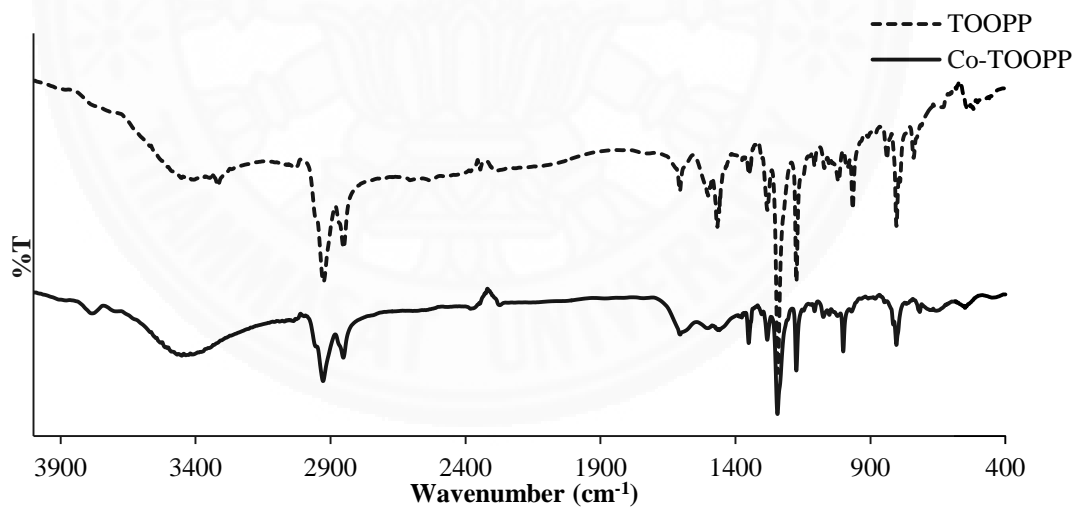


**Fig. C6** The IR spectra of TOOPP **6** and Co-TOOPP **11** in KBr

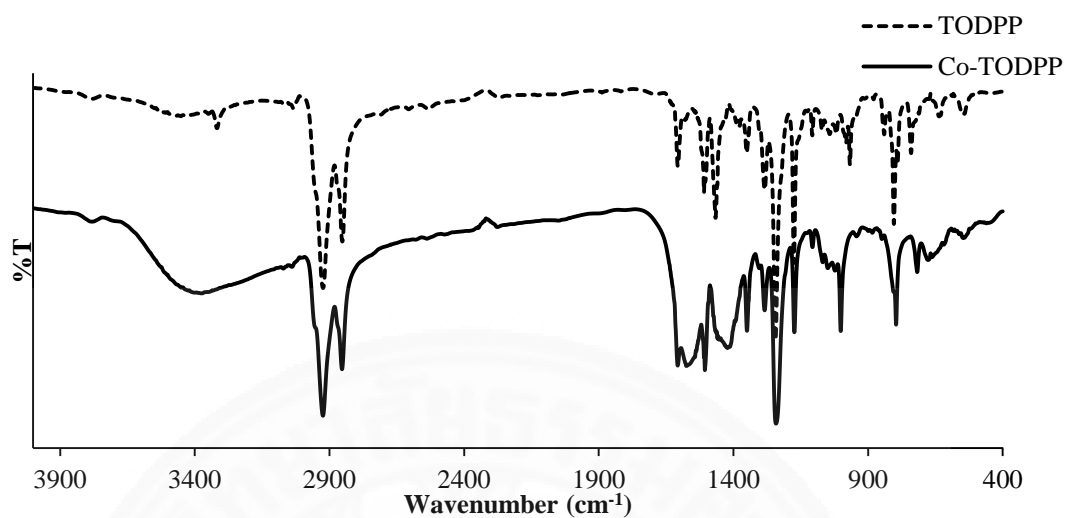


**Fig. C7** The IR spectra of TODPP **7** and Co-TODPP **12** in KBr

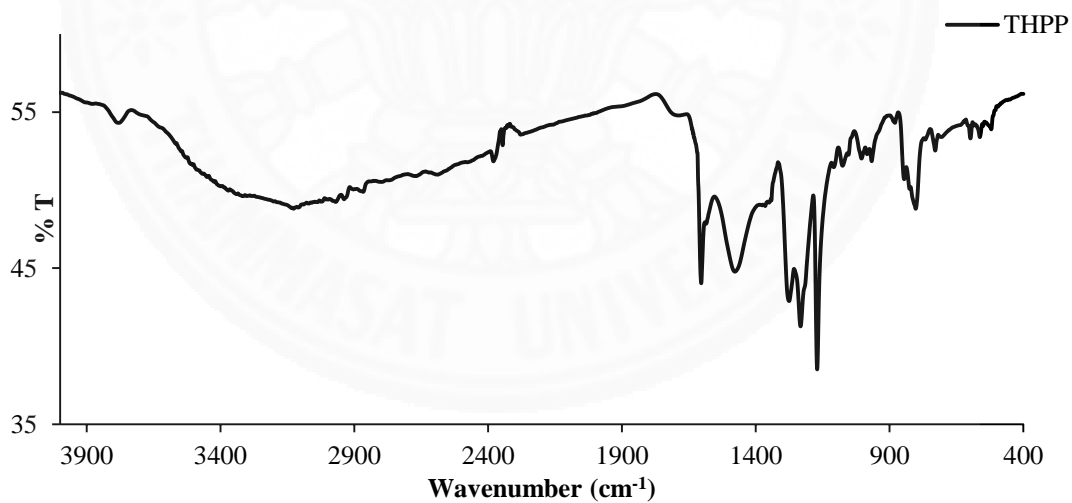
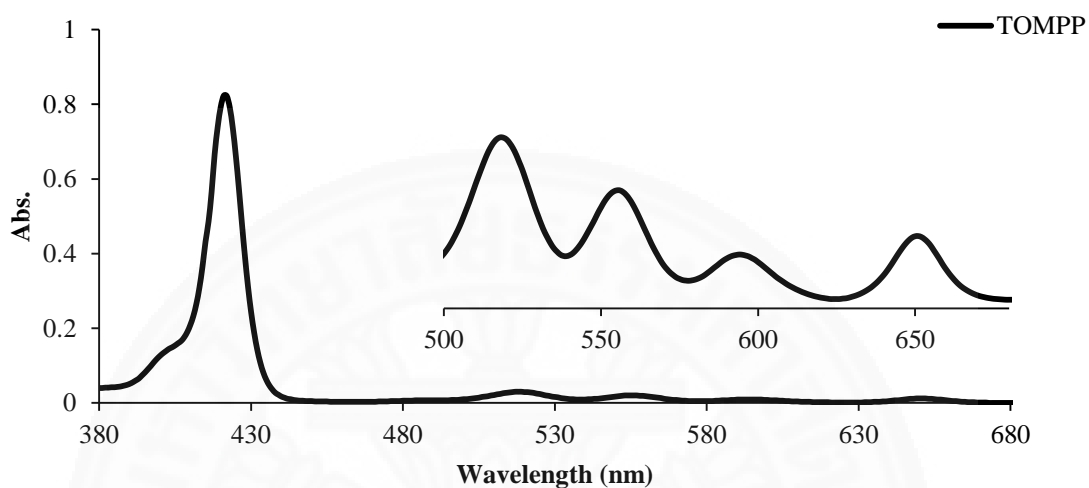


**Fig. C8** The IR spectrum of THPP **8** in KBr

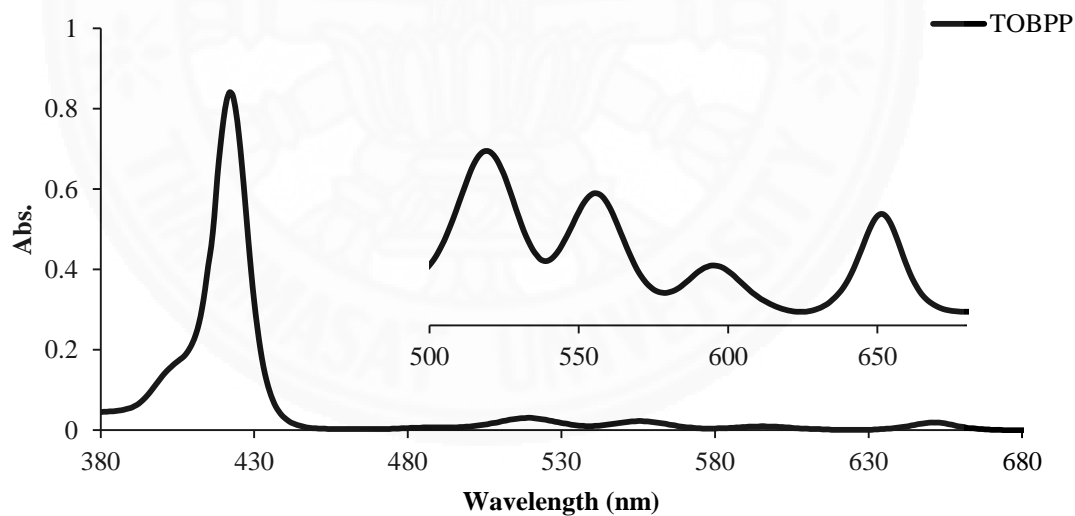
## APPENDIX D

### UV-VIS ABSORPTION SPECTRA

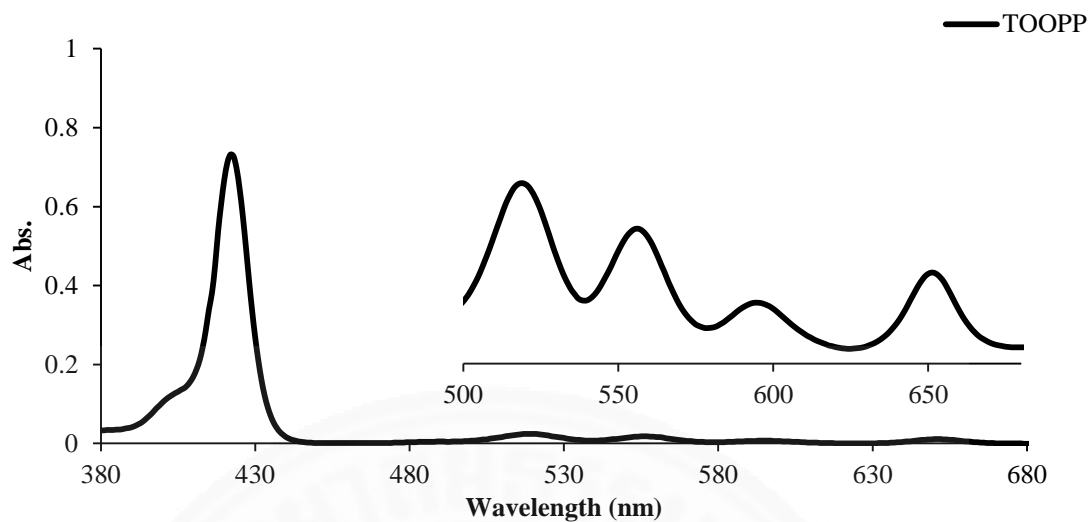
UV-Vis absorption spectra of free base ligands in dichloromethane



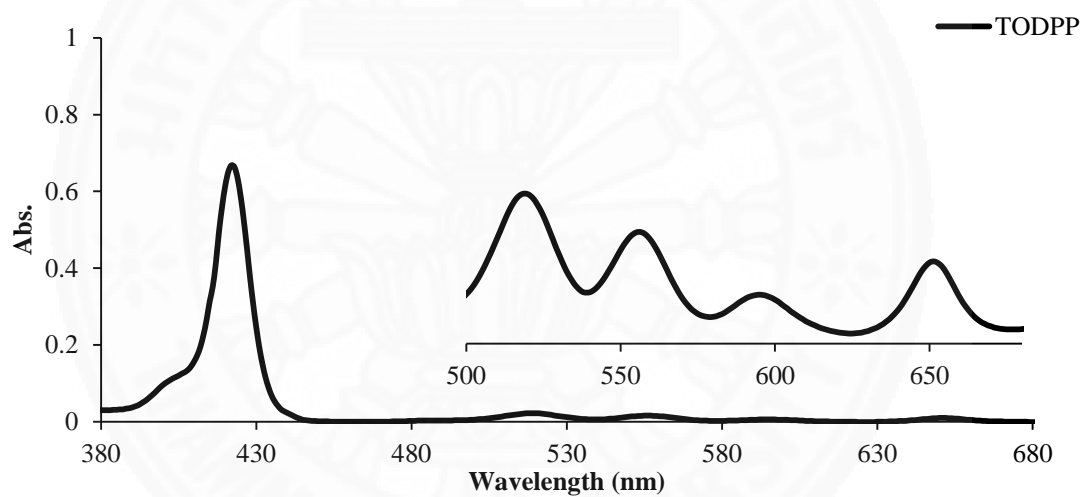
**Fig. D1** UV-Vis absorption spectra of TOMPP 4



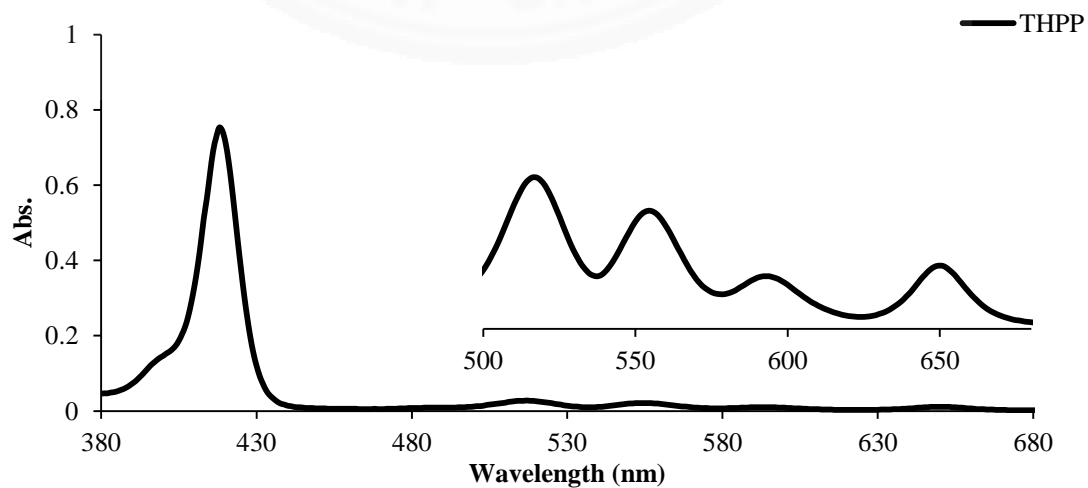
**Fig. D2** UV-Vis absorption spectra of TOBPP 5



**Fig. D3** UV-Vis absorption spectra of TOOPP 6

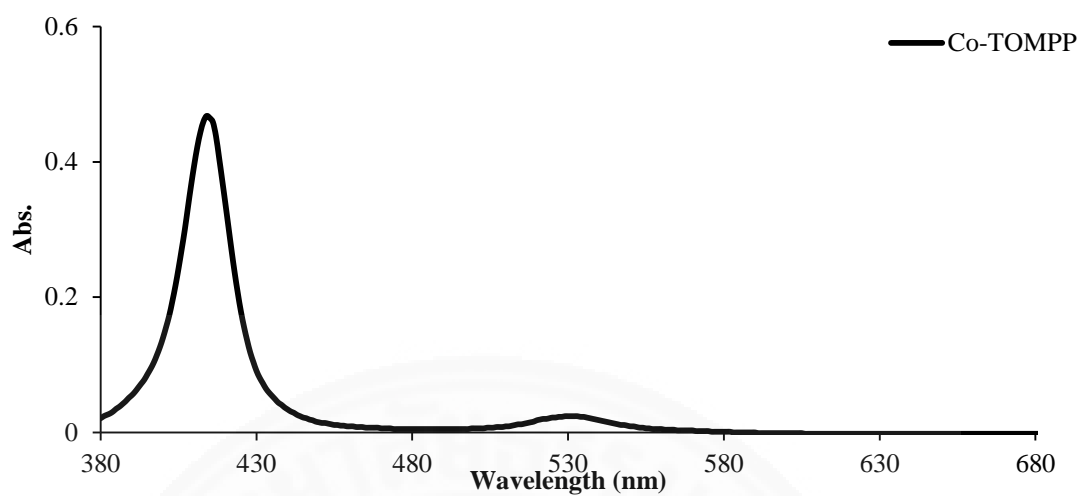


**Fig. D4** UV-Vis absorption spectra of TODPP 7

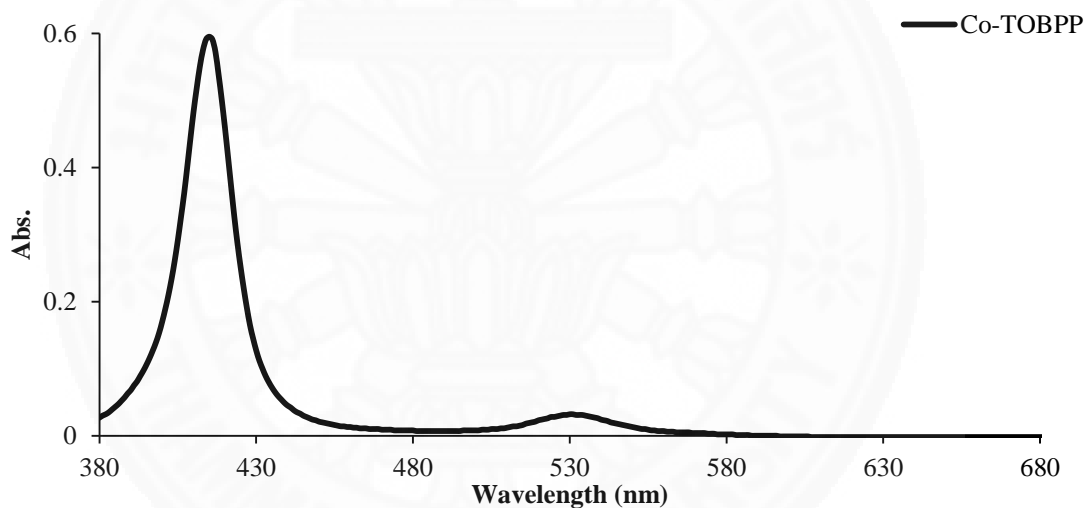


**Fig. D5** UV-Vis absorption spectra of THPP 8

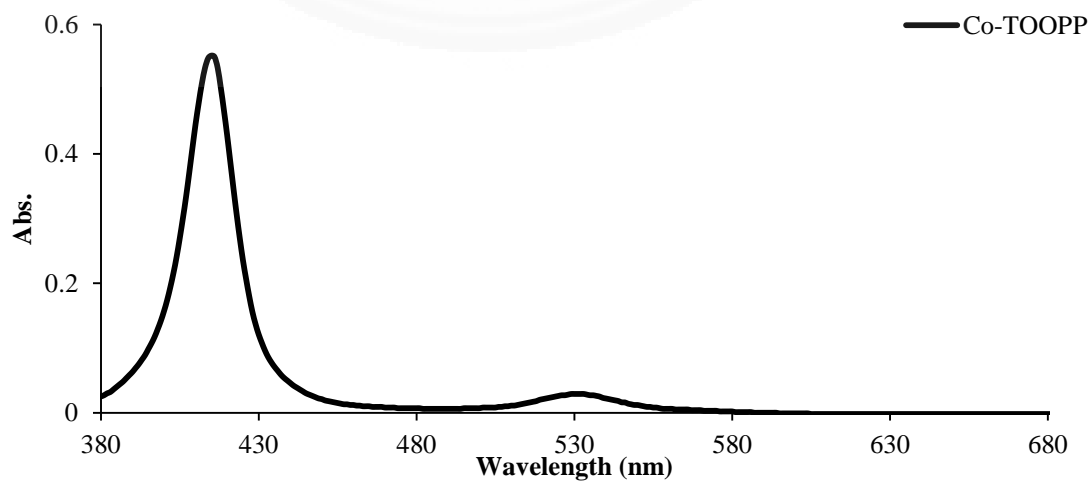
UV-Vis absorption spectra of cobalt(II) porphyrins in dichloromethane



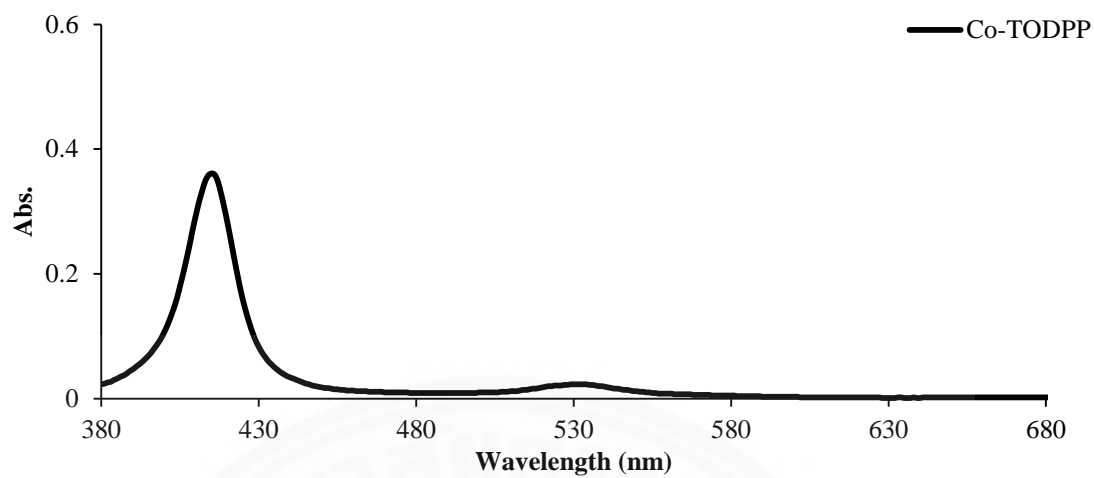
**Fig. D6** UV-Vis absorption spectra of Co-TOMPP **9**



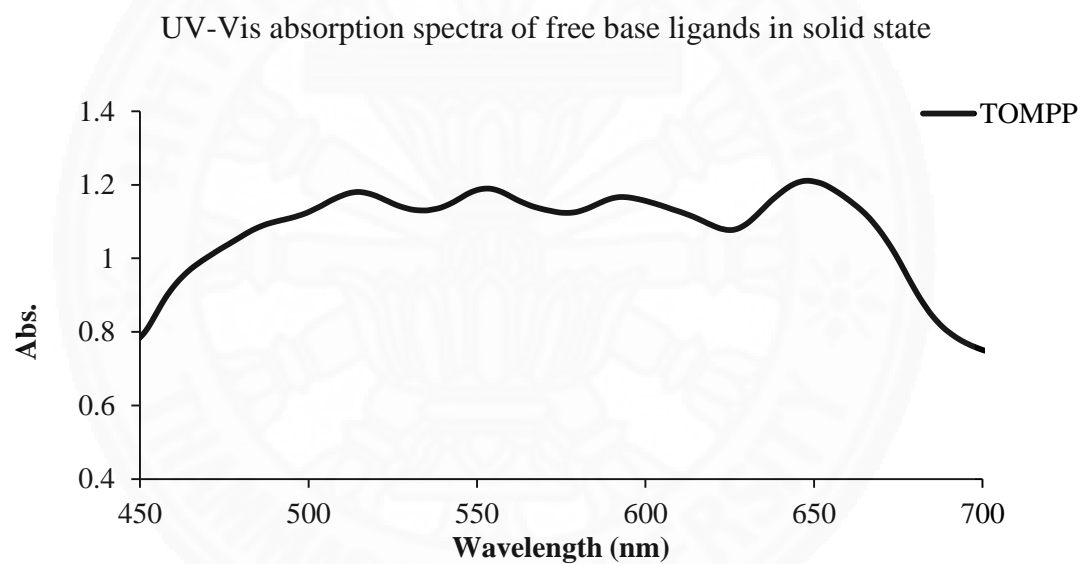
**Fig. D7** UV-Vis absorption spectra of Co-TOBPP **10**



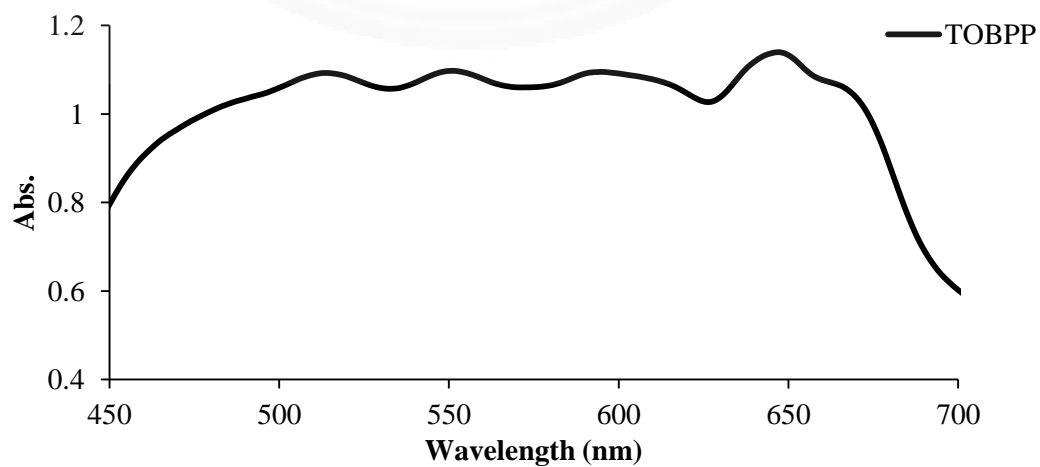
**Fig. D8** UV-Vis absorption spectra of Co-TOOPP **1**



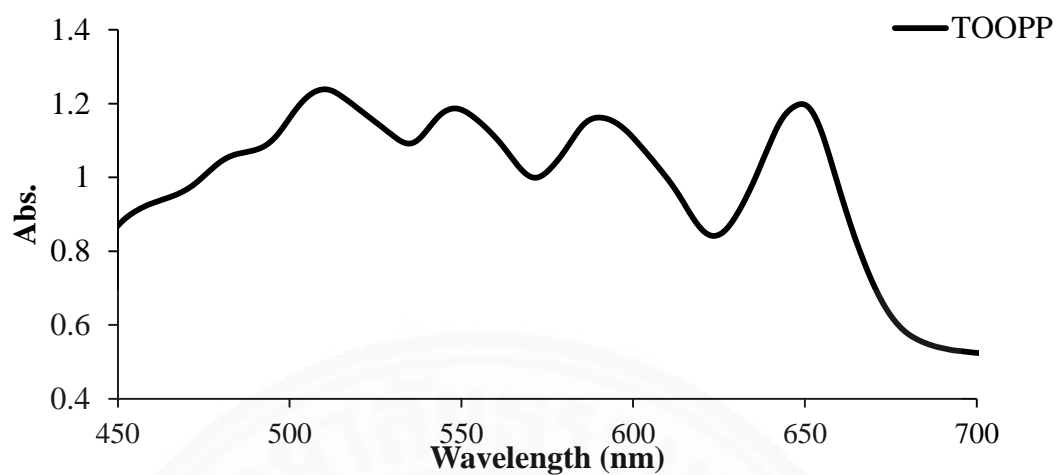
**Fig. D9** UV-Vis absorption spectra of Co-TODPP 12



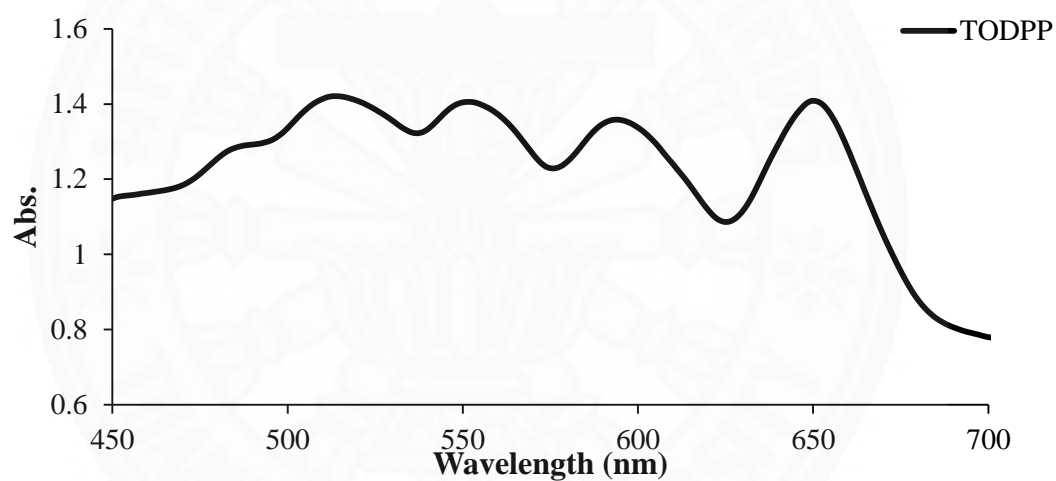
**Fig. D10** UV-Vis absorption spectra of TOMPP 4



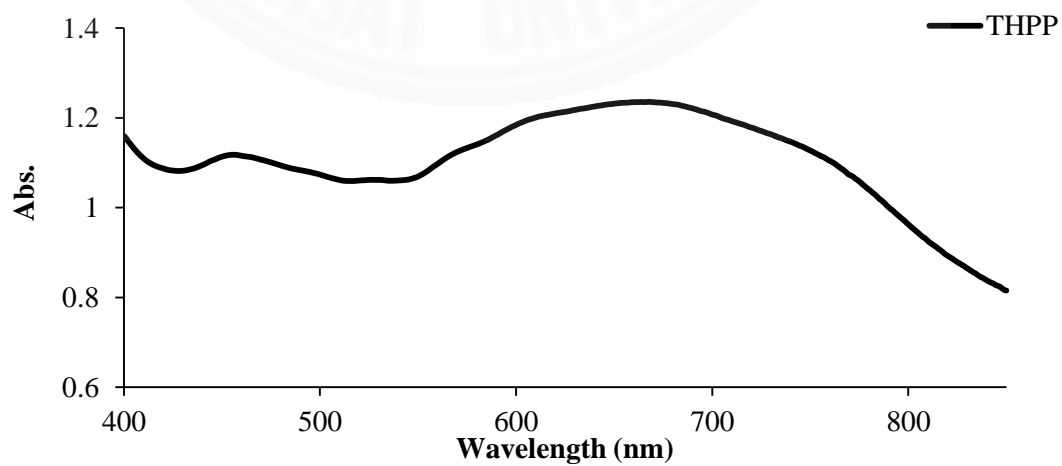
**Fig. D11** UV-Vis absorption spectra of TOBPP 5



**Fig. D12** UV-Vis absorption spectra of TOOPP 6

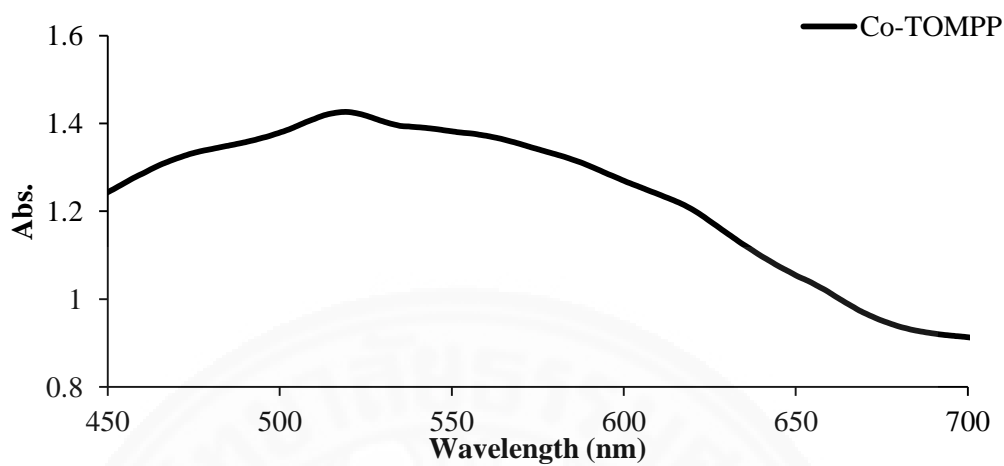


**Fig. D13** UV-Vis absorption spectra of TODPP 7

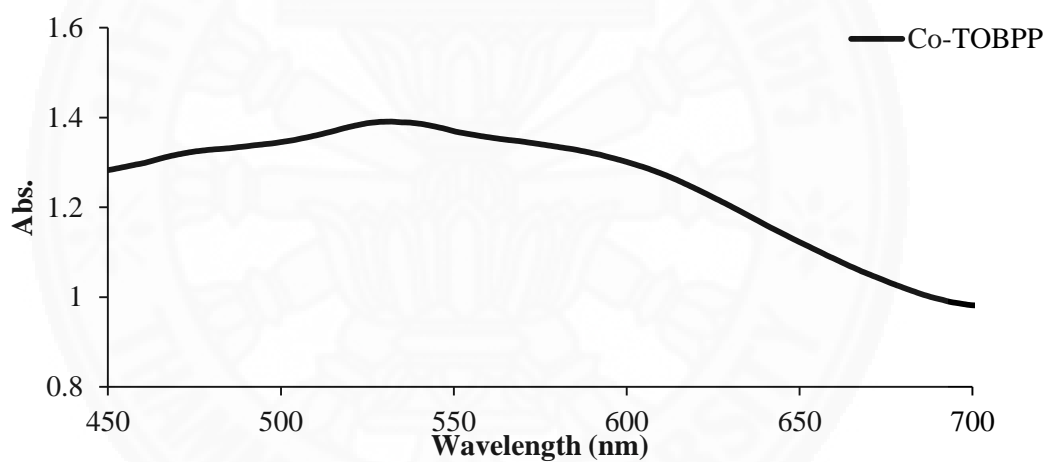


**Fig. D14** UV-Vis absorption spectra of THPP 8

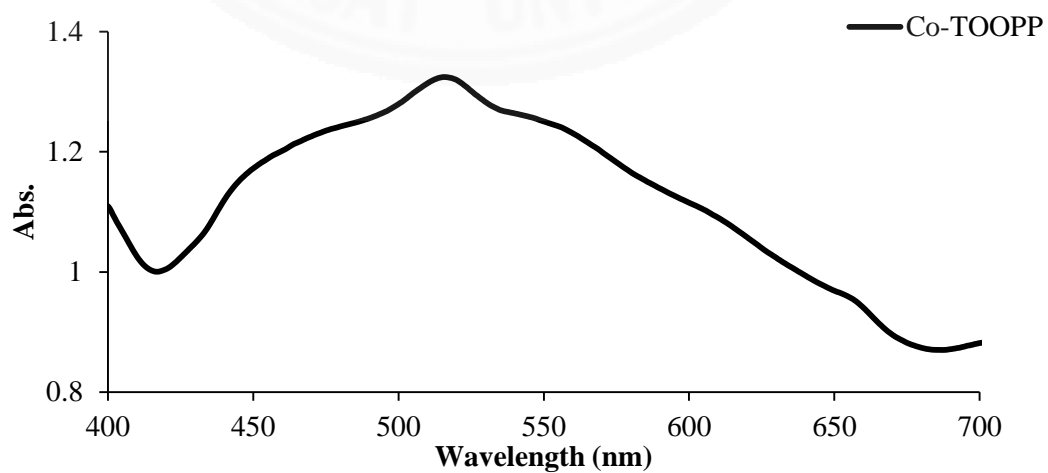
UV-Vis absorption spectra of cobalt(II) porphyrin in solid state



**Fig. D15** UV-Vis absorption spectra of Co-TOMPP **9**

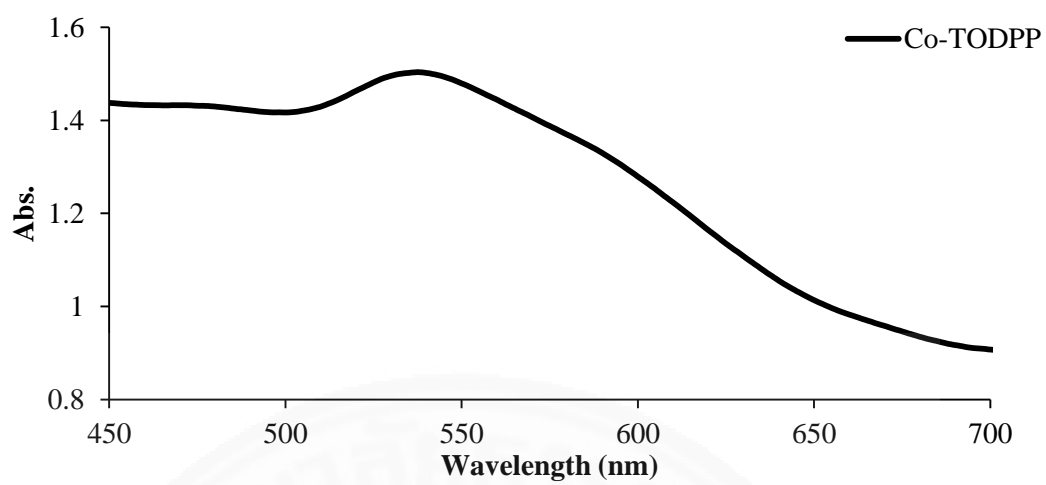


**Fig. D16** UV-Vis absorption spectra of Co-TOBPP **10**



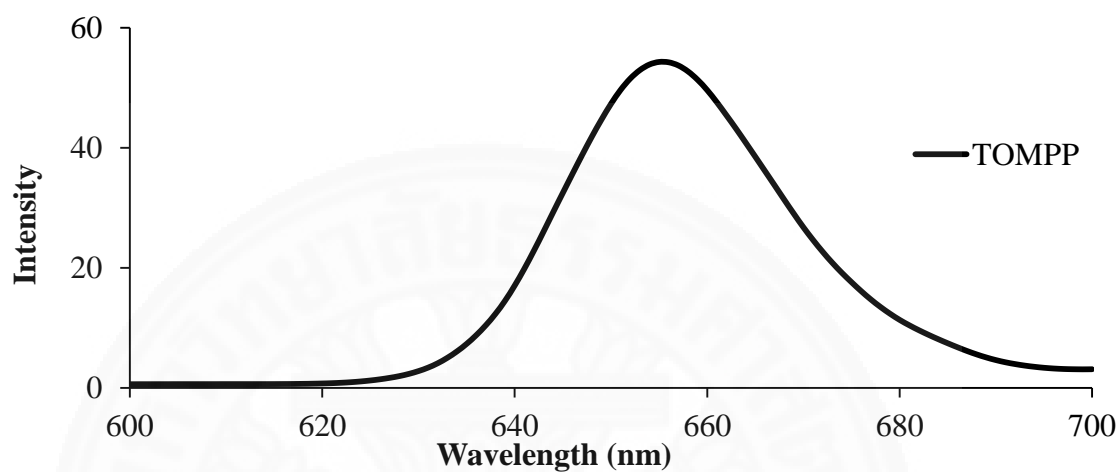
**Fig. D17** UV-Vis absorption spectra of Co-TOOPP **11**



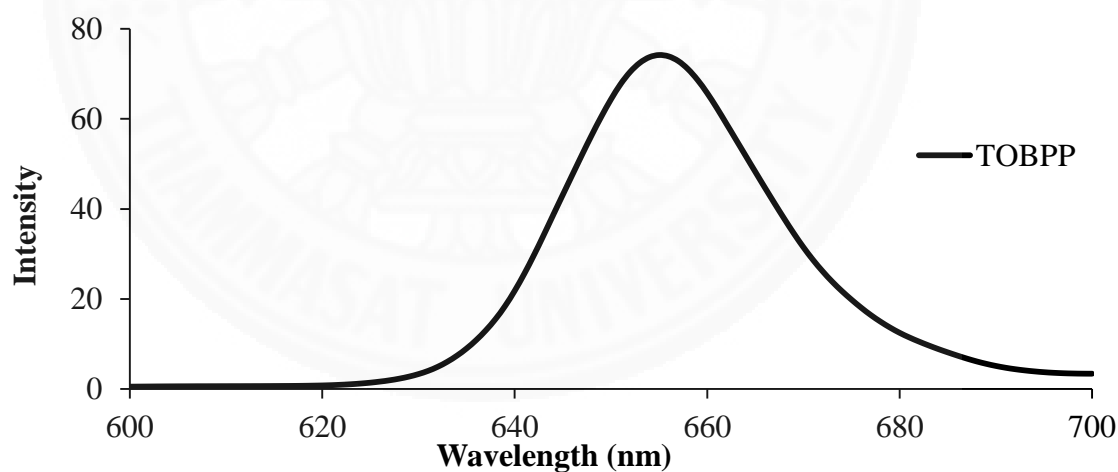


**Fig. D18** UV-Vis absorption spectra of Co-TODPP 12

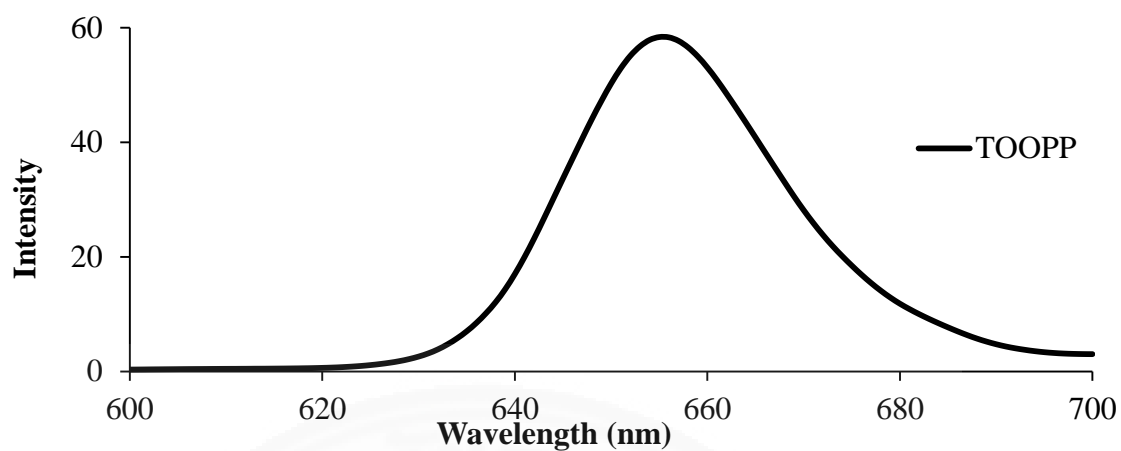
**APPENDIX E**  
**FLUORESCENCE SPECTRA**  
Fluorescence spectra of free base porphyrins



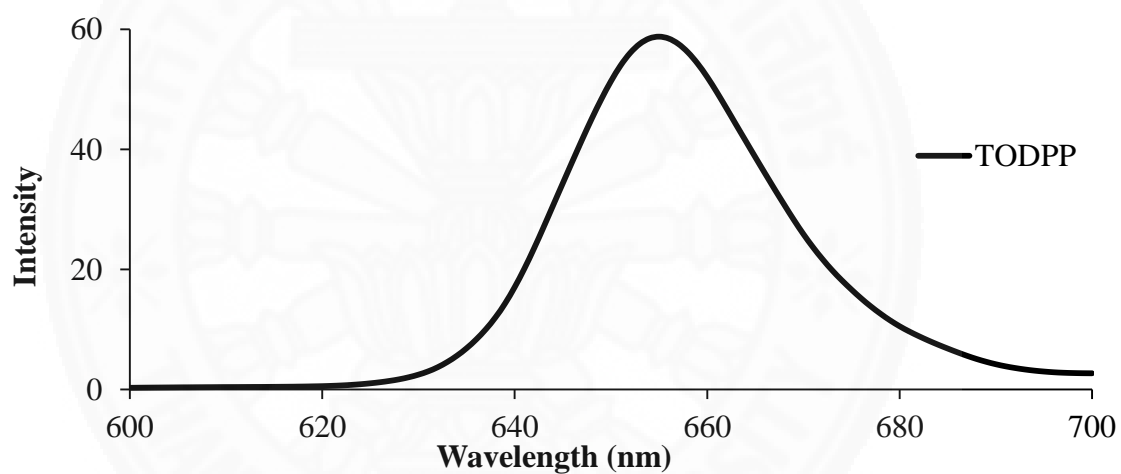
**Fig. E1** Fluorescence spectra of TOMPP 4 in CH<sub>2</sub>Cl<sub>2</sub>



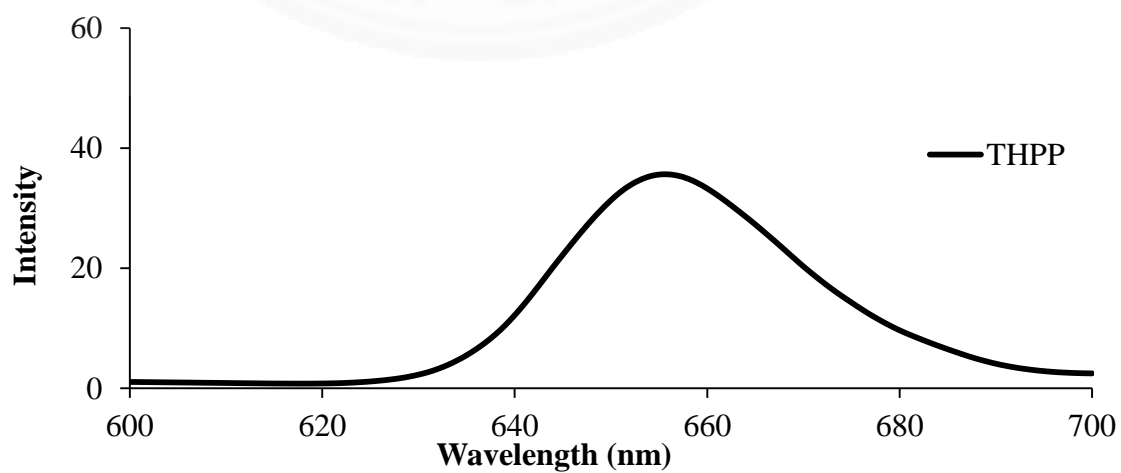
**Fig. E2** Fluorescence spectra of TOBPP 5 in CH<sub>2</sub>Cl<sub>2</sub>



**Fig. E3** Fluorescence spectra of TOOPP 6 in CH<sub>2</sub>Cl<sub>2</sub>



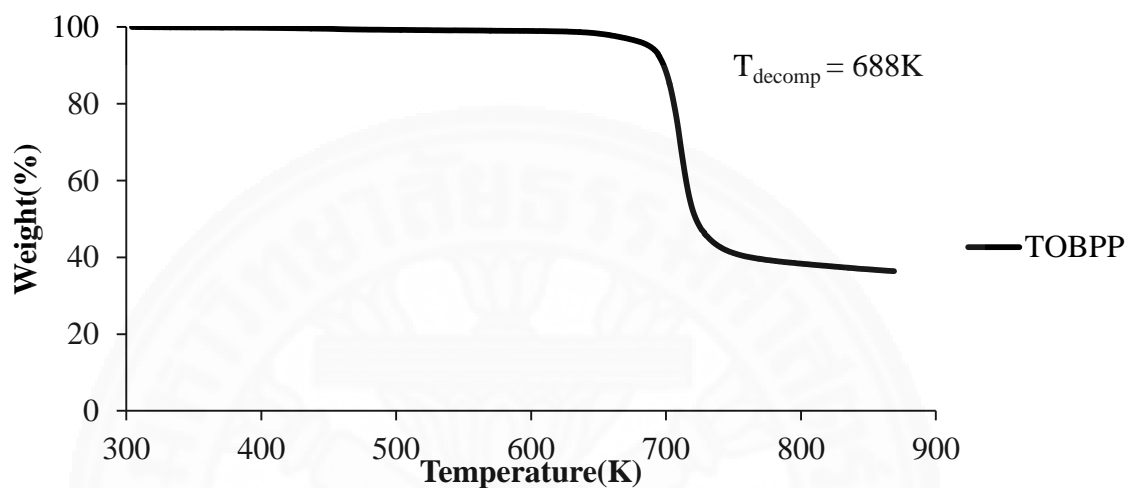
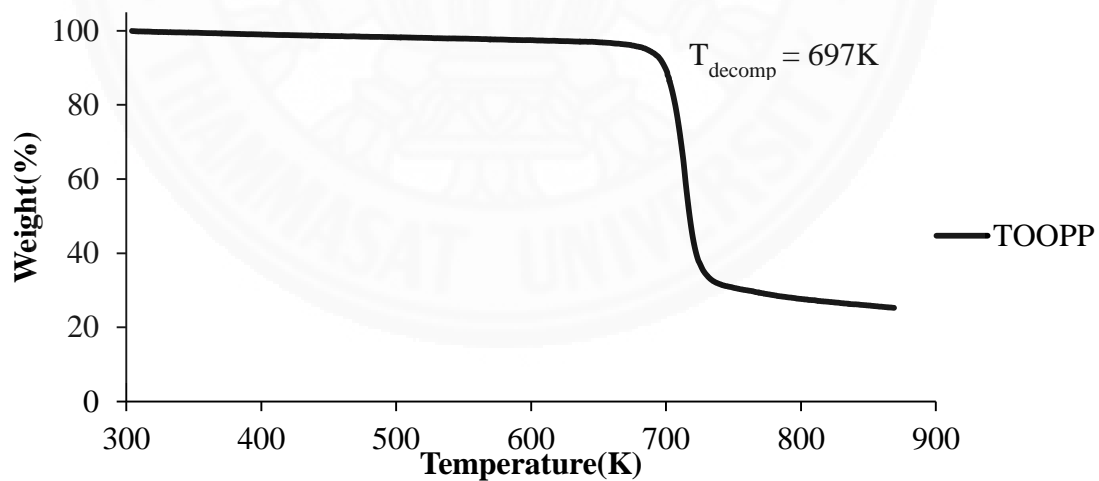
**Fig. E4** Fluorescence spectra of TODPP 7 in CH<sub>2</sub>Cl<sub>2</sub>



**Fig. E5** Fluorescence spectra of THPP 8 in CH<sub>2</sub>Cl<sub>2</sub>

**APPENDIX F****THERMOGRAVIMETRIC ANALYSIS (TGA)**

Thermogravimetric analysis (TGA) curves for free base ligands

**Fig. F1** Thermogravimetric analysis (TGA) curves of TOBPP **5****Fig. F2** Thermogravimetric analysis (TGA) curves of TOOPP **6**

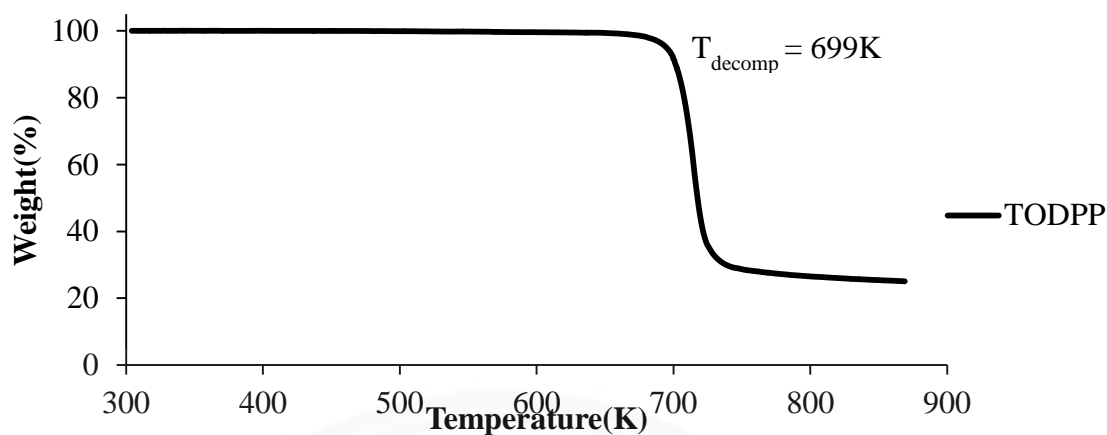


**Fig. F3** Thermogravimetric analysis (TGA) curves of TODPP 7

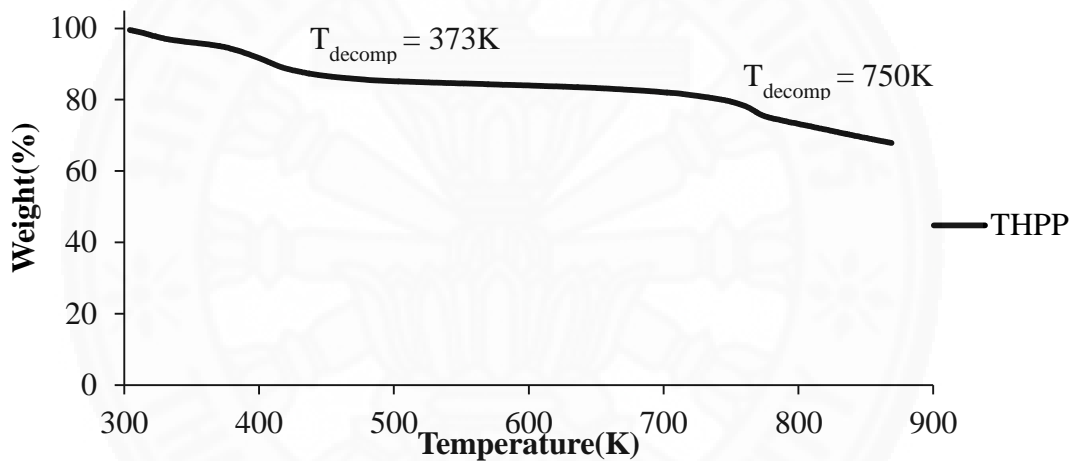


**Fig. F4** Thermogravimetric analysis (TGA) curves of THPP 8

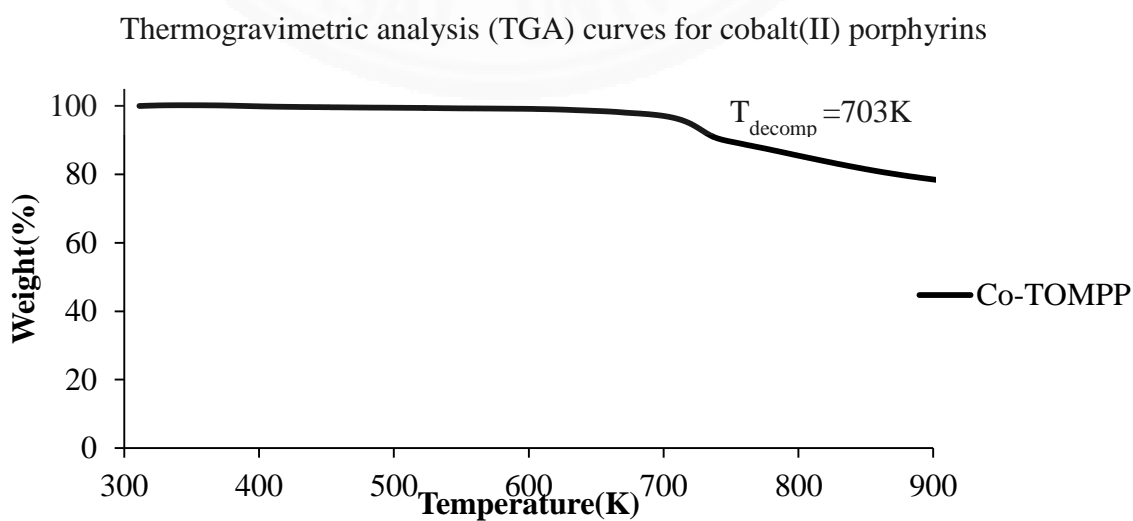


**Fig. F5** Thermogravimetric analysis (TGA) curves of Co-TOMPP 9

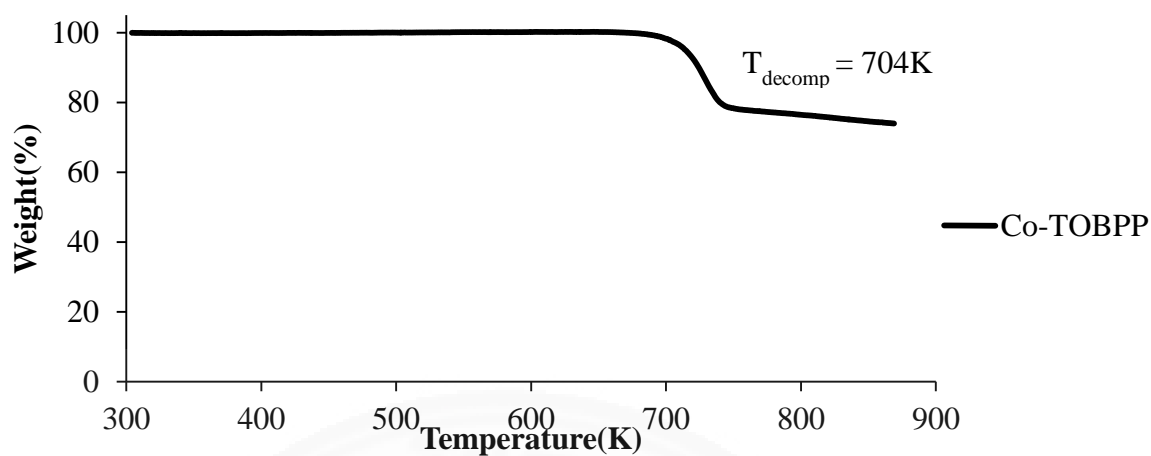


**Fig. F6** Thermogravimetric analysis (TGA) curves of Co-TOBPP 10

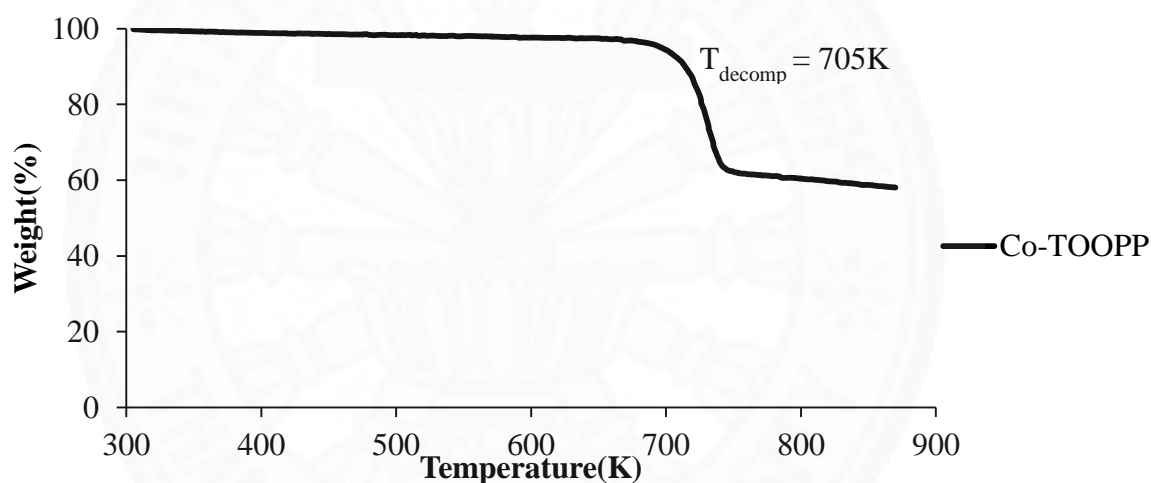


**Fig. F7** Thermogravimetric analysis (TGA) curves of Co-TOOPP 11

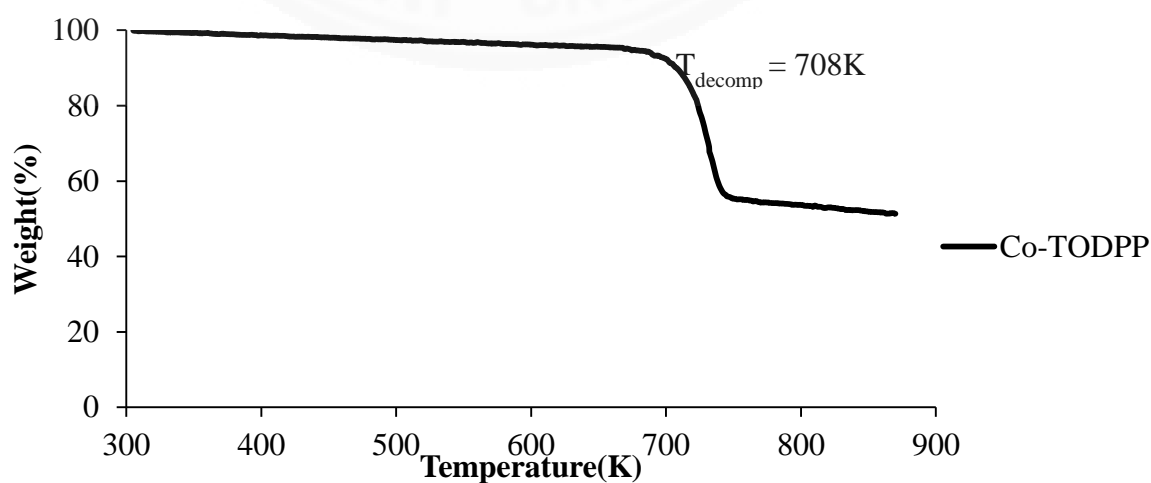


**Fig. F8** Thermogravimetric analysis (TGA) curves of Co-TODPP 12

## BIOGRAPHY

Name	Mr. Wootthiphan Jantayot
Date of Birth	September 24, 1990
Educational Attainment	2012 : Bachelor of Science in Chemistry, Thammasat University

### Publications

Poster presentation at The 39<sup>th</sup> Congress on Science and Technology of Thailand (STT 39)

Participated in a competition of invention at Institute of Intellectual Property and Business Thammasat University (TUIPI 2013)

Participated in Pure and Applied Chemistry International Conference (PACCON 2013)

Poster presentation at The 40<sup>th</sup> Congress on Science and Technology of Thailand (STT 40)

Poster Presentation at Pure and Applied Chemistry International Conference (PACCON 2014)

Paper publishing in Thai Journal of Science and Technology (2014)

Paper publishing in European Journal of Scientific Research, Volume 124 Issue 1 (2014)

Poster Presentation at Pure and Applied Chemistry International Conference (PACCON 2015)